The roles of NHE9 in vesicular trafficking and pH regulation

by

Mark Jacunski

Department of Physiology

McGill University, Montreal

April 2015

A thesis submitted to McGill University in partial fulfillment of the requirements of the degree of Master's of Science

ABSTRACT

Alkali cation/proton exchangers (NHE/SLC9A family) are integral membrane transporters involved in both cellular and systemic pH regulation, among other functions. Members of this family share 25-68% protein sequence identity and vary in both their tissue distribution and subcellular localization. The NHE9 isoform is widely-expressed and present in a subset of early and recycling endosomes that are involved in cargo trafficking and signaling. Interestingly, numerous genetic and expression analyses have linked imbalances in NHE9 function to neurodevelopmental conditions, including autism and attention deficit/hyperactivity. Recent experiments indicate that NHE9 co-localizes with the AMPA receptor subunit GRIA1 in vesicles that traffic during long-term synaptic plasticity, a process that is thought to underlie learning and memory. Furthermore, a recent study using autism-associated variants of NHE9 has indicated that decreased NHE9 function leads to vesicular acidification and deficits in cargo trafficking. However, a detailed analysis of all autism-associated variants was not carried out. To this end, we analyzed the subcellular localization of NHE9 and its autism-associated variants, measured transferrin uptake into recycling endosomes by flow cytometry, and determined vesicular pH by fluorescence ratiometric imaging. None of the exogenously-expressed autism-associated variants mislocalized in HeLa or AP-1 cells. In disagreement with a previous report, we found that only the autism-associated variant Ser438Pro presented significant functional deficits. Moreover, we identified several putative interacting proteins of NHE9 by yeast two-hybrid screening of a human brain cDNA library. These data have begun to shed new insight into the mechanisms underlying the regulation of NHE9 and its involvement in neurodevelopmental disorders.

RÉSUMÉ

Les échangeurs de cations alcalins/protons (famille de NHE/SLC9A) sont des transporteurs intégraux membranaires qui effectuent la régulation cellulaire et systémique du pH, entre autres fonctions. Les membres de cette famille ont de 25 à 68% similarité de la séquence polypeptidique mais diffèrent dans leurs expressions aux niveaux des tissus et leurs localisations sous-cellulaires. L'isoforme NHE9 est exprimé dans une majorité de tissus, et est localisé dans un sous-ensemble d'endosomes précoces et d'endosomes de recyclage, qui sont impliqués dans le transport des molécules et dans la signalisation. Curieusement, de nombreuses analyses génétiques et d'expression ont lié les déséquilibres de la fonction de NHE9 aux conditions neurodéveloppmentales, comme l'autisme et les troubles déficitaires de l'attention avec hyperactivité. Des expériences récentes indiquent que NHE9 se localise avec la sous-unité GRIA1 du récepteur AMPA dans des vésicules qui se déplacent pendant la plasticité synaptique à long terme, un processus qui est probablement à la base de l'apprentissage. Cependant, une analyse détaillée des mutants associés à l'autisme n'a pas encore été faite. Dans ce but, nous avons analysé la localisation sous-cellulaire de NHE9 et ses mutants associés à l'autisme, mesuré l'endocytose de transferrine par la cytometrie en flux, et déterminé le pH vésiculaire par l'imagerie ratiométrique de fluorescence. Aucune des variantes associées avec l'autisme n'est mal localisée dans les cellules HeLa ou AP-1, et seule la variante Ser438Pro, a des réductions de fonctions. En plus, en utilisant la technique double hybride en levures sur une banque d'ADNc du cerveau humain, nous avons identifié plusieurs partenaires d'interaction putatifs de NHE9. Ces données commencent à dévoiler les mécanismes moléculaires qui sous-tendent la régulation de NHE9 dans les conditions neurodéveloppmentales.

ACKNOWLEDGMENTS

Many of the interactions I have had during my study as a Master's student have made an impact. The tremendous change I see in myself (which hopefully has been for the better), as a researcher, as an individual, as a writer, as a teacher, and as a thinker, could not have been achieved without everything from casual quips to formal presentations. Despite my ambition, I do not want to attempt thanking everyone for everything. However, it's worth listing some key groups that have helped me during this degree.

My mentors and students in the laboratory: Prof. John Orlowski, Alina Ilie, Annie Boucher, Tushare Jinadasa, William Lau, and Mylene Lessard, for insightful conversations, guidance, challenges, suggestions, jokes, and support. Prof. John Orlowski and Alina Ilie for helping to revise the thesis, and Annie Boucher for revising the abstract, in both languages no less.

My family, and particularly, my parents: for countless inputs, including but not limited to general discussions, fun, and financial support.

The first floor of the Bellini: for some of the best discussions, both serious and not, that I have ever partaken in; adventures; challenges; and guidance. A special thanks goes out to the Imaging and Flow Cytometry Core Facilities.

My supervisory committee: for being very open and available not only for guidance but also for collaboration.

Canadian Institutes of Health Research: for funding which allowed me to focus on my project to my heart's content. The University and the Department also provided funding, for which I am thankful.

The Rod Roy Ski & Snowboard School: without which engaging in skiing would have been very limited, and with which I feel my experiences were both formative and amazing.

And last, but not least, to my thesis examiner, for offering to review my thesis, to optimize it and to clarify it where the curse of knowledge and imperfect writing has mired meaning and overlooked details.

ABBREVIATIONS AND ACRONYMS

7AAD ------ 7-aminoactinomycin D
αMEM ----- alpha modification of Eagle's minimal essential medium
A ---------- alanine
ADAM8 ---- a disintegrin and metalloproteinase domain family member 8
AMPA ------ α-amino-3-hydroxy-5-methyl-4-isoxazoleproprionic acid
ANOVA ---- analysis of variance
AP-1 --------- Chinese hamster ovary cell line lacking plasmalemmal alkali cation/proton exchange
AP-2 -------- adaptor protein 2
ARF --------- adenosine diphosphate ribosylation factor
ARNO ------ ARF nucleotide-binding site opener
ATP -------- adenosine triphosphate
AMP ------- adenosine monophosphate
AMPK ------ AMP-activated protein kinase
C ---------- cysteine if used in reference to polypeptide chain, carbon atom otherwise
C2C12 ----- mouse myoblast cell line
Ca ---------- calcium
Cl ---------- chlorine
CCCP ------ carbonyl cyanide m-chlorophenyl hydrazine
cDNA ------ complementary DNA
CFTR ------- cystic fibrosis transmembrane conductance regulator
ChFP ------- monoclonal cherry fluorescent protein, also known as mCherry
CHP -------- calcineurin B homologous protein
CLC --------- chloride channel
CTT --------- carboxy-terminal tail
D ---------- aspartic acid
DBD ------- DNA-binding domain
DMEM ---- Dulbecco's modified Eagle's medium
DMSO ----- dimethylsulfoxide
DNA ------- deoxyribonucleic acid
DTT -------- dithiothreitol
E ---------- glutamic acid
EDTA ------ ethylenediaminetetraacedic acid
EndoH ----- endo-B-N-acetylglucosaminidase H
FITC -------- fluorescein isothyocyanate
GFP -------- enhanced green fluorescent protein, also known as EGFP
GLAST ----- glutamate aspartate transporter
GluA1 ----- product of GRIA1 human gene, subunit of AMPA-type ionotropic glutamate receptor
GST -------- glutathione-S-transferase
GTP -------- guanosine triphosphate
GTPase --- guanosine triphosphatase
HEK293T -- Human embryonic kidney cell line clone 293 expressing the large T antigen

HeLa ------- Henrietta Lacks' cervical cancer cell line
H ---------- hydrogen, except in reference to the HKD domain, where it signifies histidine
HA ---------- human influenza hemagglutinin peptide
HEPES ----- 4-(2-hydroxyethyl)-1-piperazineethanesulfonic acid
HKD -------- conserved polypeptide chain motif consisting of the following sequence: HXKXXXXD where X indicates any amino acid
I ---------- isoleucine
IgG --------- immunoglobulin gamma
K ---------- potassium when referring to ions and small compounds, lysine when referring to peptides
L ---------- leucine
MEM ------ minimal essential medium
Mg --------- magnesium
mRNA ----- messenger RNA
MES -------- 2-(N-morpholino)ethanesulfonic acid
N ---------- asparagine
Na ---------- sodium
NHE -------- sodium/proton exchanger, also known as alkali cation/proton exchanger
O ---------- oxygen
P, Pro ------ proline
PBS --------- phosphate buffered saline pH 7.4
PBS-CM --- PBS 1 mM $MgCl_2$, 0.1 mM $CaCl_2$ pH 8.0
PCR -------- polymerase chain reaction
pH --------- negative logarithm of the effective proton concentration
PLD --------- phospholipase D
PNGase F - peptide-N-glucosidase F
Q ---------- glutamine
RACK ------ receptor for activated C kinase
RNA -------- ribonucleic acid
S, Ser ------ serine, except in the name of the biotinylating reagent, where it refers to sulfur
SD ---------- synthetic dropout
SDS -------- sodium dodecyl sulfate
SDS-PAGE - SDS polyacrylamide gel electrophoresis
SH-SY5Y --- human neuroblastoma cell line
siRNA ------ small interfering RNA
SLC --------- solute carrier gene family
T ---------- threonine
TAD -------- transcription-activating domain
Tfn --------- transferrin
Trk---------- tropomyosin receptor kinase
V ---------- valine
V-ATPase - vacuolar-type proton ATPase pump
X-Gal ------ 5-bromo-4-chloro-3-indolyl-β-D-galactopyranoside
Y ---------- tyrosine

CONTRIBUTION OF AUTHORS

Chapter 1: Effects of autism-associated mutations on (Na^+, K^+)/H^+ exchanger NHE9 function in vesicular trafficking and pH homeostasis

Mark Jacunski, Alina Ilie, Annie Boucher, John Orlowski

M. J. designed research, carried out experiments, analysed results, and wrote the chapter. A. I. designed research. J. O. designed research, analysed results, and revised the chapter. A. B. purified the anti-NHE9 antibody used in immunofluorescence of organotypic cultures. We acknowledge Francois Charron and Rebecca Anne McKinney for preparing organotypic cultures. We further acknowledge Gergely Lukacs and Pirjo Apaja for advice regarding ratiometric imaging analysis.

Chapter 2: Juxta-membranal cytoplasmic tail of (Na^+, K^+)/H^+ exchanger NHE9 interacts with PLD3

Mark Jacunski, Mylene Lessard, Mica Das Gupta, Annie Boucher, John Orlowski

M. J. designed research, carried out experiments, analysed results, and wrote the chapter. M. L. carried out immunoprecipitation experiments with PLD3. M. D. G. carried out part of the yeast two-hybrid screen. A. B. purified the anti-NHE9 antibody generated in-house. J. O. designed research, analysed results, and revised the chapter.

Appendix A: Endomembrane (Na^+, K^+)/H^+ exchanger glycosylation affects the stability and resident vesicle pH

Mark Jacunski, Alina Ilie, Annie Boucher, John Orlowski

M. J. designed research, carried out experiments (all, at least in part), analysed results, and wrote the chapter. A. I. designed research, participated in the maturation experiment, and analysed results. A. B. participated in cycloheximide chase and transferrin uptake experiments, and purified the anti-NHE9 antibody generated in-house. J. O. designed research, analysed results, and revised the chapter. We acknowledge Gergely Lukacs and Pirjo Apaja for advice regarding ratiometric imaging analysis.

TABLE OF CONTENTS

GENERAL INTRODUCTION

Cellular pH Homeostasis

The acid-base balance of a cell, its sub-compartments, and its surrounding environment is a fundamental chemical property which governs many aspects of cellular physiology. At a molecular level, a cell is a biochemical microcosm whose constituent macromolecules are affected by the balance of acids and bases; molecules shift from protonated to deprotonated states which can affect their biochemical properties (1). In particular, altering the charge of ionisable amino acids that make up proteins – the macromolecules most directly responsible for cellular activities – can in turn affect the manner in which these amino acids interact with one another and with other molecules to determine the structure and function of proteins.

In this way, the activities of many proteins may be modulated as a function of the acid-base balance – the pH – in a physiologically meaningful manner, but can also be aberrantly affected under certain pathophysiological conditions that disrupt pH homeostasis. For example, acidification of the stomach lumen is important for pepsinogen auto-activation, and thus gastric protein degradation (2) as well as for the iron release from internalized ligand-bound transferrin receptor complexes in early endosomes (3). At the cell and tissue level, changes in pH have also been implicated in processes such as proliferation (4) and extracellular matrix digestion (5). Conversely, in pronounced intracellular acidosis the function of the cardiac human ether-a-go-go related gene products inward rectifying channel decreases, which can lead to arrhythmias and death (6). Since many proteins can be profoundly affected by the acid-base balance, it is not surprising that cells have evolved numerous mechanisms for regulating it.

Regulation of pH is a necessary feature of all cells in order to manage the constant flux of acid equivalents. In particular, metabolic processes are a constant source of proton equivalents since they tend to yield oxidized, acidic products (7). Moreover, both the higher extracellular proton concentration and the negative potential of the cell provide a driving force for the influx of protons (7). Given that many processes not only specifically affect the pH, but are affected by it, it is imperative to understand the molecular mechanisms that govern pH homeostasis.

Cellular pH can be regulated by two main means: by buffering protons or acid equivalents, and by expelling them extracellularly or sequestering them into subcellular compartments. For instance, carbonic anhydrases – a group of enzymes responsible for catalyzing the equilibrium reaction between carbon dioxide and water, and carbonic acid – contributes to the buffering capacity because carbonic acid readily dissociates into bicarbonate and protons (8). While the buffering capacity is central to pH homeostasis, it is limited. However, the transport of protons across membrane compartments by a number of protein families offers the cell a more active means of controlling pH.

The transport of protons would be futile without the ability to contain those protons. The sequestration of protons from different compartments can occur because lipid bilayers are by themselves infinitesimally permeable to protons. Transporting significant amounts of protons requires proteins integral to the membrane (7). Among these proteins are primary active transporters that harness the energy generated by ATP hydrolysis to move substrates against their electrochemical gradients, such as the ubiquitously-expressed vacuolar-type proton ATPase (V-ATPase) (9), or the gastric proton/potassium ATPase (10). However, these primary active transport systems fulfill more specialized roles in cells and tissues, and do not make major contributions to cytoplasmic pH homeostasis. Instead, cells have evolved a variety of secondary active transport systems which contribute to pH regulation by using the gradients established by other primary active transport systems such as the Na^+/K^+ ATPase, which is ubiquitous and abundant in the plasma membrane (11).

A major acidifying mechanism that cells possess is through anion exchange (7). In particular, bicarbonate/chloride (HCO_3^-/Cl^-) exchange mediated by the widely-expressed SLC4A2 (anion exchanger isoform 2) is activated by alkalinity and leads to bicarbonate efflux in exchange for chloride to neutralize cytoplasmic pH (12, 13). Bicarbonate transport can also occur in the opposite direction, to alkalinize the cell, through co-transport with sodium (7). This Na^+-HCO_3^- co-transport is mediated by SLC4A4, 5, 7, 8, and 10, which differ in both their tissue expression and their stoichiometry (12, 14-19). Regardless of the stoichiometry, the importance of bicarbonate flux through these transporters allows for pH regulation in many physiological settings; defects

in these transporters are linked to a variety of phenotypes ranging from neurological disorders (20) to metabolic acidosis through ineffective renal reabsorption of bicarbonate (21).

Members of the alkali cation/proton (Na^+, K^+/H^+) exchanger family (SLC9A1-9, or NHE1-9) are likewise involved in cytoplasmic alkalinisation (22), functioning as homodimers (23). They differ not only in their tissue distribution, but also in their sub-cellular localization. Paralogs NHE1-5 are selective to Na^+/H^+ exchange and function predominantly on the plasma membrane, though NHE3 and 5 are in dynamic equilibrium with an endosomal pool (24, 25). On the other hand, paralogs NHE6-9 localize to intracellular compartments and their exchange has been shown to be non-selective to either potassium or sodium in exchange for proton (26-28), which will be explored further in the following section on vesicular pH. Members of the NHE family function in other processes which in some cases are distinct from their roles in pH homeostasis (23). One particular example is the activation of NHE1, 2, and 4 by cell shrinkage (29, 30), yielding net sodium chloride uptake when functionally coupled to the anion exchangers SLC4A1 and 2 (31-33). The net intake of sodium chloride increases the osmolarity, which leads to osmosis to restore cell volume.

Only those alkali cation/proton exchanger paralogs which are present on the membrane can effectively regulate cytoplasmic pH (7). For most cells, NHE1 plays this housekeeping role (23); proton binding and transport rises not only with increasing proton concentrations but likely also by allosteric interactions with protons to regulate cytoplasmic pH (34). However, in some cell types, NHE1 localization is restricted, being present only in certain domains of the plasma membrane, such as the basolateral membrane in certain epithelia (22, 35-37), or the transverse tubules of cardiomyocytes (38). While NHE1 is still involved in cytoplasmic pH regulation in these settings, it may also have more specialized roles. For instance, in the basolateral membrane of medullary thick ascending limb of nephrons, NHE1 contributes to transepithelial bicarbonate transport, thus playing a role in systemic ion regulation (39).

Other paralogs of the NHE family also participate in cellular pH regulation, albeit in more specific circumstances. For instance, NHE5 is expressed preferentially in neurons and is present not only on the cell surface but also in an endosomal pool (25). Maintaining an internal pool of

NHE5 offers an additional control for Na^+/H^+ exchange for the purpose of cytoplasmic pH regulation. For instance, low pH often coincides with high adenosine monophosphate (AMP), as when neuronal activity is high. In these circumstances, AMP-activated protein kinase (AMPK) phosphorylates NHE5 which then accumulates at the plasma membrane where it can regulate neuronal cytoplasmic pH (40). In addition, NHE5 has also been shown to function on its resident endosomes, acidifying their lumen and affecting their trafficking (41).

Cytoplasmic pH is controlled by numerous mechanisms involving both buffering and transport. Though maintaining pH homeostasis is a key function of these mechanisms, certain processes involve shifts in the pH, such as migration and cell division. Furthermore, there are certain cellular processes which function best in particular environments that may be unlike the cytoplasm. Lysosomes house a multitude of hydrolases involved in macromolecular catabolism, which occurs in a lumen which can reach pH levels below 5.0 (42). This is one of the evolutionary reasons for the existence of intracellular compartments; cells can sequester certain processes to their own compartments. Here too, biological processes can affect the pH and, and inversely, the pH can affect biological processes.

Vesicular pH Regulation

Intracellular compartments house cargo, biochemical reactions, scaffold signaling cascades, traffic throughout the cell, and provide a portal for communication with the cell's external environment (7, 43). Many of these compartments can be categorized into exocytic and endocytic vesicular pathways. The canonical exocytic pathway begins with both protein and lipid synthesis and modification in the endoplasmic reticulum, continuing through further modification in the Golgi apparatus, and eventually targeting to another compartment or to the exoplasm via exocytosis (44). Conversely, the canonical endocytic pathway begins with plasmalemmal cargo which are internalized to early endosomes, from which cargo are either returned to the plasmalemma by recycling endosomes or eventually degraded by trafficking through late endosomes and finally lysosomes (44). In reality, the two pathways are intertwined: trafficking to a compartment from one pathway does not signify that trafficking will only continue along that pathway. Mammalian cells also contain other compartments such as mitochondria,

peroxisomes, and the nucleus, which, for the most part, do not directly partake in vesicular trafficking (43, 45) and will not be discussed further here.

Vesicle cargo trafficking can be investigated by examining sub-cellular localization relative to compartmental-specific biochemical processes. Many members of the RAB family of small GTPases play central roles in compartment-specific processes and are commonly used as markers of vesicular identity (**Figure 1**). In humans, the family is made up of about 70 paralogs which are part of distinct signaling pathways that are in part responsible for distinct vesicular functions (43). For instance, activation of RAB4 in neurons facilitates sorting of certain internalized glutamate ionotropic channels to be recycled back to the plasma membrane for continued function (46). Similarly, the activation of RAB5 during low-density lipoprotein receptor-dependent internalization is responsible for recruiting both membrane tethering complexes as well as RAB7 for eventual trafficking to lysosomes for degradation (47, 48). Thus, many RAB proteins are relevant molecular markers of vesicle types due to their central roles in compartment-specific biochemistry.

Another set of molecules which are key determinants of vesicle function are phosphoinositides (**Figure 1**). Phosphoinositides are lipids with an inositol ring phosphorylated at one to three positions: 3, 4, and/or 5. Like the RABs, the different phosphoinositide species with different combinations of phosphorylated positions reside on different cellular sub-compartments, though generally with a wider range than that of RABs (49). Much like RABs mediate vesicular functions by protein-protein interactions, proteins can also be regulated by interactions with lipids. One possible form of interaction is that of integral membrane proteins' transmembrane domains contacting adjacent lipids. This is exemplified by a prominent hypothesis of mechanotransduction channel gating due to membrane tension, in which lipids adjacent to mechanotransduction channels alter the conformation of the channel pore to allow for ion conductance (50). A second form of interaction is that of proteins interacting with specific lipids or lipid domains, as in the requirement of phosphoinositide-4,5-bisphosphate in recruiting adaptor protein 2 (AP-2) for the formation of clathrin coats in endocytosis (49). Phosphoinositides take part in both mechanisms, acting as important recruiters and regulators of proteins in vesicle function (49, 51).

Like the cytoplasm, each sub-cellular compartment has a finely-regulated luminal pH which is either permissive to or otherwise central to the function of that compartment (7, 9). Accordingly, vesicle types can be identified not only by specific biochemical process, but also by their luminal pH. However, direct measure of vesicle membrane ion transport and direct manipulation of vesicular proteins is limited methodologically. As a result, the causality of pH regulation for and/or by vesicular function is still murky. Nonetheless, strong correlations between the processes occurring in a vesicle and its luminal pH exist.

But how does pH regulation play into vesicle functions? A particular case is revealed at synapses, where neurons secrete neurotransmitters. In the case of small molecule neurotransmitters, such as monoamines and acetylcholine, neurotransmitters are imported into synaptic vesicles in exchange for luminal protons down their electrochemical gradient (52). The proton gradient necessary to power this neurotransmitter influx is generated by the vacuolar-type H^+-ATPase pump (V-ATPase) (52). However, numerous vesicular neurotransmitter transporters, such as those for glutamate or glycine, may be powering the transport by exchanging neurotransmitters for intraluminal chloride (52). Nonetheless, the pH gradient is still important in these cases as the chloride gradient is thought to be established primarily by balancing the charge of intraluminal protons (53).

Acidification by the V-ATPase is crucial to biochemical processes that underlie the trafficking, signaling, biochemistry of vesicles and their cargo. Vesicle acidification as a means to release iron from internalized transferrin-transferrin receptor complexes was already mentioned as an example (3), but it can also determine vesicle trafficking. For instance, acidification of early endosomes allows the ADP ribosylation factor 6 (ARF6) guanosine nucleotide exchange factor and ADP ribosylation factor nucleotide site opener (ARNO) to interact with components of the V-ATPase in order to promote sorting of internalized albumin towards degradation in the lysosomes (54). More recently, prolonged adenylate cyclase-mediated signaling by internalized parathyroid hormone ligand-receptor complexes was found to activate the V-ATPase to acidify vesicles (55). This acidification led to the dissociation of parathyroid hormone ligand-receptor complexes to quell signaling, which coincided with trafficking towards late endosomes and the Golgi to further sequester and terminate the signalling (55). Many signaling pathways have been found to

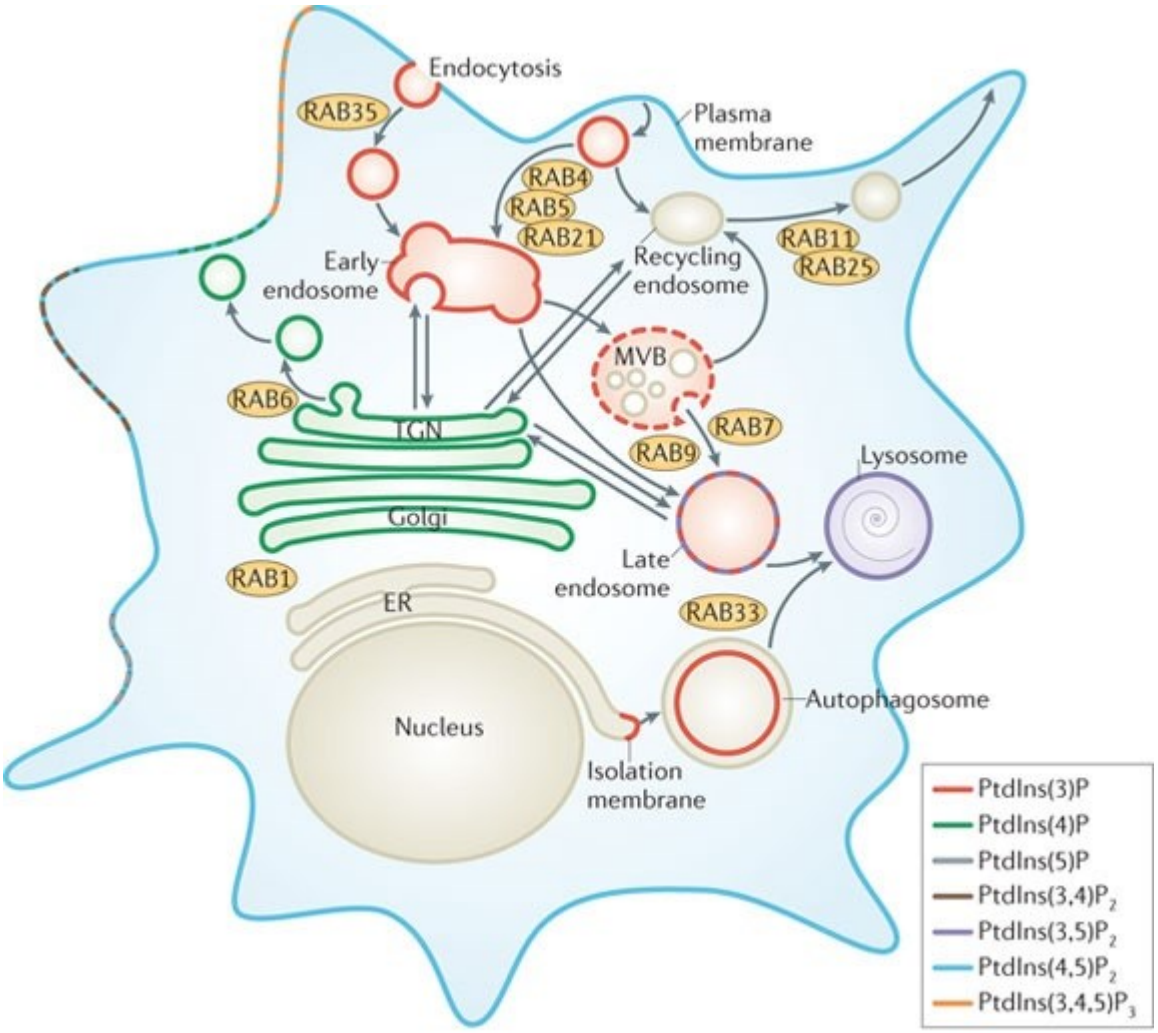

Figure 1: Canonical markers of intracellular compartments. Many small RAB GTPases participate in compartmental-specific biochemical processes and hence act markers of intracellular compartments. Similarly, phosphoinositides tend to be enriched on certain compartments, being produced on certain membranes and also participating in particular biochemical interactions. Figure adapted from (56).

proceed or to start on endomembranes, some of which have been found to correlate with pH, such as Notch signaling (57) and brain-derived neurotrophic factor signaling (58). However, unlike the examples above, the causality and underlying molecular mechanisms of such effects are still obscure.

Regardless, the V-ATPase is one of the principal determinants of vesicular pH (7). Compartment-specific biochemical events such as those involving RAB family proteins, phosphatidylinositides, can regulate V-ATPase function (9). For instance, the activation of the V-ATPase in the example of parathyroid hormone signaling occurs in part due to a phosphorylation event on an a-type subunit (55, 59). Importantly, different paralogs of the a-type subunit traffic to certain membranes (9). By differentially regulating the V-ATPases according to their subunits, each compartment could conceivably generate a different pH (7). Finally, the transport capacity of the membrane also determines the pH; the density of V-ATPases in combination with other ion transport such as chloride or alkali cation/proton exchange could dictate luminal pH by altering membrane potential, membrane conductance, and the concentration of protons (7).

Indeed, proton transport by the V-ATPase is limited thermodynamically by the energy released in ATP hydrolysis (7, 53). Proton transport would eventually be abrogated by a steep electrochemical gradient – the high intraluminal proton concentration and high intraluminal membrane potential – that the V-ATPase would have to work against (7, 9). In this case, cation efflux and anion influx of the vesicle would be required in order to dissipate the positive membrane potential and to yield a gentler electrochemical gradient against which to work (7). While insight about cation efflux from vesicles is curtailed by methodological limitations, the influx of anions such as chloride has become clearer as a result of more reliable fluorescent sensors (53).

The most prominent chloride-transporting proteins belong to the CLC family of chloride channels and transporters (53). Paralogs CLC3-7 are electrogenic secondary active transporters that exchange one intraluminal proton for two cytoplasmic chloride ions, a process that effectively dissipates the high positive intraluminal charge generated by the vacuolar H^+-ATPase (53). There is a large body of work implicating chloride transport by CLC paralogs in the function

of their resident vesicles. For example, CLC3 is necessary for the acidification of ligand-bound transferrin receptor-containing vesicles to help dissociate the ligand from the receptor (60) and increases the relative size of the acidic, lysosomal sub-compartment, which could signify an increase in lysosomal degradation activity (61). Other chloride transporting proteins have been implicated in sub-compartment pH regulation, but these results are more contentious. Specifically, the cystic fibrosis transmembrane conductance regulator (CFTR), has been controversially found to function in exocytic or recycling vesicles (62, 63). Furthermore, there are two known Golgi anion channels (GOLAC1 & 2) which contribute to chloride conductance, while also facilitating the diffusion of anions such as phosphate (64, 65). Whether this electrical shunt in the Golgi is important for luminal pH regulation remains to be determined. Regardless of the importance of chloride influx to vesicles as an electrical shunt for proton influx, it is important to note that chloride itself may have important effects on vesicle function (53). For instance, it is possible that chloride influx regulates the osmotic balance of vesicles to modify protein function or vesicular volume (53).

Contrary to the vesicular chloride influx as a balancer to proton influx, members of the alkali cation/proton (Na^+, K^+/H^+) exchangers (SLC9A or NHE) family that localize to endomembranes can either acidify or alkalinize vesicular lumen depending on the paralog or the circumstance (23). As mentioned in the preceding section on cellular pH, NHE3 and NHE5 are present and function on both the plasma membrane and endomembranes (25, 40, 66, 67). These plasmalemmal paralogs selectively exchange sodium for protons, in contrast to the non-selective endomembrane paralogs which can exchange either sodium or potassium for protons (23). Consequently, NHE3 and NHE5 most likely function in newly-formed endocytic vesicles, when the luminal fluid composition is still similar to the sodium-rich and potassium-poor extracellular solution (23, 41, 66). In these vesicles, the exchangers would mediate sodium efflux and proton influx to the vesicle, thereby acidifying the lumen. Presumably, as intraluminal sodium is depleted and the proton concentration gradient steepens, NHE3 and NHE5 function would diminish. However, some experiments indicate that the ubiquitous plasma membrane Na^+/K^+ ATPase functions on endocytic vesicles and takes part in their trafficking (68), in which case these paralogs of the NHE family could continue to function. Regardless, there is mounting evidence to

suggest that NHE3 and NHE5 participate in vesicular pH regulation. For instance, NHE3 acidifies vesicles in kidney proximal tubule cells and facilitates the endocytosis of albumin, a key homeostatic process (69). Relatedly, the neuronally-expressed NHE5 affects TrkA trafficking and acidifies internalized nerve growth factor-bound TrkA, facilitating downstream signaling which, among other effects, increases neuronal arborisation (41).

In contrast to the putatively limited but effective alkali cation/proton exchange mediated by the NHE3 and NHE5, the ubiquitously-expressed NHE6-9 are non-selective for alkali cations and can mediate potassium/proton exchange in the potassium-rich cytoplasmic environment in order to alkalinize, rather than acidify vesicles (27, 28, 70). Accordingly, these proteins can have profound effects on vesicle trafficking and signaling.

NHE6 is a resident of early and recycling vesicles (70-72), with some limited plasmalemmal presence (73, 74). The function of NHE6 has been shown to enhance several trafficking phenomena, such as transferrin uptake (75) and the exit of amyloid precursor protein from the Golgi body (76). Mutations in NHE6 have been linked to Christianson syndrome, a neurodevelopmental condition characterized by intellectual disability, ataxia, microcephaly, and epilepsy (77-79). Additionally, post-mortem expression analyses in humans have found correlations in decreases in NHE6 expression to the severity of autism (80), another neurodevelopmental condition. Two Christianson syndrome-associated mutants that have been studied in detail – Δ255ES256 and Δ370WST372 – exhibit not only greatly decreased glycosylation but also precluded endoplasmic reticulum exit, suggesting that they cause profound perturbations in protein folding (74, 81). Accordingly, the Δ370WST372 mutation does not enhance transferrin uptake and diminishes the arborization of transfected mouse primary neurons, relative to wild-type NHE6 (74). This has been corroborated with a putatively ion exchange deficient variant yielding similar results (82). Additionally, hippocampal cultures from NHE6-null mice exhibit less neuronal arborization, fewer dendritic spines, lower synaptic field potentials, as well as more acidic endosomes in the neurites (82). The acidification of these endosomes has been suggested to underlie the neuronal defects in part by the decrease in brain-derived neurotrophic factor signaling (82), a key pathway in both the development and the maintenance of the central nervous system (83, 84). Indeed, its receptor, TrkB, colocalizes with

NHE6 in neurons, and the application of brain-derived neurotrophic factor rescues the arborization of neurons in cultures from NHE6-null mice (82). Moreover, in dendritic spines NHE6 trafficking correlates with the trafficking of α-amino-3-hydroxy-5-methyl-4-isoxazolepropionic acid (AMPA)-type glutamate receptors during synaptic plasticity (85). Altogether, these results support the association of NHE6 with neurodevelopmental conditions such as Christianson syndrome and autism, and they suggest that NHE6 plays important roles in sub-cellular trafficking and signaling mechanisms, in part through vesicular pH regulation.

Conversely, not much is known about either the physiological role of NHE7 or the molecular processes in which it is involved (22, 23). NHE7 is a resident of the trans-Golgi network and, like NHE6, is present at the plasma membrane in small amounts (86). It remains unclear whether NHE7 contributes to ion homeostasis at either the trans-Golgi network or the plasma membrane (22). A recent study concluded that NHE7 was sodium-specific and led to increased transferrin trafficking by acidifying endosomes (87), in striking contrast to the highly similar paralog NHE6 (68% at the primary sequence level), but this is not supported by previous studies (27).

NHE8 resides in the trans-Golgi network, early and late endosomes, and multivesicular bodies in most cells (22, 23). Much of the work on NHE8 has been dedicated to its plasmalemmal localization in kidney proximal tubules and the small intestine, and not much is known about its function on endomembranes. Nonetheless, one study found that preventing NHE8 function by either RNA interference or a putatively dominant negative variant perturbed steady-state vesicular trafficking without altering steady-state pH (88). Indeed, multivesicular bodies, as well as other acidic vesicles were found to be enlarged and located abnormally close to the nucleus (88). Furthermore, the study found that a depletion of NHE8 increased epidermal growth factor degradation, which occurs in acidic vesicles (88). This suggests that NHE8 alkalinizes late endosomes and lysosomes thus dampens their function.

Alkali Cation/Proton Exchanger Isoform 9

NHE9 resides on early and recycling vesicles in a distribution that is distinct, but overlapping with that of NHE6, and contributes to luminal alkalinisation (70). Much like NHE6,

abnormalities in NHE9 have been linked to neurodevelopmental disorders. Indeed, NHE9 was first identified by its associations to disorders such as attention deficit/hyperactivity disorder and autism. Initially, a family with a history of impulsivity and intellectual disability was found to contain a chromosomal inversion which likely resulted in a total loss of NHE9 (89). This has since been corroborated by a number of genome-wide association studies, particularly by Lasku-Su, et al. (90). Moreover, a rat model of attention deficit/hyperactivity disorder was found to have mutations which disrupted NHE9 co-precipitation with calcineurin homologous protein 1 (CHP1), but not receptor for activated C kinase 1 (RACK1) (91), though the relationship to human attention deficit/hyperactivity disorder is tenuous, and the protocols and results of their biochemical experiments are questionable.

In addition to an association with attention deficit/hyperactivity disorder, imbalances in NHE9 function have been linked to autism and epilepsy. Both a large deletion near the 5' end of the NHE9 gene (SLC9A9), as well as a number of point mutations, including a nonsense mutation at arginine 423, were linked to autism, sometimes accompanied by epilepsy (92). While the expression and function of these genotypes were not evaluated further in that study, a subsequent study demonstrated that NHE9 enhanced both transferrin uptake and glutamate uptake in mouse primary astrocytes, effects which were entirely lost by three of the evaluated mutations, V176I, L236S, and S438P (93). More recently, a post-mortem expression analysis of human brains indicated that NHE9 expression increases in correlation with the severity of autism (80). Since some of the linked mutations seem to lead to a loss of function, this latter result would suggest that a fine balance of NHE9 function is required for normal neurodevelopment. Intriguingly, NHE6, which shares a similar subcellular distribution, 58% primary sequence similarity, and linkages with neurodevelopmental conditions, was found to be down-regulated in correlation with the severity of autism, opening up even more questions about the distinct roles of these two paralogs (80).

There is substantial evidence that balanced NHE9 function is required for normal neurodevelopment. Perhaps enhancing the uptake of critical factors such as transferrin or glutamate (93) may be important for neurodevelopment, or, like NHE6, it may diminish key intracellular signaling (82). Another possibility is the persistence of aberrant or inappropriate

signals. Supporting this idea is the recent finding that NHE9 expression supports glioblastoma growth by increasing epidermal growth factor signaling as well as migration and proliferation, two effects which may stem from sustained epidermal growth factor signals (94).

Research Rationale and Objectives

While numerous studies have associated NHE9 function to neurodevelopment, the biochemical mechanisms underlying these functions remain obscure. Remarkably, despite the ubiquitous expression of NHE9, there have not been any strong associations with the function of other organ systems. A neuron-specific trafficking or signaling event involving NHE9-containing endosomes may be responsible for the limited effects of any disruption in NHE9 function. However, many alternative explanations exist: compensation by other members of the NHE family, anatomical and cellular complexity of central nervous system development (95), and even peripheral dysfunction, such as compromised immune function of epithelia, which may profoundly affect neurodevelopment (96-98).

The function of NHE9 in regulating vesicular trafficking and pH regulation remains obscured. The exchanger could act equally as an ion transporter in addition to a scaffolding protein to mediate its neurodevelopmental function. Given the similarity to its paralogs, it is likely to function as an alkali cation/proton exchanger, and its long cytoplasmic carboxy-terminal tail is probably involved in many intermolecular interactions. Rao and colleagues have begun to study the role of wild-type and autism-associated mutant forms (V176I, L236S, S438P) of NHE9 on the trafficking of transferrin receptor-containing vesicles (93). In our study, we will expand their experiments to include other autism-associated mutations (P117T, D495N, Q609K) as well as a putatively ion exchange deficient variant (D244N). Including an ion exchange deficient variant would be central to distinguishing between the scaffolding and the ion exchange functions of NHE9. Moreover, we will measure transferrin uptake during the linear range of its uptake, rather than at steady state, which we believe is a better indicator of endocytosis rather than capacity. Finally, we intend to measure pH over multiple time points in an effort to determine when in transferrin endocytosis is NHE9 function important.

Confirming these findings in a system which contains minimal NHE9, such as human cervical cancer HeLa cells, or AP-1 cells – a Chinese hamster ovary cell line devoid of plasmalemmal sodium-proton exchange activity, as well as NHE6 and NHE9 – may shed new light on the function of NHE9, particularly if expanded to all the currently-known autism-associated mutations, in addition to a putatively ion exchange-deficient mutation (D244N) which we developed. To this end, my first objective was to study the sub-cellular localization of NHE9 and its mutants transiently transfected into either HeLa or AP-1 cells in an attempt to identify those with the greatest defects in trafficking. Next, I aimed to measure transferrin uptake in HeLa cells using flow cytometry. My final objective was to determine whether NHE9 is involved in vesicular pH regulation and whether the mutants affected this aspect of function, I measured vesicular pH using transferrin conjugated to fluorescein isothiocyanate in wide-field fluorescence ratiometric imaging, in contrast to the flow cytometry-based method used by Kondapalli et al. We believe this method has two advantages. First, using this method we can measure pH in individual regions of interest. This factor will potentially allow us to distinguish between NHE9-containing and NHE9-lacking transferrin-containing vesicles, particularly at early points in transferrin endocytosis where transferrin is less broadly localized. Second, we will be able to carry out the imaging in a solution of our choice, rather than a flow cytometer's sheath fluid, which allows us to be more confident in our pH-clamping during ratiometric calibration. Eventually, characterizing NHE9 and the mentioned mutations in these experiments will provide tools and insights for continuing study on the mechanisms underlying the link between vesicular pH, trafficking, and neurodevelopment.

Investigating what protein-protein interactions SLC9A9 is involved in may provide a firm grasp of the place of SLC9A9 in cellular homeostasis and, in particular, in neurodevelopment. Hence, an additional goal was to complete a yeast two-hybrid protein-protein interaction screen of a human brain cDNA library with the carboxy terminal cytoplasmic tail of SLC9A9. From this I identified twenty-six putative interacting partners. Most of the potential interactions remain uncharacterized, but I pursued further study of phospholipase D 3 because of its implications in sub-cellular trafficking as well as differentiation (99, 100). While the relevance of this interaction,

if any, remains elusive, my experiments have opened a potential avenue of research on the association of SLC9A9 with neurodevelopment.

CHAPTER 1

Effects of autism-associated mutations on (Na^+, K^+)/H^+ exchanger NHE9 function in vesicular trafficking and pH homeostasis

Mark Jacunski, Alina Ilie, Annie Boucher, John Orlowski

N. B. Supplemental data for this chapter appears in Appendix B.

Introduction

The development of the mammalian nervous system is among the most complicated and fascinating biological processes. The process involves the differentiation of multipotential cells (101), their timely migration (83, 102), and eventually their settlement and arborization to produce a network capable of computation (103, 104). All of these events are governed by underlying signaling events, many of which involve coordinated sub-cellular trafficking events. Receptors which are synthesized in the rough endoplasmic reticulum must appropriately traffic to the plasma membrane to receive and convey the signals which underlie the development and function of the central nervous system. Importantly, when activated, some receptors' signaling leads to further trafficking during which signaling can continue. One of the most prominently studied instances occurs with G protein-coupled receptor signaling leading to internalization through interactions with β-arrestins (105). Depending on the receptor-β-arrestin couple, receptors can be sequestered internally, returned to the plasma membrane, to the Golgi, or to the lysosomes for degradation (43, 106). Indeed, biochemical events which occur during extended signaling throughout trafficking can influence the signaling itself. This influence could be indirect, for example by sequestering the receptor and thereby preventing new signaling events (107), or it could be direct, perhaps by acidifying, destabilizing receptor-ligand interactions ceasing signaling (55). The appropriate signaling of canonical biochemical cascades is central to brain development, but crucially, these signals often involve sub-cellular trafficking events which have not been extensively investigated (57, 108).

One protein which could contribute to these sub-cellular trafficking events is the endomembrane alkali cation/proton exchanger (NHE or SLC9A) isoform 9 (NHE9). A number of genetic and expression analyses in humans have found an association with altered NHE9 function and neurodevelopmental conditions. Genetic studies in families and genome-wide association studies suggest that altered NHE9 function can result in attention deficit/hyperactivity disorder or autism, sometimes accompanied by epilepsy (89-92). While many of the mutations have not been investigated in great detail, some appear to lead to a complete loss of function, as in a chromosomal inversion including the 5' end of the NHE9 gene in a family with intellectual disability and impulsivity identified as attention deficit/hyperactivity disorder (89), or a major

promoter mutation and a nonsense mutation in autistic individuals with recent shared ancestry (92). Whether the associations with autism that are not apparent loss-of-function mutations contribute towards neurodevelopmental disruptions remains unclear.

Interestingly, mutations in NHE6 – a closely-related paralog of NHE9 with 58% similarity at the polypeptide sequence level and a similar sub-cellular distribution – have also been associated with neurodevelopmental conditions including such symptoms as intellectual disability, ataxia, and microcephaly (77). Paradoxically, a post-mortem expression analysis in humans indicated that the severity of autism correlated with increased NHE9 expression but decreased NHE6 expression (80). The mechanisms which underlie this distinction, if it is indeed causally related to neurodevelopmental conditions, are intriguing and unclear; how two such related proteins both in sub-cellular localization and ion exchange function can yield such different results is unknown.

Since the mechanisms underlying the relationship between NHE9 function and neurodevelopment, if any, is less certain that that of NHE6, we elected to evaluate NHE9 function and the effects of reported autism-associated mutations. In addition to the seven autism-associated mutations studied here, we identified and constructed a putatively ion exchange-deficient variant of NHE9, identified by homology studies with other members of the NHE family. We focussed our experiments on transferrin in immortalized cell culture as this gave us the greatest capabilities to study the effects of NHE9 and its variants on cargo uptake as well as vesicular pH. NHE9 localizes to early and recycling endosomes (70), and transferrin is trafficked through early endosomes to recycling endosomes when internalized (109). This process has been used to assess the function of both wild-type and autism associated mutant forms (V176I, L236S, S438P) of NHE9 already (93), but we aim to expand the experiments to include not only other autism-associated mutations (P117T, D495N, Q609K) but also a putatively ion exchange deficient variant (D244N). Using an ion exchange deficient variant would allow us to distinguish between the scaffolding and the ion exchange functions of NHE9. In addition, we will make two methodological alterations. First, we will measure transferrin uptake during the linear range of its uptake, rather than at steady state, which we believe is a better indicator of endocytosis, rather than total uptake capacity. Second, we intend to measure pH over multiple time points to

evaluate how NHE9 and the mentioned variants may be contributing to pH regulation and trafficking of transferrin both over the linear range and in the steady state.

From the present study, our results indicate that in an immortalized cell culture system overexpressing NHE9, the mutations do not significantly affect the subcellular distribution of NHE9. Furthermore, we show that while most of the mutations affected transferrin uptake, only two did so significantly: the autism-associated mutation S438P and the putatively ion-exchange deficient variant D244N. Importantly, we found that the enhancement of transferrin endocytosis is not directly related to the pH of transferrin-containing vesicles. Nonetheless, we found that the mutations generally acidified transferrin-containing vesicles relative to wild-type NHE9. These results suggest that NHE9 contributes to neurodevelopment through a complex interaction between altered trafficking and altered ion exchange function.

Materials and Methods

Reagents

All chemical compounds were purchased from Bioshop Canada or Thermo Fisher Scientific, unless otherwise indicated. Restriction endonucleases and VENT® polymerase were purchased from New England Biolabs. Small interfering RNA pools were purchased from GE Healthcare: siGENOME SMARTpool of either negative control #2 (UAAGGCUAUGAAGAGAUAC, AUGUAUUGGCCUGUAUUAG, AUGAACGUGAAUUGCUCAA, UGGUUUACAUGUCGACUAA), NHE6 (GUUCAAAUCUAUUGGAAUC, GAAACCGGCCUUGCUAUGA, GAUGAUGUUUGCUGGUCUU, UAUAAGGGUUGGUGUUGAU) or NHE9 (CAACAUCAAUCCUCAUCAA, GAUAGUUGCUGUUCUCUUC, GAUGUGGAAUGCAUUGUAA, CAACUCUGCUGGUUAAUAU). Bafilomycin A1 was purchased from LC Laboratories. Rabbit polyclonal antibody to NHE9 was generated by injecting rabbits with affinity-purified glutathione S-transferase (GST)-tagged NHE9 residues p.581-645 (a region which is well-conserved between orthologs but not paralogs), collecting serum, and affinity-purifying as described elsewhere (85). Rabbit polyclonal antibody against NHE6 was generated similarly, as described elsewhere (85).

Cell culture

Cells were grown on polystyrene dishes (BD Falcon) in humid air at 37 °C and 5% CO_2. Both HeLa and AP-1 Chinese Hamster Ovary cells lacking plasmalemmal alkali cation/proton exchange activity (29) were maintained in alpha modification of Eagle's minimum essential medium (αMEM) (Invitrogen) at 10% fetal bovine serum (Invitrogen), 1% penicillin/streptomycin (Invitrogen), 25 mM $NaHCO_3$ (pH 7.4), henceforth referred to as serum-supplemented medium. HeLa cells were used until passage 19, and AP-1 cells were used to passage 13. For plating onto glass coverslips, glass coverslips were coated with poly-L-lysine (Sigma) (37 °C 2 h to overnight at 0.1 mg/mL in water, followed by four water washes) for HeLa cell culture, and coated with fibronectin (Sigma) for AP-1 cell culture (37 °C for 2 h or overnight at 4 °C with 3.75 µg/mL fibronectin in phosphate buffered saline [PBS], followed by four PBS washes). For live-cell imaging, cells were transferred to HEPES-buffered (i. e., HCO_3^--free) Dulbecco's modification of minimum essential media (DMEM) lacking phenol red between 12 and 24 h prior to imaging.

Plasmids and molecular cloning

Human NHE9 was cloned from a human brain cDNA library using polymerase chain reaction (PCR) methodology. Further PCR mutagenesis added a hemagglutinin tag (YPYDVPDYAS) to the carboxy terminal tail of NHE9 ($NHE9_{HA}$), and inserting it into the mammalian expression vector pcDNA3.1 (Invitrogen) using the restriction endonucleases *KpnI* and *XbaI*. NHE9 was also inserted into pAc-GFP-N1 (ClonTech) using the restriction endonucleases *KpnI* and *BamHI*, creating a carboxy terminal fusion with green fluorescent protein (GFP). In addition, this vector was further modified by inserting monomeric Cherry fluorescent protein (ChFP) between the sites for *BamHI* and *NotI*, replacing GFP. Mutations in NHE9 were generated by two-step polymerase chain reaction-based mutagenesis and sub-cloned into the same three fusion constructs (i. e., HA, GFP, and ChFP. Amino terminal fusions of small RAB GTPases 4, 5, 7, and 11 were obtained from the laboratory of Prof. Terry Hebert (McGill University).

Plasmid transfection of HeLa cells

Plasmids were transfected into HeLa cells when grown to 10-40% confluence using liposomal-mediated FuGENE6 (Promega) transfection. Transfection mixtures were prepared in

approximately one twelfth of the cell media volume of αMEM, according to manufacturer protocols. One μg of DNA was used per 35-mm plate. For 20-mm wells, as was used in for imaging experiments, 0.5 μg of DNA was transfected. For 60-mm plates used in flow cytometry-based endocytosis assays, 4 μg of DNA was transfected. In brief, for every μg of plasmid DNA, 3 μL of FuGENE6 was first mixed into the serum-free media and allowed to stand for 5 min. After, plasmid DNA was added and the tubes were gently mixed. Following an additional 20 min incubation, transfection mixtures were added to cells. Cells were fed after overnight incubation in normal growth conditions.

Plasmid transfection of AP-1 cells

AP-1 cells were transfected at 20-70% confluence, depending on the experiment. Lipofectamine2000 (Life Technologies) transfection mixtures were prepared in approximately one fifteenth of the cell media volume of serum-free αMEM, according to manufacturer protocols. One μg of DNA was used per 35-mm plate. For 20-mm wells, as was used in for imaging experiments, 0.5 μg of DNA was transfected. Briefly, for every μg of plasmid DNA, 2.5 μL of Lipofectamine2000 was first mixed into the serum-free media and allowed to stand for 5 min. Plasmid DNA was subsequently added and the tubes were gently flicked to mix. After an additional 20 min incubation, transfection mixtures were added to cells bathed in serum-free αMEM for AP-1. Cells were fed after 5 h of incubation in normal growing conditions.

Lysis of Mammalian Cell Cultures and Protein Detection

Cells were washed twice with ice-cold phosphate buffered saline (PBS) pH 7.4 and scraped into immunoprecipitation buffer (PBS, 0.25% sodium deoxycholate, 0.5% Nonidet-P40, and protease inhibitor cocktail [Roche]). After incubating at 4 °C for 30 min, lysates were clarified by centrifuging at 16,100 x *g* for 20 min at 4 °C. Samples were then taken for protein concentration measurement (Biorad DC™ Protein Assay Kit), and for total lysate samples. Laemmli loading buffer (0.1 M Tris pH 6.8, 25% glycerol, 3.7% SDS, 200 mM dithiothreitol [DTT]) was added to all samples for protein separation by 9% acrylamide sodium dodecyl sulfate poly acrylamide gel electrophoresis (SDS-PAGE). Gel contents were transferred onto Immobilon-P (Millipore) membranes, blocked with 5% skim milk PBS, and blotted with the appropriate primary antibodies

(mouse monoclonal anti-HA 1:5000 (Covance), rabbit polyclonal anti-GFP 1:2000 (Life Technologies), or rabbit polyclonal anti-NHE9 1:1000, rabbit polyclonal anti-NHE6 1:3000) in 5% skim milk 0.1% Tween-20 PBS, washed four times with 0.1% Tween-20 PBS, then blotted with either goat anti-mouse IgG constant fragment conjugated to horseradish peroxidase (Jackson ImmunoResearch) at 1:5000 dilution or goat anti-rabbit IgG constant fragment conjugated to horseradish peroxidase (Jackson ImmunoResearch) at 1:10000 dilution. Detection was carried by providing substrate with the ECL™ blotting detection reagents (GE Healthcare), and using traditional film-based exposure and development methods. Developed films were scanned using the "Scan Film" function from HP Solution Center and a HP ScanJet G4050.

Laser-scanning confocal fluorescence microscopy and analysis

Following two washes with PBS, cells were fixed in 4% formaldehyde in PBS pH 7.4 for 20 min. For immunocytochemistry, cells were subsequently washed thrice with PBS and permeabilized for 20 min with 0.1% saponin in PBS pH 7.4. Permeabilized cells were washed then blocked with coverslip staining solution (0.01% saponin, 0.4% glycine, 10% goat serum in PBS) by incubating for 45 min. Primary antibodies were diluted into the same solution and incubated with the cells for 1 h at room temperature or overnight at 4 °C (rabbit polyclonal anti-HA diluted at 1:2000 [Abcam]; 3E10 mouse monoclonal anti-MYC tag diluted at 1:250 [Millipore]; rabbit polyclonal anti-NHE9 diluted at 1:500). After four washes with coverslip staining solution, secondary antibodies were diluted into the same solution and left to bathe the cells for 1 h at room temperature, protected from light (AlexaFluor-conjugated secondary antibodies [Molecular Probes] were diluted at 1:2000, in particular, goat anti-rabbit IgG constant fragment conjugated to either AlexaFluor568 was used in combination with goat anti-mouse IgG constant fragment conjugated to the AlexaFluor488). Cells were washed thrice with PBS and once with water prior to mounting onto glass slides in Aqua Poly/Mount (Polysciences). Slides were imaged after overnight drying at room temperature protected from light. A Carl Zeiss MicroImaging laser-scanning confocal microscope 710 on an Axiovert 200 M and using a plan-Apochromat 63x/1.4 numerical aperture oil objective and ZEN 2011 software were used for image acquisition. Each experiment made use of the same acquisition parameters.

When imaging for subsequent colocalization analysis, in addition to keeping all imaging parameters constant, the distribution of emission intensities was monitored in case of laser power fluctuations and other changes. The following acquisition parameters were used: z-axis images were separated by 0.3 µm, at an x-y sample pixel size of 0.54 µm by 0.54 µm. Images were acquired as an average of two 12-bit linear scans. Only low-to-medium-expressing cells were chosen for acquisition, exhibiting only a minute amount of saturation, if any. Three independent trials with at least three cells were used for quantification. The three-dimensional images were deconvoluted using Huygen's Essential (Scientific Volume Imaging) with manual estimations of the background and maximum intensities as described previously (110). Finally, the images were analyzed by Imaris 7.2 (Bitplane) with manual but consistent thresholding in order to exclude any remaining extraneous signal (110). $_{MYC}$RAB11 staining exhibited low intensities and high background and thus were thresholded differently than $_{GFP}$RAB4, 5, and 7 micrographs to better reflect a slow recycling vesicular distribution. This may have modestly inflated measures of Mander's coincidence coefficients for RAB11, but does not change any conclusions stemming from the micrographs or their analysis. Mander's coincidence coefficients were statistically analyzed first by confirming homogeneity of variances by the Bartlett test (111), then by parametric type II one-way analysis of variance (ANOVA).

Micrographs shown here were adjusted in order to better display results. First, digital offset was removed manually. Next, each channel was scaled separately to display all intensities over the entire bit range, permitting for some saturation.

Small interfering RNA transfection and knockdown assessment

HeLa cells in 6-well plates (BD Falcon) were transfected at 50-75% confluence using Dharmafect1 transfection reagent (GE Healthcare) using manufacturer protocols. In brief, two tubes were prepared for each culture: one tube with 10 µL of 20 µM siGENOME SMARTpool siRNA in siRNA resuspension buffer (GE Healthcare) and 190 µL of serum-free αMEM; the other tube with 5 µL of Dharmafect1 transfection reagent and 195 µL of serum-free αMEM. After 5 min of incubation, tube contents were mixed and allowed to stand for an additional 20 min. Transfection mixtures were subsequently added to 1.6 mL of αMEM with 10% fetal bovine serum and 25 mM $NaHCO_3$

pH 7.4 to bathe the cells. Cells were washed with αMEM with 10% fetal bovine serum and 25 mM $NaHCO_3$ pH 7.4 both overnight and after approximately 48 h, and lysed for protein separation and immunoblotting, or transferrin uptake, after 72 h. Cells were lysed as noted in the section on mammalian cell lysis.

Flow cytometry-based transferrin uptake assay

HeLa cells in 60-mm polystyrene dishes (BD Falcon) were serum-starved 48-hour post-transfection by washing then incubating in 4 mL serum-free αMEM for 2 h in normal growing conditions. Next, transferrin conjugated to AlexaFluor633 (Tfn-Alexa^{633}) (Molecular Probes) at 10 µg/mL in 2.5 mL in serum-free αMEM was loaded onto cells for 10 min in normal growing conditions. Immediately following the allotted time for uptake, cells were washed with 4 mL αMEM 10% FBS 1% penicillin/streptomycin and then incubated in 4 mL of the serum-supplemented αMEM for 1 min in normal growing conditions. Following two 3-mL washes with PBS, cells were incubated with 0.5 mL 10 mg/mL trypsin (Invitrogen) in PBS for 7 min at 37 °C. Cells were resuspended by adding 3.5 mL serum-supplemented αMEM and then centrifuged at 200 x *g* for 5 min. The supernatant was aspirated and the cell pellets were resuspended in 0.5 mL PBS, adding 5 µL 7-aminoactinomycin D (7AAD, purchased from Affymetrix eBioscience) to each tube. A BD LSRII flow cytometer and BD FACSDiva software were used for data acquisition and analysis. For each trial, the following compensation controls were used to optimize acquisition and analysis: non-transfected, GFP-transfected, Tfn-Alexa^{633}-loaded, and 7AAD-stained cells. The following lasers and filters were used: 488-nm laser (488/10-nm filter for side scatter, 695/40-nm filter for 7AAD, 530/30-nm filter for GFP); 633-nm laser (660/20-nm filter for AlexaFluor633). Finally, total cellular Tfn-Alexa^{633} medians were obtained by excluding intensities in this channel which were exhibited by the compensation controls that were not loaded with Tfn-Alexa^{633}. For four independent trials, the median total cellular Tfn-Alexa^{633} fluorescence for 10^4 live, transfected cells were compared relative to all non-transfected cells from the same trial, i. e. from each plate that was from the same batch of processed plates. The relative values from four independent experiments were statistically analysed. The Bartlett test revealed that variances were homogeneous, validating the use of a parametric type II one-way ANOVA for statistical analysis, assuming a normal distribution of median total cellular Tfn-Alexa^{633} fluorescence.

Fluorescence ratiometric imaging analysis for intracellular pH measurements

HeLa cells were grown on poly-L-lysine-coated glass coverslips and transfected approximately 24 h after plating as described in the section on plasmid transfection of HeLa cells. Following overnight incubation with the transfection mixture, the medium was changed to 10% fetal bovine serum-supplemented HEPES-buffered DMEM and the cells were grown for an additional night in 0% CO_2 37 °C humid air.

To load the cells with transferrin, cells were serum-starved with a serum-free HEPES-buffered DMEM wash followed by two 20-min incubations in 0% CO_2 humid air at 37°C. Next, the cells were incubated with fluorescein isothiocyanate-conjugated human transferrin (Tfn_{FITC}) (Molecular Probes) at 1 µg/µL in serum-free HEPES-buffered DMEM for the indicated amount of time in 0% CO_2 humid air at 37 °C. Cells were subsequently washed twice with 10% fetal bovine serum-supplemented HEPES-buffered DMEM, keeping the second wash for a 30 s chase period, to allow for both internalization and unbinding of remaining plasmalemmal Tfn_{FITC}. Following a wash with a modified Ringer's solution (140 mM NaCl, 5 mM KCl, 10 mM HEPES, 10 mM glucose, 1 mM $CaCl_2$, 1 mM $MgCl_2$, pH 7.3) cells were imaged in the same solution at room temperature within two minutes of each time point, and within thirty minutes for pH calibration. A Carl Zeiss MicroImaging AxioObserver Z1 inverted microscope using a plan-Apochromat 63X/1.4 numerical aperture oil immersion objective and equipped with a X-Cite 120Q fluorescence illumination system (Lumen Dynamics Group Inc.) and a Evolve 512 electron multiplying charged-coupled device camera (Photometrics Technology) with MetaFluor software (Molecular Devices) was used for image acquisition and vesicle region of interest selection. Using 440-, 490-, and 570-nm lasers and acquiring with a long-pass 525 nm filter allowed for optimization of both high signal and low channel cross-talk while imaging FITC and ChFP. For each time point and construct, three images were acquired and 20-275 vesicles selected, depending on the time point and the cell. Distributions of pH values were analysed using Origin 7.5 software (OriginLab).

Standard curves for the experiments were also obtained as described elsewhere (112), with some modifications. In brief, cell culture and imaging was carried out in the same way; cells were imaged in potassium-rich buffer (10 mM NaCl, 10 mM glucose, 135 mM KCl, 1 mM $CaCl_2$, 1 mM $MgCl_2$), buffered with MES for pH's under 6.0 or with HEPES for pH's at 6.0 and above, and

pH was adjusted using either HCl or KOH. However, proton concentrations were equilibrated by adding a number of proton ionophores in addition to 10 µM nigericin immediately prior to imaging: 10 µM monensin, 25 µM carbonyl cyanide m-chlorophenyl hydrazine (CCCP). Furthermore, the V-ATPase was inhibited through the addition of 0.4 µM bafilomycin. Cells were washed thrice over eight minutes to allow for proton equilibration prior to imaging. Cells were imaged at pH 4.5, 5.5, 6.0, 6.3, 6.6, 7.2, and 8.3, thrice independently for untransfected HeLa cells, and twice each for ChFP-transfected and $NHE9_{ChFP}$-transfected cells.

Results

An imbalance in NHE9 function has been linked to neurodevelopmental disorders such as attention deficit/hyperactivity disorder (89) and autism (80, 92). Although NHE9 is ubiquitously expressed (70), its expression in the brain has not been examined in detail. Analysis of *in situ* hybridization of NHE9 mRNA of adult mouse brain from the *Allen Developing Mouse Brain Atlas (113)* indicates a relatively high level of expression the cerebral cortex, the hippocampus, and the olfactory bulb (data not shown), the former two being particularly involved in higher-level cognitive processes. Furthermore, NHE9 is expressed during post-natal development in the mouse brain, and colocalizes with α-amino-3-hydroxy-5-methyl-4-isoxazolepropionic acid (AMPA) receptor subunit GRIA1 (also known as GluA1) in mouse organotypic hippocampal cultures (**Figure 1A**). Interestingly, in these cultures, the trafficking of NHE9 and GRIA1 during long-term synaptic plasticity – a process which underlies learning – is correlated (data not shown, manuscript in preparation [Das Gupta, et al.]). Altogether, these results support the importance of NHE9 function in the developing central nervous system.

Some of the autism-associated variants of NHE9 have been functionally investigated (93), but the results remain unconfirmed and three out of six of the associated mutations have not been characterized (**Figure 1B**). As an additional tool, we constructed a putatively ion exchange deficient mutant form (D244N), which we identified by homology studies with other members of the NHE family. As our model, we chose the immortalized cervical cancer cell line HeLa and exogenous overexpression systems to characterize the mutants because of the ease of culturing and manipulating the cells. Moreover, HeLa cells express a minute amount of NHE9 as detected by immunoblotting lysates using a NHE9-specific antibody generated in-house, when compared

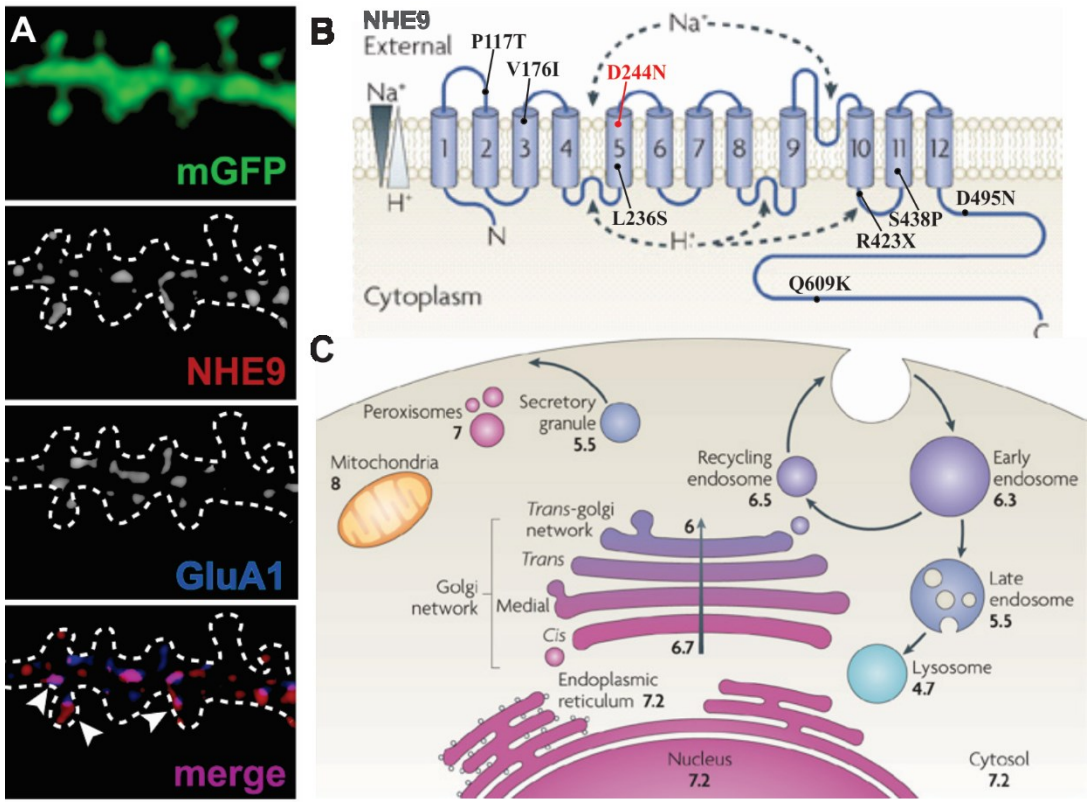

Figure 1: NHE9 expression, localization, and structure. NHE9 is expressed in neurons, as shown by the mouse organotypic hippocampal culture micrographs displayed in panel A. A dendrite from a neuron expressing farnesylated (i. e. membranal) green fluorescent protein (mGFP) by the neuron-specific Thy1 promoter was immunostained for NHE9 and GluA1, which appear in a punctate pattern throughout the dendrite and colocalizes extensively. (B) The structure of NHE9 is thought to be similar to other paralogs of the NHE family, with the mutations used in this study indicated here, schematized using polypeptide sequence alignment and the topological model proposed by Wakabayashi (114). Mutations shown in black have been associated with autism. The mutation in red, D244N, is a putatively ion exchange deficient mutant which we identified by homology. The R423X nonsense mutations did not express and will not be discussed further. (C) In the cell, NHE9 is present in a subset of early and recycling endosomes distinct but overlapping with that of NHE9. Panels B and C are modified from (7).

to other immortalized cell culture lines such as SH-SY5Y human neuroblastoma and human embryonic kidney (HEK293T) cells (**Figure 3A, Supplementary Figure 1**). In order to verify the use of this model for the study of NHE9 function, we sought to more precisely define the sub-cellular localization of NHE9 in HeLa cells. Prior reports and unpublished data from our laboratory indicate that NHE9 is present on a distinct but overlapping pool of early and recycling endosomes with that of NHE6 (70)(**Figure 1C**).

Hence, we analyzed the sub-cellular localization of NHE9 fused to monoclonal Cherry fluorescent protein (ChFP) at the carboxy terminus ($NHE9_{ChFP}$) in relation to a number of small RAB GTPases that are associated with distinct sub-cellular compartments and therefore can serve as convenient molecular markers of those compartments (43)(**Figure 2**). Though there is some overlap with other compartments: RAB4 is a fast recycling and early endosomal marker; RAB5 is an early endosomal marker; RAB7 is a late endosomal marker; and RAB11 is a slow recycling endosomal marker (43). Our micrographs indicate that NHE9 colocalizes most strongly with the slow recycling endosomal marker RAB11, and much less so with the other markers (**Figure 2A**, top and bottom panels). This is reflected by the quantification of colocalization using the Mander's coefficients (**Figure 2B**). The results are similar in AP-1 cells (**Supplemental Figure 2, Supplementary Figure 3A**), a derivative of the Chinese hamster ovary immortalized cell line which lacks plasmalemmal alkali cation/proton exchange activity. Together, these results indicate that in spite of the exogenous overexpression of NHE9, NHE9 retains a distinct sub-cellular localization in HeLa and AP-1 cells, suggesting that the cell models are appropriate for further study.

The localization of proteins often depends on many biochemical interactions and signaling cascades which are in turn dependent on the structure and function of the protein in question. Since neither the autism-associated nor the putatively ion exchange-deficient variants of NHE9 have had their sub-cellular localization quantitatively analyzed to our knowledge, we chose to analyze their localization, using human influenza hemagglutinin peptide (HA) carboxy terminus-tagged fusions of NHE9 (**Figure 3B**), in relation to RAB11 in HeLa cells. Any major shift towards retention in the endoplasmic reticulum or degradation via the lysosomes could have been noted

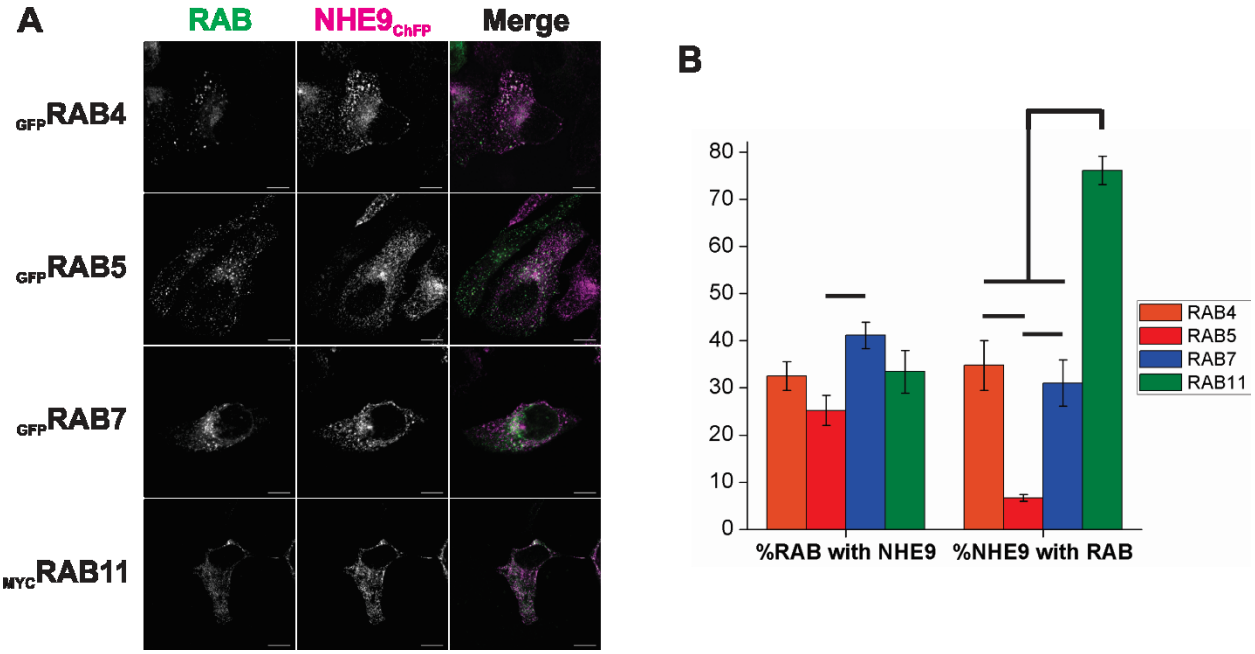

Figure 2: NHE9 is present in early and recycling endosomes in HeLa cells. At least ten micrographs from a total of three independent experiments acquired with identical imaging parameters were used for colocalization analysis. Imaging the green channel was adjusted identically for all RAB11 immunostainings, as the signal was considerably weaker. A representative sample of micrographs is shown in panel A. MYC tag secondary immunostaining was done with goat anti-mouse IgG conjugated to AlexaFluor488. After deconvolution and manual thresholding, Mander's coefficients of coincidence were obtained using Imaris 7.0 software, which recapitulates our qualitative findings (B). NHE9 signal coincides most with RAB11, a slow recycling endosomal marker. Scale bar represents 10 µm. Error bars represent standard error of the mean. Significant differences indicate $p < 0.05$ by type II one-factor ANOVA.

as a reduction in the Mander's coefficients of NHE9 with RAB11. Micrographs of $NHE9_{HA}$ variants and $_{MYC}$RAB11 immunostainings indicate that none of the studied mutations significantly affect the sub-cellular localization (**Figure 3C**). This is reflected by Mander's coefficient quantifications of co-incidence (**Figure 3D**). This experiment was reproduced in AP-1 cells with similar results. However, in these cells there are some statistically significant differences between the Mander's coefficients, but none of them were consistent enough among the NHE9 variants to warrant further investigation (**Supplementary Figure 3**).

Though mutations in NHE9 do not affect its sub-cellular localization significantly when overexpressed in HeLa cells, these observations did not discriminate between any potential states of flux, such as endocytosis. To this end, we first examined the localization of NHE9, in a carboxy terminal fusion to enhanced green fluorescent protein (GFP), with two archetypal endocytic cargos: transferrin and epidermal growth factor (**Figure 4A**). Transferrin is trafficked through early and sorting endosomes to recycling endosomes (109), and at steady-state (i. e. following 40 minutes of internalization), colocalizes extensively with NHE9 (**Figure 4A**, top panels). Conversely, epidermal growth factor, which also traffics through early and sorting endosomes, but then is further sorted to late endosomes for eventual degradation in lysosomes (115), does not colocalize with NHE9 even at early time points (i. e., following 10 minutes of internalization) (**Figure 4A**, bottom panels). The reason for the differences between internalization times is due in part to the targeting of the two cargo: epidermal growth factor is degraded and with limited quantities of fluorophore-conjugated epidermal growth factor, longer internalization times would lead to losses in fluorescence; transferrin is recycled and can continue to accumulate in vesicles without major losses to degradation.

Since NHE9 and transferrin are trafficked to the same compartments, we chose to measure transferrin uptake in HeLa cells using a flow-cytometry based approach in order to evaluate the trafficking function of NHE9 and its variants (**Figure 4B**). Forty-eight hours after transfecting GFP or $NHE9_{GFP}$ variants, total cellular Tfn-$Alexa^{633}$ fluorescence was measured in 7-aminoactinomycin D (7AAD)-negative (i. e., live cells (116)) and GFP-positive cells after ten minutes of internalization, normalizing to the uptake of non-transfected cells from the same trial (**Figure 4D**). We chose a ten-minute time point because previous experiments with NHE6 indicate

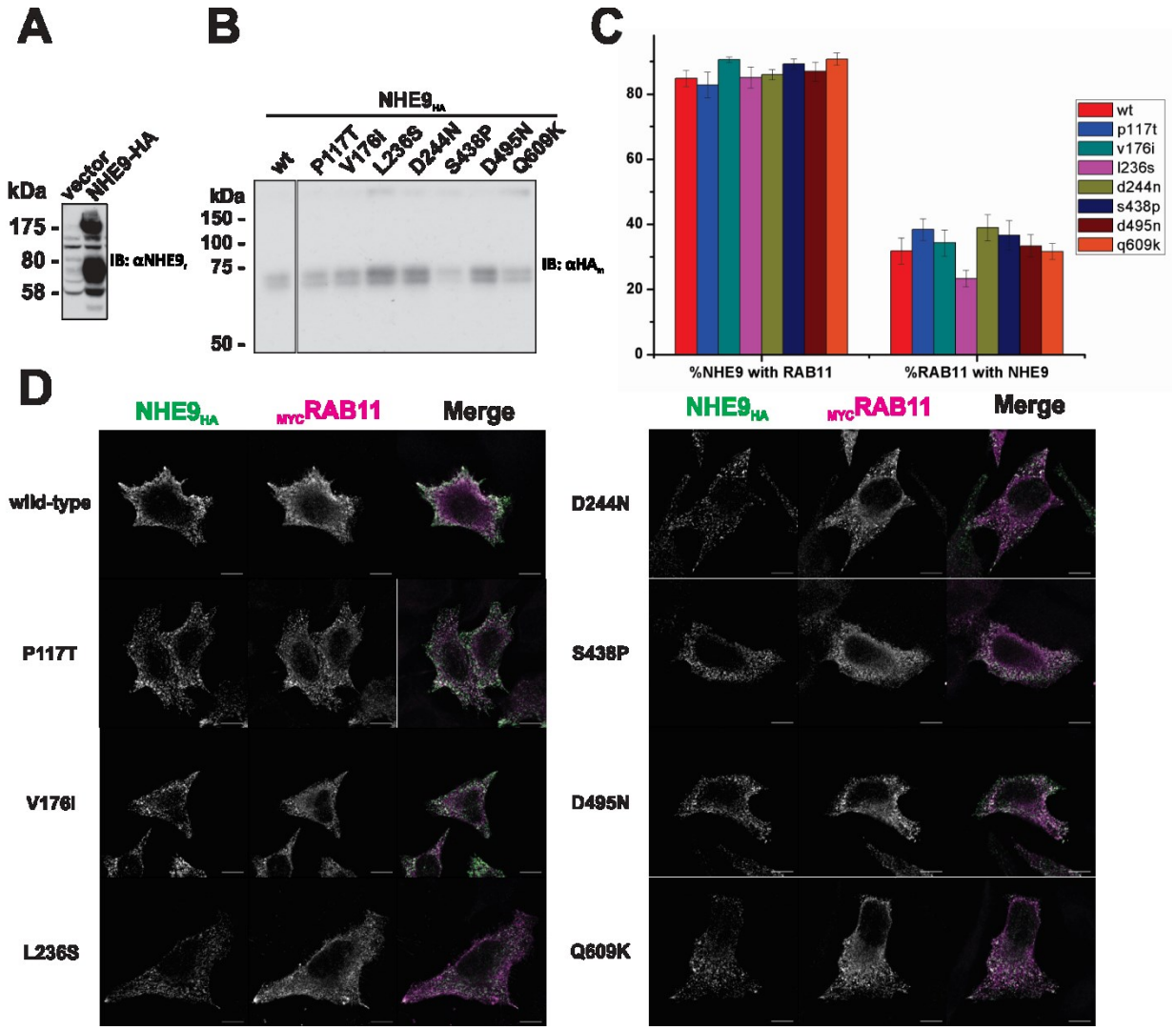

Figure 3: Autism-associated variants do not affect the sub-cellular localization of NHE9 in HeLa cells. HeLa cells express a minute amount of NHE9, visible only after heavy overexposure of immunoblots (A). Autism-associated variants and the putatively ion exchange variant p.D244N in carboxy terminal HA-tagged forms were expressed in HeLa cells and lysed to assess expression (B). Any variation in signal strength was not found consistently and thus did not warrant further investigation. None of the variants' sub-cellular localization relative to RAB11 differed significantly (C), as indicated by Mander's coefficients of coincidence. This quantification recapitulates our qualitative assessment of the micrographs, at least ten of which were used for analysis from three separate experiments (D). Scale bar represents 10 µm. Error bars represent standard error of the mean. Significant differences indicate $p < 0.05$ by type II one-factor ANOVA.

that this time point is well within the linear range of endocytosis and introduces less variation than shorter time points (data not shown). Overexpressing wild-type $NHE9_{GFP}$ enhances transferrin uptake to more than 150% of GFP-expressing cells. Furthermore, variants P117T and V176I did not affect transferrin endocytosis. Though variants L236S, D495N, and Q609K showed reduced enhancement of transferrin endocytosis, these differences were not significantly different from wild-type. However, both the putatively ion-exchange deficient D244N and the autism-associated S438P presented significant defects in the enhancement of transferrin endocytosis; the total cellular transferrin fluorescence was not significantly different from that of GFP-expressing cells and was significantly different from $NHE9_{GFP}$-expressing cells.

HeLa cells contain some endogenous NHE9, overexpression of which leads to an enhancement of transferrin endocytosis. However, it remains unknown if this small amount of NHE9 plays a significant role in endocytosis or trafficking of transferrin in these cells. Moreover, since NHE6 does express relatively strongly in HeLa cells and also enhances transferrin uptake, it is unknown if the two cooperate in transferrin uptake. Hence, we used a short interfering RNA (siRNA) approach to eliminate NHE6 and/or NHE9 with the flow cytometry-based transferrin endocytosis assay (**Figure 5A**). As expected, knocking down NHE6 decreased transferrin uptake (75), but knocking down NHE9 had no discernible effect (**Figure 5B**), though neither result was statistically significant. Furthermore, by concomitantly knocking down NHE6 and NHE9, we observed no additional decrease in transferrin uptake (**Figure 5C**). Thus, while NHE9 overexpression significantly enhances transferrin uptake in these cells, endogenous NHE9 levels are too low to make an impact on this process.

To determine whether the ion exchange function of NHE9 was affected by the mutations we measured the pH of transferrin- and NHE9- containing vesicles using wide-field fluorescence ratiometric imaging analysis (**Figure 6**). We manually picked vesicles which contained not only $NHE9_{ChFP}$ signals (**Figure 6A**) but also Tfn_{FITC} signal. Tfn_{FITC} was excited with a wavelength of 490 nm followed by 440 nm, and the ratio obtained was converted to a pH value using calibrations which were done thrice independently for non-transfected cells and twice independently each for ChFP-expressing cells and $NHE9_{ChFP}$-expressing cells (**Figure 6B**). We observed that just transfecting cells with ChFP decreased transferrin luminal pH (**Figure 6C, Supplementary Figure**

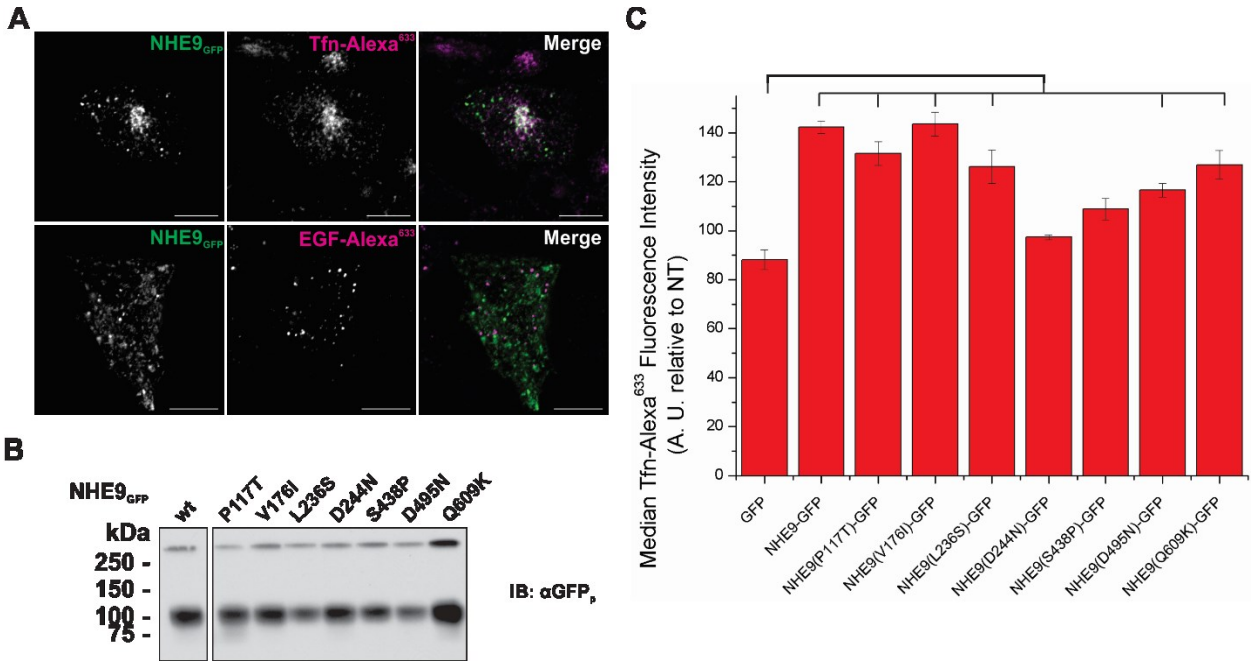

Figure 4: NHE9 enhances transferrin uptake. In HeLa cells, NHE9 colocalizes with the archetypal recycling endosome cargo transferrin (Tfn), and does not colocalize with the archetypal cargo which traffics towards the degradative lysosomes, epidermal growth factor (EGF) (A). $NHE9_{GFP}$ variants were transfected into HeLa cells to assess that expression was not perturbed (B). A flow cytometry-based transferrin endocytosis assay indicated that $NHE9_{GFP}$ enhances transferrin uptake to about 1.5X that of cells expressing GFP-alone (C). Of the autism-associated variants, only the S438P variant was not significantly different from control, in addition to the putative ion exchange deficient D244N variant. However, most other mutations exhibited some decreased enhancement of transferrin uptake. Scale bars represent 10 µm. Error bars represent standard error of the mean. Significant differences are $p < 0.05$ by type II one-factor ANOVA.

4). This effect may be related to the decreased transferrin uptake of GFP-expressing cells, relative to non-transfected cells (about 85%) (**Figure 4C**). Compared to ChFP-expressing cells, NHE9 tended to alkalinize vesicular pH, as expected. However, the effects of the mutations on the pH of these vesicles did not always correspond to the enhancement of transferrin uptake. Nonetheless, for most of the variants, specifically V176I, L236S, S438P, D495N, Q609K, the decreased alkalinisation corresponds to the diminished transferrin uptake. On a different note, the relative pH values among the variants remained largely consistent over the entire time course, from 2.5, 10, and 40 min (**Supplementary Figure 4**), suggesting that throughout the trafficking processes measured by this experiment, NHE9 tends to alkalinise vesicles.

Discussion

The development of the central nervous system is determined by a multitude of signaling pathways that depend on the appropriate trafficking of signaling molecules (102, 103, 108). Trafficking molecules can be affected by the lumenal pH, and can influence how receptors traffic or whether ligands remain attached to their receptors if internalized, for instance (48, 56). NHE9 is one such element that may contribute to neurodevelopment by impacting vesicular trafficking and pH regulation. Signaling molecules may bind NHE9 to alter its trafficking or its alkali cation/proton exchange activity. In moving protons, NHE9 can contribute to vesicular pH, which in turn may have biochemical effects on other signaling molecules. Additionally, NHE9 itself may act as a scaffold for further signals or trafficking processes; the carboxy terminal tail is a long cytoplasmic polypeptide chain without a prominent secondary structure (23).

We studied the function of NHE9 and a number of variants found in autistic individuals to gain insight on the role of NHE9 in the trafficking events which may influence neurodevelopment. Only a subset of these mutations have previously been studied – V176I, L236S, and S438P – and for those, a complete loss of function was found in both the enhancement of transferrin and glutamate endocytosis, as well as in vesicular alkalinisation (93). Importantly, the other mutations have not been studied to our knowledge and we extended our experiments to include a putatively ion-exchange deficient variant, D244N. Like the previous study, we used transferrin as an archetypal recycling endosome cargo to measure the effects of NHE9 on trafficking and

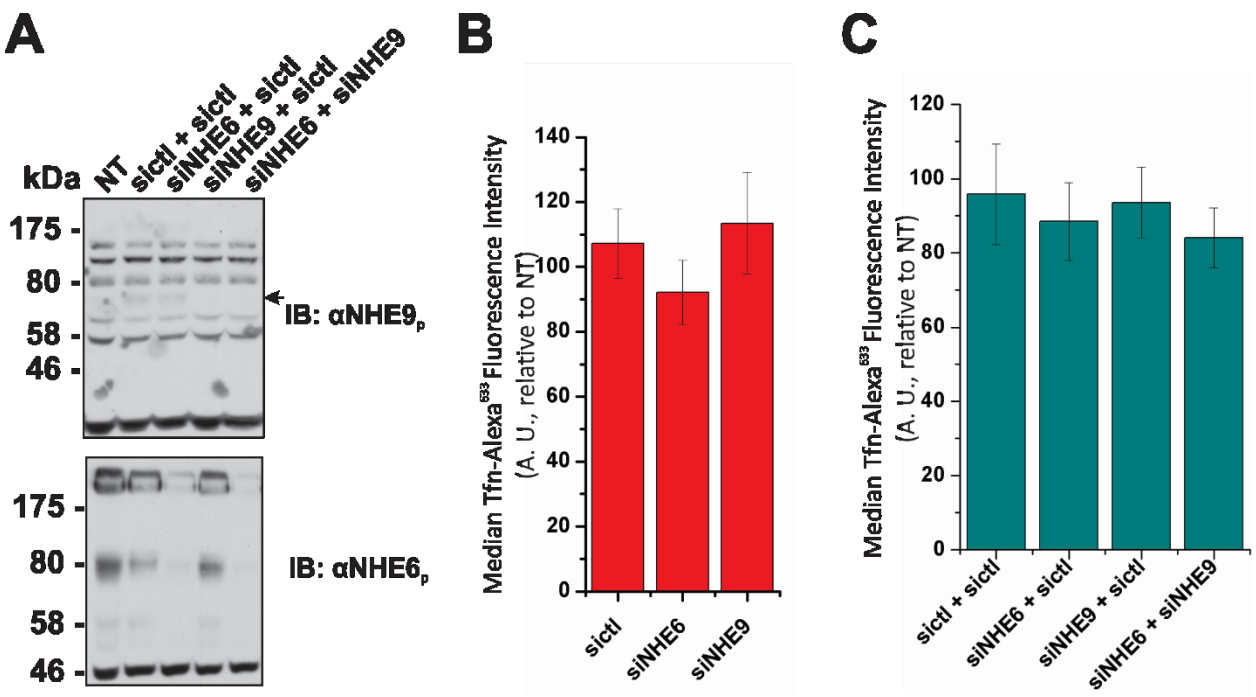

Figure 5: Endogenous NHE6 and NHE9 do not collaborate in transferrin uptake in HeLa cells. RNA interference was confirmed at the protein level by immunoblotting for endogenous NHE6 and NHE9 (A). The levels of NHE9 are very low in HeLa cells and require significant over-exposure to visualize. Using a small interfering RNA approach we were able to strongly reduce NHE6 and/or NHE9. However, our cultures were somewhat inconsistent in transferrin uptake at 5 min and we did not find that our knockdowns had significant effects on transferrin uptake in this time frame (B, C). However, knocking down NHE6 did tend to decrease transferrin uptake (B, C). Conversely, knocking down NHE9 did not affect transferrin uptake significantly, whether NHE6 was present or not (B, C). This could be explained by the low endogenous levels of NHE9; HeLa cells do not utilize NHE9 for transferrin uptake to a significant extent. Error bars represent standard error of the mean. A type II one-factor ANOVA was used for statistical analysis, using $p < 0.05$ as significant values.

vesicular pH regulation. In our study, we used both HeLa and AP-1 cell lines, which contain a minute amount of NHE9, which should better isolate any effects of NHE9 on cellular physiology.

In our investigation, we showed that in a heterologous system of overexpression, none of the variants affected the sub-cellular localization of NHE9 in either HeLa or AP-1 cells. We also confirmed that NHE9 enhanced transferrin uptake in HeLa cells, but we found that most of the mutations did not significantly perturb this function, with the exception of D244N, the putative ion exchange-deficient variant, and S438P, an autism-associated variant. This is in contrast with previous studies that showed that the autism-associated V176I, L236S, and S438P variants all completely precluded the enhancement of transferrin uptake (93, 94). Interestingly, we found that at steady state, NHE9 did alkalinize vesicles and that this effect was diminished by the mutations in a manner that largely corresponded with the effects on the enhancement of transferrin uptake. Paradoxically, the putatively ion exchange deficient D244N variant which indicated almost no enhancement of transferrin uptake also indicated more alkaline transferrin-containing vesicles. Moreover, cells overexpressing P117T exhibited acidic transferrin-containing vesicles while transferrin endocytosis was not significantly affected. While all the other variants passed through a lower pH compartment, possibly the early endosomes, prior to reaching a more alkaline steady-state pH, when D244N was expressed transferrin-containing vesicles remained relatively alkaline. Hence, one potential explanation of seeming lack of acidification of vesicular pH in HeLa cells expressing the D244N variant of NHE9 is that transferrin is not being effectively trafficked to early endosomes, which may also explain why the capacity for transferrin endocytosis was lesser in these cells. However, the molecular and cellular mechanisms underlying this result are obscure.

Our use of transferrin does not serve to confirm causality of NHE9's association with autism, epilepsy, and attention-deficit hyperactivity disorder. However, it does provide us with an important tool to evaluate NHE9 function and a consistent method to compare all nine of the variants studied here. NHE9 colocalizes with transferrin to a great extent at steady state, after 40 min of transferrin uptake. Like NHE6, we found that the structure and function of NHE9 is important in transferrin uptake; overexpression of either NHE6 or NHE9 greatly enhances uptake. One interesting means to widen our knowledge of cellular trafficking and endocytosis would be

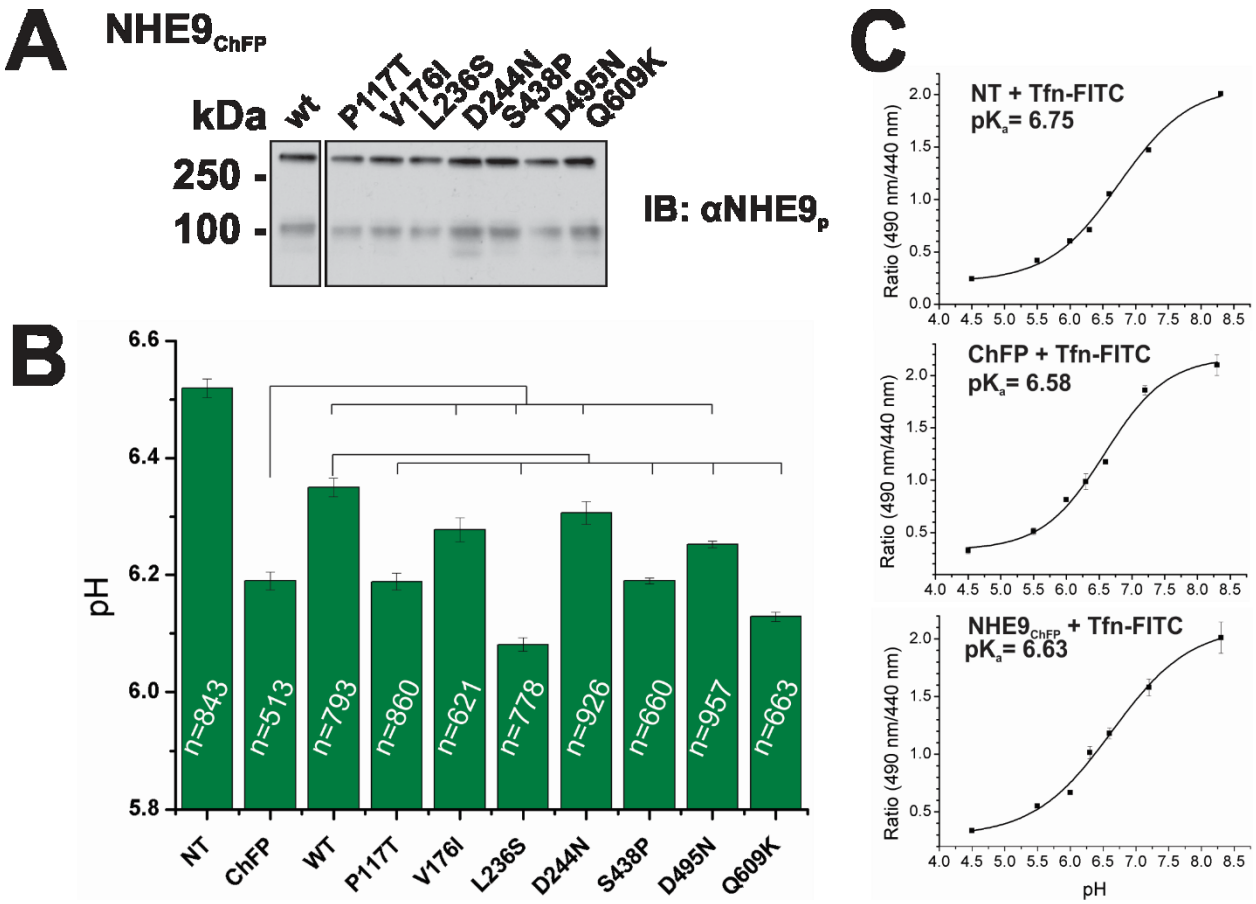

Figure 6: NHE9 contributes to the pH regulation of transferrin-containing vesicles. We used fluorescein isothiocyanate-conjugated transferrin for ratiometric imaging analysis in HeLa cells, and chose ChFP as a fusion to identify transfected cells and NHE9-containing vesicles. The expression of ChFP-fused constructs indicated that proteins were produced as expected (A). Just transfecting ChFP lowered the pH of transferrin-containing vesicles, which was alkalinized when wild-type NHE9 was expressed (B). For most NHE9 variants studied here, the decrease in alkalinisation corresponded somewhat with the effects on transferrin uptake. The major exception is the putatively ion-exchange deficient variant D244N, for which pH remained alkaline (see Supplemental Figure 4) Calibration curves for untransfected, ChFP-transfected, and $NHE9_{ChFP}$-transfected cells are shown in panel C, which were obtained by incubating cells at the shown pH values with 10 µM nigericin, 10 µM monensin, 25 µM carbonyl cyanide m-chlorophenyl hydrazine, 0.4 µm bafilomycin and fitting ratios to a sigmoidal curve according to a modified Henderson-Hasselbach equation (112). Significant values have $p < 0.05$. Error bars represent standard error of the mean. For the pH bar graph, a type II one-way ANOVA was used.

to repeat our flow cytometry-based endocytosis assay with cargo which colocalizes minimally with NHE9. Here, we could distinguish how much of the effects of NHE9 are due to its effects at the trafficking vesicles in question, and how much are due to other effects relating to bulk vesicular trafficking.

A technical limitation of our intravesicular pH measurement stems from signal leak from filters. Despite some effort, we cannot rule out that our ChFP signals impacted our pH measurements unpredictably. We used cells whose ChFP signal did not saturate, at intensities which we empirically determined to have infinitesimal or indistinguishable effects in the 490 nm channel (data not shown). However, high ChFP signal did visibly leak into the 490 nm channel. This was easily visualized in the ChFP-expressing cells because of the cytoplasmic distribution of the fluorescence, but the leak was difficult to assess in $NHE9_{ChFP}$-expressing cells, as we expected almost every region with $NHE9_{ChFP}$ signal to also contain Tfn_{FITC} signal. Although calibration curves should take into account any background fluorescence emission, the use of a particularly fluorescent molecule which can in some cases leak into other channels, such as ChFP, may confound the results. During calibration, the pH is equilibrated throughout the cell using ionophores, in which case ChFP – alone or fused to a protein – would be immersed in the calibration pH. However, the physicochemical consequences of the pH in which transferrin is bathed (intravesicular rather than cytoplasmic) would not be recapitulated when imaging cells which are not treated with proton ionophores. Hence, our measurements of pH in cells expressing ChFP and fusions thereof have less reliability because the calibration does not faithfully control for physicochemical variation of ChFP due to pH. This argument could be extend to background fluorescence, but its effects are considered negligible. Overall, we maintain that we can compare all the results which contained ChFP signal but we are less confident in comparing these results to cells which were not transfected.

Studying the effects of NHE9 on transferrin uptake may not provide direct insights on the role of NHE9 in neurodevelopment. However, this study does provide a means to measure the function of NHE9. Unfortunately, without more detailed molecular dissection we cannot be certain whether these effects are related to the ion exchange function of NHE9, a scaffolding role, or perhaps a combination of the two. Nevertheless, we showed that a putatively ion

exchange-deficient isoform is indeed likely to be ion-exchange deficient, and that the ion exchange function is related to the facilitation of transferrin trafficking. The information on the function of NHE9 and its variants drawn from this work should allow one to extend these studies to trafficking in neurodevelopment.

CHAPTER 2

Juxta-membranal cytoplasmic tail of (Na^+, K^+)/H^+ exchanger NHE9 interacts with PLD3

Mark Jacunski, Mylene Lessard, Mica Das Gupta, John Orlowski

In the first chapter we studied how NHE9 might influence trafficking in the cell using the archetypal recycling endosome cargo transferrin. Using techniques involving this cargo, we were also able to assess how autism-associated variants of NHE9 may affect these functions in trafficking. We found that transferrin vesicle trafficking is not directly related to the luminal pH of those vesicles. NHE9 seems to play roles in both the acidification and the alkalinisation of vesicles to enhance transferrin uptake. In an effort to begin to extend these insights into the context of neurodevelopment, we sought to find protein interacting partners of NHE9 and to characterize how, when, and why such an interactions may be important to cellular physiology.

Introduction

Alkali cation/proton exchanger isoform 9 (NHE9, also known as SLC9A9) is widely-expressed and is among the most recently-discovered NHE family members (89). Much of our knowledge of NHE9 comes from genetic and expression analyses, which have associated imbalances in NHE9 function to neurodevelopmental conditions, including autism (80, 92) and attention deficit hyperactivity disorder (89, 90). An early, broad study indicated that NHE9 was present in recycling endosomes and implicated it in luminal pH regulation in that compartment (70). The recycling endosomes are vesicles which are involved in receiving cargo from early vesicles, the Golgi apparatus, or the plasma membrane, sequestering them or trafficking them elsewhere, all while potentially affecting the biochemical interactions that the cargo makes (43, 108). By altering the pH, or by taking part in these interactions itself, NHE9 may play a central role in cargo trafficking and signaling cascades that are crucial to neurodevelopment. However, the precise mechanisms underlying any associations with neurodevelopmental conditions remain unclear.

In an effort to uncover the role of NHE9 in cellular physiology, our group has shown that NHE9 overexpression can enhance transferrin endocytosis and regulate the pH of transferrin-containing vesicles in immortalized cells (manuscript in preparation). Similarly, in an earlier study the group of Rajini Rao found that NHE9 has the same function in mouse primary astrocytes, in addition to increasing glutamate uptake (93). Moreover, this group found that NHE9 increased proliferation and migration in glioblastoma cells, possibly mediated in part by epidermal growth factor signaling (94). However, these investigations neither addressed the molecular mechanisms underlying the functions of NHE9, nor did they clarify how imbalances in NHE9 seem to only affect neurodevelopment, despite its widespread expression. Indeed, while astrocytes are an important component of neurodevelopment (102) and glutamate uptake is a necessary phenomenon in synapse function (117), these studies did not shed light on the roles of NHE9 in neurons during neurodevelopment and neuron function.

To this end, we screened a human brain cDNA library for protein-protein interactions with the cytoplasmic carboxy terminal tail of NHE9. Among twenty-six putative interacting partners,

phospholipase D isoform 3 (PLD3) stood out due to its neuronal expression pattern and some implications in neurogenic differentiation, as well as trafficking and signaling events in general (100). The phospholipase D family is canonically involved in the degradation of phosphatidylcholine to choline and phosphatidic acid (118, 119). The precise mechanisms of the enzymes' influence on signaling events remains uncertain, though evidence suggest that phosphatidic acid can facilitate membrane fission events by appropriately bending the lipid bilayer, while also interacting with proteins to exert changes on signaling (118). Interestingly, only PLD1 and PLD2 have been shown to possess this canonical activity, while the other isoforms, including PLD3, seem not to (120). Nonetheless, PLD3 contains the appropriate catalytic HKD domains without any evident perturbations (100). Moreover, the viral proteins with which PLD3 shares the greatest similarity seem to be able to exert influence over trafficking and signaling independently of the canonical enzymatic activity (121).

The most definitive investigation of PLD3 function was conducted in the context of myogenic differentiation (100). PLD3 expression rises during C2C12 murine myoblast myotube formation and facilitates its progression (100). Moreover, stressing the endoplasmic reticulum – a phenomenon often found in cellular differentiation – increases the expression of PLD3, possibly to facilitate and quicken the process (100). Whether this putative function also occurs in neurons remains unclear despite indications that PLD3 may also be involved in neurogenic differentiation and neuron function (99, 100).

In our investigation, we found that PLD3 binds most strongly to residues of the cytoplasmic carboxy terminal tail of NHE9 close to its emergence from the lipid bilayer. However, qualitative colocalization analysis by laser scanning confocal microscopy did not indicate that the two protein resided in the same compartments, either in HEK293T cells or in SH-SY5Y neuroblastoma cells. Nevertheless, we believe the interaction to be relatively specific: we found that PLD3 does not immunoprecipitate NHE6, which shares 58% similarity with NHE9 at the level of the polypeptide sequence throughout the protein, and also shares great similarity in the putative binding domain in the carboxy terminal tail. Additionally, we found that another non-canonical member of the PLD family which shares a similar sub-cellular distribution, PLD4,

precipitates similarly with the NHE paralogs used. Hence, the interaction between NHE9 and PLD3 warrants greater investigation.

Materials and Methods

Reagents

All chemical compounds were purchased from Bioshop Canada or Thermo Fisher Scientific, unless otherwise indicated. Restriction endonucleases and VENT polymerase were purchased from New England Biolabs.

Yeast two-hybrid screening

Plasmids used in yeast two-hybrid screening were obtained with the Matchmaker Gold Yeast Two-Hybrid System (ClonTech). A human brain cDNA library was cloned in yeast expression vector pACT2 by the manufacturer. NHE9 carboxy-terminal tail (CTT) (p.482-645) was cloned in yeast expression vector pAS2-1 between EcoRI and BamHI restriction sites by engineering using polymerase chain reaction (PCR). Insertion of cDNA sequences resulted in the generation of a bait fusion protein GAL4 p.1-147 DNA-binding domain (DBD) and NHE9 CTT (GAL4DBD-NHE9CTT) and prey fusion proteins comprising the GAL4 p.768-881 transcription-activating domain (TAD) and a cDNA from a human brain library (GAL4TAD-Prey).

The bait which was used to screen an estimated $1.82*10^7$ independent clones was a fusion between GAL4 p.1-147 DBD and NHE9 p.482-645 CTT cloned in pAS2-1 vector which also expresses TRP1 gene, producing a key enzyme for *de novo* tryptophan synthesis. The prey fusions with GAL4 p.768-881 TAD cloned in pACT2 vector which also expressed the LEU2 gene, producing an enzyme necessary for *de novo* leucine synthesis. The plasmids were co-transformed into *Saccharomyces cerevisiae* strain AH109 (MATa, trp1-901, leu2-3, 112, ura3-52, his3-200, gal4Δ, gal80Δ, LYS2::$GAL1_{UAS}$-$GAL1_{TATA}$-HIS3, $GAL2_{UAS}$-$GAL2_{TATA}$-ADE2, ura3::$MEL1_{UAS}$-$MEL1_{TATA}$-lacZ) using the lithium acetate method (122). As a negative control for the lacZ expression assay – to ensure that bait fusion protein could not interact with GAL4 TAD and that prey fusion proteins could not interact with GAL4 DBD, and that neither fusion could induce the expression of lacZ alone – each fusion protein was transformed alone with the corresponding portion of GAL4. Colonies from the negative control assay remained white when in the presence of X-Gal (5-

bromo-4-chloro-3-indolyl-β-galacto-pyranoside), a substance which generates blue-green metabolites upon β-galactosidase catalysis – β-galactosidase being the product of lacZ. This indicates that unwanted cross-reactivity and reporter activation did not occur. The following technical controls were generated from AH109 yeast cells for the β-galactosidase reporter assay: yeast transformed with pCL1, which encodes wild-type GAL4 and serves as a positive control; yeast transformed with pTD1-1, which encodes GAL4 DBD fused with SV40 large T-antigen p.84-708, and pVA3, which encodes GAL4 TAD fused with p53 p.72-390, which also serves as a positive control as those fragments of SV40 large T-antigen and p53 have been shown to interact (123); yeast transformed with pTD1-1 and pLAM5'-1 which encodes a GAL4 TAD fused with lamin C p.66-230 and serves as a negative control. Positive transformants were grown on synthetic dropout (SD) selection media (SD/-Leu/-Trp, 6.7 g/L yeast nitrogen base, 20 g/L glucose) at 30 °C. Reconstituted GAL4 binds to promoter regions of ADE2 and HIS3 – required for *de novo* adenine and histidine synthesis, respectively – and promotes their expression. These genes serve as reporters for interaction, in addition to lacZ. To screen, transformants were grown on synthetic dropout selection media (SD/-Ade/-His/-Leu/-Trp) at 30 °C and tested for β-galactosidase activity by colony lift-filter assay.

Colony lift-filter assay involves transferring yeast colonies to a filter paper by pressing filter paper into yeast colonies growing on media. Filter papers with colonies are flash-frozen in liquid nitrogen for 10 seconds, and allowed to thaw. Following thawing, they are placed on filter papers soaked in X-Gal Z-buffer pH 7.0 (33.4 mg/ 100mL X-Gal, 0.27% β-mercaptoethanol, 1.61 g/100 mL Na_2HPO4, 0.55 g/100 mL NaH_2PO4, 75 mg/100 mL KCl, 25 mg/100 mL MgS). Positive clones which were strongly coloured blue-green before negative controls, i. e. pTD1+pLAM5'-1-transformed yeast, were restreaked and the process repeated until all resulting colonies tested positive for β-galactosidase activity.

Following the above, plasmids were isolated from three separate positive colonies as identified by the colony lift-filter assay, and inserts were sequenced. Seventy-nine unique sequences were identified from about 250 clones. Using the Basic Local Alignment Sequence Tool (National Center for Biotechnology Information), ClustalW2 (European Biotechnology Institute)

(124), and VectorNTi® (Life Technologies), sequences were aligned with known full-length cDNAs and verified to be in frame in the coding sequence.

Cell culture

Cells were grown on polystyrene plates (BD Falcon) in humid air at 37 °C and 5% CO_2. HEK293T cells were maintained in alpha modification of Eagle's minimum essential (Invitrogen) at 10% fetal bovine serum (Invitrogen) and 1% penicillin/streptomycin (Invitrogen). SH-SY5Y human neuroblastoma cells were maintained in Dulbecco's Modified Eagle's Medium and nutrient mixture F-12 mixed in a 1:1 ratio (DMEM/F12) (Gibco) with an additional 10% fetal bovine serum. HEK293T were used until passage 19 and SH-SY5Y cells were used until passage 16. For plating onto glass coverslips, glass coverslips were coated with fibronectin (Sigma) (37 °C for 2 h or overnight at 4 °C with 375 µg/mL fibronectin in phosphate buffered saline [PBS], followed by four PBS washes). For live cell imaging, cells were transferred to HEPES-buffered (i. e., CO_2 independent) DMEM between 12 and 24 h prior to imaging.

Plasmids and molecular cloning

Human NHE9 was cloned out of a human brain cDNA library and further polymerase chain reaction added a hemagglutinin tag (YPTSCPSYAS) to the carboxy terminal tail of NHE9, and inserting it into mammalian expression vector pcDNA3.1 (Invitrogen) using the restriction endonucleases *KpnI* and *XbaI*. Human PLD3 was received from Michael Frohman (Stony Brook University), subcloned with a carboxy terminal fusion with a FLAG epitope (DYKDDDDK), inserted into pcDNA3.1 between *XbaI* and *BamHI*. Human PLD4 was also received from Michael Frohman, but was kept as an insert in a pcDNA3-His-MYC vector, which conferred a carboxy terminal fusion of PLD4 with six consecutive His codons and a MYC epitope (EQKLISEEDL). Mutants were generated by two-step polymerase chain reaction-based mutagenesis and sub-cloned to the same three fusions: HA, GFP, and ChFP for NHE9 and FLAG for PLD3.

Plasmid transfection of HEK293T cells

Plasmids were transfected into HEK293T cells using liposomal-mediated FuGENE6 (Promega) transfection when grown to 10-20% confluence in 10-cm dishes. Transfection mixtures were prepared in approximately one twelfth of the cell media volume of αMEM, according to

manufacturer protocols. For immunoprecipitation experiments involving PLD3, a total of 8 µg of DNA was transfected, 3 µg of pcDNA3-PLD3-FLAG, and a total of 5 µg of either pcDNA3 alone, or in a mixture with plasmids expressing the NHE paralogs used in this study, so as to equalize the expression between the paralogs. For the immunoprecipitation of PLD4, 3 µg each of PLD4 and either pcDNA3 or NHE-containing plasmid were used, without adjusting for expression. For 20-mm wells, as were used for imaging, 0.5 µg of each construct were used. In brief, for every microgram of plasmid DNA, 3 µL of FuGENE6 was first mixed into the serum-free media and allowed to stand for 5 min. After, plasmid DNA was added and the tubes were gently flicked to mix. Following an additional 20 min incubation, transfection mixtures were added to cells. Cells were fed after overnight incubation in normal growing conditions.

Plasmid transfection of SH-SY5Y cells

SH-SY5Y cells were transfected when at 20-70% confluence, depending on the experiment. Lipofectamine2000 (Life Technologies) transfection mixtures were prepared in approximately one fifteenth of the cell media volume of OptiMEM (Gibco) for SH-SY5Y cells, according to manufacturer protocols. For 20-mm wells, 0.5 µg of each construct were used. Briefly, for every microgram of plasmid DNA, 2.5 µL of Lipofectamine2000 was first mixed into the serum-free media and allowed to stand for 5 min. Plasmid DNA was subsequently added and the tubes were gently flicked to mix. After an additional 20 min incubation, transfection mixtures were added to cells bathed in OptiMEM. Cells were fed after 5 h of incubation in normal growing conditions.

Lysis of Mammalian Cell Cultures and Protein Detection

Cells were washed twice with ice-cold phosphate buffered saline (PBS) pH 7.4 and scraped into immunoprecipitation buffer (PBS, 0.25% sodium deoxycholate, 0.5% Nonidet-P40, and protease inhibitor cocktail [Roche]). After incubating at 4 °C for 30 min, lysates were clarified by centrifuging at 16,100 x *g* for 20 min at 4 °C. Samples were then taken for protein concentration measurement (Biorad DC™ Protein Assay Kit), and for total lysate samples. Laemmli loading buffer (0.1 M Tris pH 6.8, 25% glycerol, 3.7% SDS, 100 mM dithiothreitol [DTT]) was added to all samples for protein separation (total lysates and beads), for which 9% acrylamide sodium dodecyl sulfate poly acrylamide gel electrophoresis (SDS-PAGE) was used. Protein were transferred onto

Immobilon-P (Millipore) membranes, blocked with 5% skim milk PBS, and blotted with the appropriate primary antibodies (mouse monoclonal anti-HA 1:5000 [Covance], M2 mouse monoclonal anti-FLAG 1:5000 [Sigma]) in 5% skim milk 0.1% Tween-20 PBS, washed four times with 0.1% Tween-20 PBS, then blotted with either goat anti-mouse IgG constant fragment conjugated to horseradish peroxidase (Jackson ImmunoResearch) at 1:5000 dilution or goat anti-rabbit IgG constant (Jackson ImmunoResearch) fragment conjugated to horseradish peroxidase at 1:10000 dilution. Detection was carried by providing substrate with the ECL™ blotting detection reagents (GE Healthcare), and using traditional film-based exposure and development methods. Developed films were scanned using the "Scan Film" function from HP Solution Center and a HP ScanJet G4050.

Immunoprecipitation

Forty-eight hours after transfection, cells in 10-cm dishes were lysed as described in the section on mammalian cell lysis. Approximately equal amounts and concentrations of protein (adjusted with immunoprecipitation buffer) were loaded onto 100 µL of thrice pre-washed 50% Protein G Sepharose Beads 4 Fast Flow slurry (GE Life Sciences) for each condition in order to pre-clear lysates for non-specific binding to the beads. After 2 h of rocking at 4 °C, lysate-bead colloids were centrifuged at 100 x *g* for 30 sec and supernatants were collected. These supernatants were then incubated with 3 µg of the appropriate antibodies (rabbit polyclonal of either non-specific IgG [Southern Biotech] or anti-HA [Abcam]) overnight with rocking at 4 °C. Samples were subsequently loaded onto 100 µL of thrice pre-washed 50% bead slurry for 2 h of rocking at 4 °C. After, beads were washed four times with 650 µL of immunoprecipitation buffer, obtaining and discarding the supernatant by centrifuging at 100 x *g* for 30 sec. Following the washes, Laemmli loading buffer (0.1 M Tris pH 6.8, 25% glycerol, 3.7% SDS, 100 mM dithiothreitol [DTT]) was added to all samples for protein separation (total lysates and beads). Protein separation, immunoblotting, detection, and analysis was carried out as described in the section on mammalian cell culture lysis.

Glutathione-S-transferase pull-down

Glutathione-S-transferase (GST) fusion proteins were prepared by transforming Epicurian Coli BL21-Codon Plus™ strain (Stratagene) *Escherichia coli* with pGEX-2T (Amersham Biosciences) plasmids, either without an insert or with the indicated fragments of NHE9 inserted. Bacterial cultures of 3 mL of 2YT medium were grown overnight at 37 °C with shaking supplemented with 100 µg/mL ampicillin. After, 50 mL of 2YT medium supplemented with 100 µg/mL ampicillin was inoculated with 2 mL of this culture and grown at 37 °C until an optical density of 0.6 at 600 nm. The culture was transferred to grow at 30 °C and expression of glutathione-S-transferase and fusions was induced by adding isopropyl β-D-1-thiogalactopyranoside to 0.4 mM and maintaining cultures at 30 °C with shaking for 3 h. Cultures were subsequently pelleted by centrifuging at 4,000 x *g* for 20 min at 4 °C, discarding the supernatant. Pellets were resuspended in 1 mL of GST lysis buffer (0.5% Nonidet P-40, 100 µL EDTA, protease inhibitor cocktail in PBS) and sonicated thrice for 30 sec on ice with 30 sec of cooling in between. Lysates were then centrifuged at 16.1 kG for 30 min at 4 °C and the pellet discarded. Expression of GST and its fusions was qualitatively determined by incubating lysates with beads for 2 h, as noted in the section on immunoprecipitation, though with pre-washed 50% glutathione Sepharose beads (GE Life Science). After four 650-µL washes with GST lysis buffer, beads were loaded and separated through SDS-PAGE as noted in the section on mammalian cell lysis, and visualized using either Coomassie stain or transferring and staining the membrane by using Ponceau stain.

For GST pull-down with phospholipase D isoform 3, HEK293T cells in 10-cm dishes, 48 h after transfection of pcDNA3-PLD3$_{FLAG}$ were lysed and prepared for GST pull-down as noted under the section for lysis of mammalian cell cultures. GST and fusions were adjusted for expression by diluting in GST lysis buffer and loading appropriate amounts onto pre-washed 50% glutathione Sepharose beads and incubating at 4 °C for 2 h with rocking. The beads were washed with 650 µL buffer – twice with GST lysis buffer, and twice with immunoprecipitation buffer – before being loaded with equal amounts of cell lysates containing PLD3$_{FLAG}$. The lysate-bead mixtures were then incubated for an additional 2 h with rocking at 4 °C followed by four washes with immunoprecipitation buffer. After, beads were loaded and separated as noted in the section on

immunoprecipitation. Following immunoblotting and detection thereof, membranes were Ponceau stained to verify the binding and expression of GST and the GST fusions.

Laser-scanning confocal fluorescence microscopy and analysis

Following two washes with PBS, cells were fixed in 4% formaldehyde in PBS pH 7.4 for 20 min. For immunocytochemistry, cells were washed thrice with PBS and permeabilized for 20 min with 0.1% saponin in PBS pH 7.4. Permeabilized cells were washed then blocked with coverslip staining solution (0.01% saponin, 0.4% glycine, 10% goat serum in PBS) by incubating for 45 min. Primary antibodies were diluted into the same solution and incubated with the cells for 1 h at room temperature or overnight at 4 °C (rabbit polyclonal anti-HA diluted at 1:2000 [Abcam]; M2 mouse monoclonal anti-FLAG [Sigma] diluted at 1:2000). After four washes with coverslip staining solution, secondary antibodies were diluted into the same solution and left to bathe the cells for 1 h at room temperature protected from light (goat anti-rabbit IgG constant fragment conjugated to AlexaFluor488 and goat anti-mouse IgG constant fragment conjugated to AlexaFluor568 [Molecular Probes]). Cells were washed thrice with PBS and once with water prior to mounting onto glass slides in Aqua Poly/Mount mounting medium (Polysciences). Slides were imaged after overnight drying at room temperature protected from light. A Zeiss laser-scanning confocal microscope 710 and ZEN 2011 software were used for image acquisition. Each experiment made us of the same acquisition parameters. Z-axis images were separated by 0.3 µm, at an x-y sample pixel size of 0.54 µm by 0.54 µm. Images were acquired as an average of two 12-bit images. Only low-to-medium-expressing cells were chosen for acquisition.

Micrographs shown here were adjusted in order to better display results: First, digital offset was removed manually. Next, each channel was scaled separately to display all intensities over the entire bit range, permitting for some oversaturation.

Results

NHE9 is an alkali cation/proton exchanger with emerging roles in regulating vesicular trafficking and pH (93). These roles in vesicle function may be central to physiological cargo delivery and manipulation, and indeed may underlie the associations of imbalances in NHE9 to

Short Name	Full Name
Adhesion, Cytoskeleton, Cell Identity, Scaffolding	
CNTN2	Axonal Contactin 2
ZYX	Zyxin
GPHN	Gephyrin
PCDHGC3	Protocadherin gamma subfamily C, 3
DCAF7	DDB1 and CUL4 associated factor 7
JMJD8	Jumonji domain containing 8
Trafficking and Protein Chaperone	
DNAJB6	DNAJB6 DnaJ (Hsp40) homolog, subfamily B, member 6
VPS4A	Vacuolar protein sorting 4 homolog A
Other Signaling	
COPS5	COP9 constitutive photomorphogenic homolog subunit 5
RSU1	Ras suppressor protein 1
PLEKHB1	Pleckstrin homology domain containing, family B (evectins) member 1
NOMO1	NODAL modulator 1
PLD3	Phospholipase D family, member 3
MESP1	Mesoderm posterior 1 homolog
KLHL22	Kelch-like 22
YWHAH	Amino acid Oxygenase Activation Protein (tyrosine, tryptophan)
Metabolic	
ACAA1	Acetyl-CoA acyltransferase 1
PGP	Phosphoglycolate phosphatase
Unkown	
SDF2	Stromal cell-derived factor 2
Nucleotide Interaction and Association	
CLP1	Cleavage and polyadenylation factor I subunit 1
DDX56	DEAD box helicase 56
HNRNPF	Heterogeneous nuclear ribonucleoprotein F
HNRNPH2	Heterogenous nuclear ribonucleoprotein H2
TOX4	TOX high mobility group box family member 4
EEF2	Eukaryotic translation elongation factor 2
PNPT1	Polyribonucleotide nucleotidyltransferase 1
TRIM27	Tripartite motif containing 27

Table 1: Putative interacting partners of NHE9. A yeast two-hybrid screen of a human brain cDNA library using the carboxy terminal tail of NHE9 as bait (p.482-645) yielded twenty-six interacting partners, listed here.

neurodevelopmental disorders, such as autism and attention deficit hyperactivity disorder (80, 89, 90, 92). Recent studies indicate that NHE9 influences the trafficking of such cargo as transferrin, glutamate, and epidermal growth factor, and leads to increases in epidermal growth factor signaling (93, 94). However, to date there have not been reports of NHE9 function in the context of the developing nervous system. In an effort to reveal protein-protein interactions that NHE9 makes in this system, we performed a yeast two-hybrid screen of a human brain cDNA library using the cytoplasmic carboxy terminal tail of NHE9 (p.482-645), which we identified by a combination of hydropathy analysis and polypeptide sequence alignment with paralogs of the NHE family. Using this technique we screened an estimated $1.82*10^7$ clones as described in the materials and methods section (**Figure 1**) and found twenty-six putative interacting partners (**Table 1**), including phospholipase D isoform 3 (PLD3).

Since PLD3 localizes to the endoplasmic reticulum and all NHE paralogs are transmembrane proteins – which are synthesized in the rough endoplasmic reticulum – we aimed to determine the specificity of the interaction between NHE9 and PLD3 by immunoprecipitating carboxy terminal hemaglutannin-tagged NHE family members 1, 5, 6, 7, and 9 ($NHE\underline{X}_{HA}$, where $\underline{X}$ is the isoform number) and immunoblotting for carboxy terminal FLAG-tagged PLD3 ($PLD3_{FLAG}$) from transiently transfected into human embryonic kidney cells cell line 293 expressing the large T antigen (HEK293T) cells. We found that PLD3 co-immunoprecipitated with NHE5, 7, and 9 most strongly, but also to some extent with NHE1 (**Figure 2**, left panel). Surprisingly, PLD3 did not co-immunoprecipitate with NHE6, in spite of the high degree of similarity at the level of the polypeptide sequence (>58%) with NHE7 and 9 (**Figure 2**, left panel). Additionally, we performed the experiment with two variants of PLD3 of interest: V232M, a late-onset Alzheimer's Disease-associated mutation (125), and K418R, a putatively catalytically inactive mutant (100). We found that co-immunoprecipitation was not greatly affected by these mutations (**Figure 2**, centre and right panels).

To further dissect the nature of the interaction between NHE9 and PLD3 in an *in vitro* pull-down assay, we generated a number of glutathione-S-transferase (GST) fusions with fragments of the carboxy terminal tail of NHE9 – p.482-645 – the bait used in the yeast two-hybrid assay. Each fragment spanned about fifty amino acid residues, and overlapped by about fifteen residues

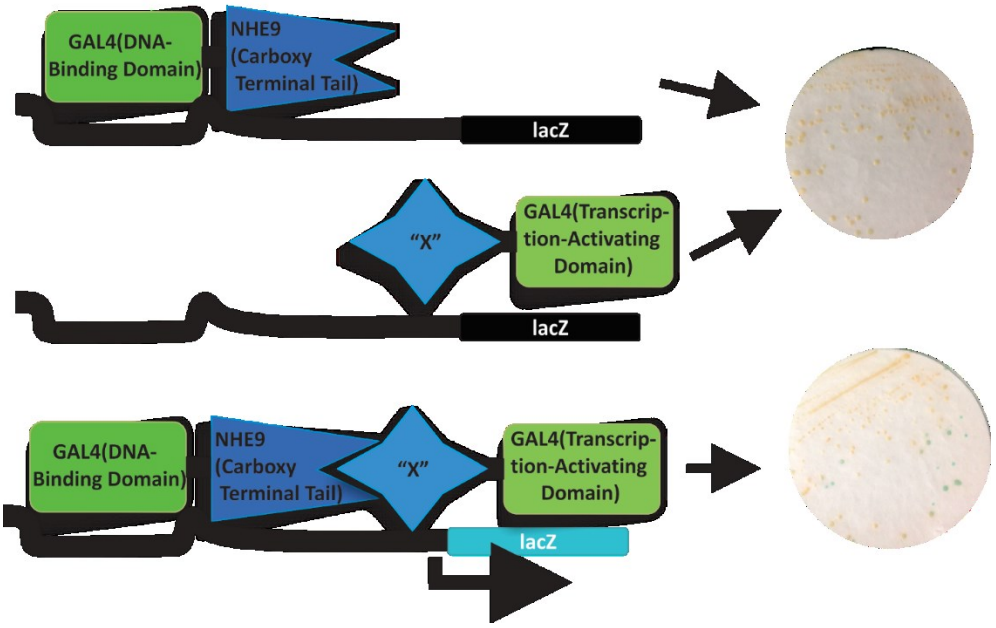

Figure 1: Schematic of the yeast-hybrid screen. In the traditional yeast two-hybrid screen, a positive hit only occurs when two hybrid proteins interact: one peptide fused to the GAL4 DNA-binding domain; another peptide fused to the GAL4 transcription-activating domain. A colony lift-filter assay indicates expression of the lac operon when colonies turn blue (below). In the yeast two-hybrid screen used here, yeast was grown on media which selected for each plasmid, as well as for two additional proteins whose transcription is promoted by GAL4.

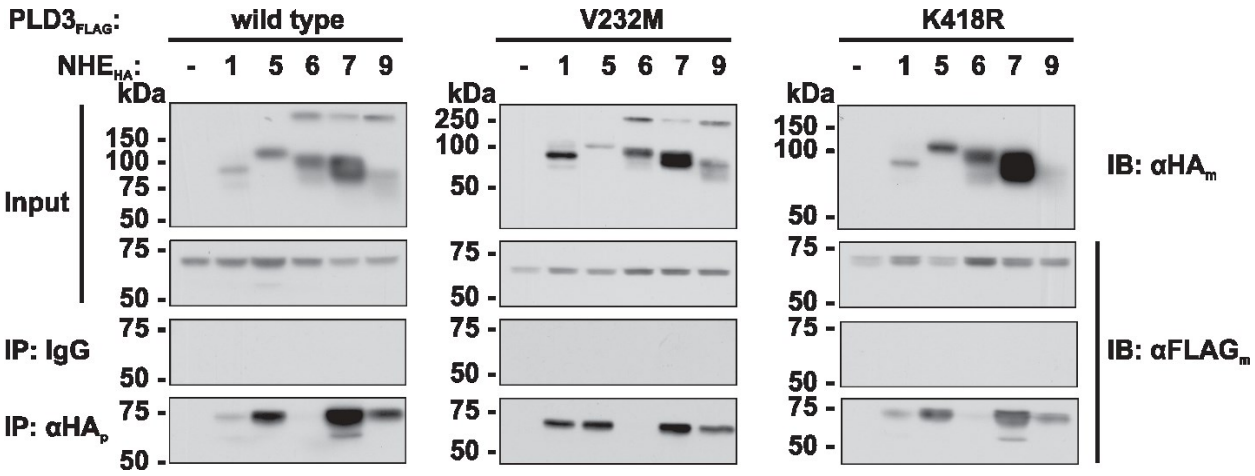

Figure 2: PLD3 co-immunoprecipitates with some NHE paralogs. (Left) In lysates of HEK293T cells transiently transfected with $PLD3_{FLAG}$ and HA-tagged NHE paralogs, PLD3 co-immunoprecipitates with NHE5, 7, and 9, and to a lesser extent with NHE1, but insignificantly to NHE6, despite the great deal of similarity at the primary sequence between NHE6, 7, 9 (>58%). This pattern was not strongly altered by either of two mutations in PLD3, a late-onset Alzheimer's disease-linked V232M, and a putatively catalytically inactive K418R. Each experiment was carried out independently four times.

with neighbouring fragments. Additionally, we constructed a fusion of the full carboxy terminal tail with GST. Incubating beads coated with the $_{GST}$NHE9(p.482-645) with lysates from HEK293T cells transiently transfected to express PLD3$_{FLAG}$ resulted in considerable pull-down of PLD3$_{FLAG}$, while GST alone did not (**Figure 3A**). We found that the first fragment, p.482-531, displayed similar levels of binding to PLD3$_{FLAG}$, when the lower amount of the fragment used in the pull-down assay is taken into account (**Figure 3A**). With slight overexposure of the membranes, we note that the second fragment, p.516-578, also yields PLD3$_{FLAG}$ binding while non-specific binding to GST yields little-to-none (**Figure 3A**). Paradoxically, protein alignments of NHE6, NHE7, and NHE9 indicate that residues p.482-578 of NHE9 are well-conserved, with 40-54% similarity with the NHE6 and NHE7 (**Figure 3B**), despite the inability of NHE6 to co-precipitate PLD3. Hence, we conjecture that the corresponding region of NHE6, though possibly able to bind to PLD3, is preferentially bound to another protein or otherwise inaccessible, precluding its pull-down of PLD3 in the experiments we performed.

To provide more evidence about the specificity of the interaction, we also immunoprecipitated the mentioned NHE paralogs which were co-transfected in HEK293T cells with PLD4$_{MYC}$. PLD4 is a paralog of PLD3 which is also non-canonical (119), exhibiting no phosphatidylcholine degradation activity (126). PLD3 and 4 are both single-pass transmembrane proteins which tend to localize to the endoplasmic reticulum (100, 126), but in contrast to PLD3's putatively neuronal expression, PLD4 is thought to be expressed in non-neuronal cells – microglia, in particular (127). We found that NHE1, 5, and 7 could precipitate PLD4, but NHE9 may have precipitated PLD4 more weakly than it did PLD3 (**Figure 4**). As with PLD3, NHE6 did not precipitate PLD4 (**Figure 4**). Since binding capabilities between the NHE paralogs and the PLD paralogs are not entirely conserved between the isoforms, we suggest that the interactions, and particularly the NHE9-PLD3 interaction, have specific roles in cellular physiology.

Although the NHE9 and PLD3 interaction is able to take place *in vitro*, the two proteins are expected to be largely sequestered from one another: following biosynthetic maturation and trafficking: NHE9 is a resident of early and recycling endosomes, and PLD3 remains largely in the endoplasmic reticulum. We sought to determine whether some overlap between these two distributions occurred in immortalized cell culture by immunofluorescence microscopy. Our

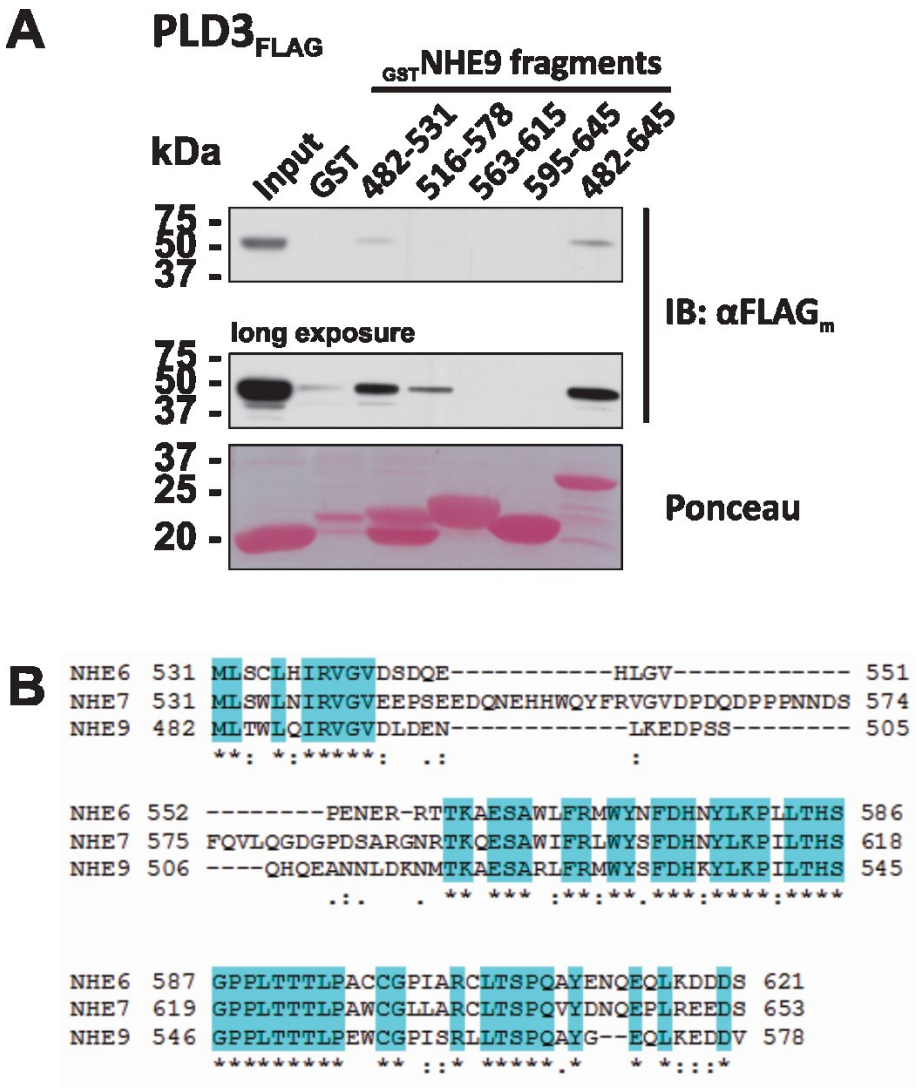

Figure 3: PLD3 binds to residues p.482-578 in the carboxy terminal cytoplasmic tail of NHE9. (A) Lysates from HEK293T cells transiently transfected with $PLD3_{FLAG}$ were incubated with beads coated with either GST alone, or GST fused to fragments of the carboxy terminal cytoplasmic tail of NHE9, whose expression can be visualized in the Ponceau staining. PLD3 bound most strongly to NHE9(p.482-531) though exhibited some specific binding to residues p.516-578, since the signal was stronger than the GST control signal. The experiment was carried out four times. (B) Alignment of paralogs NHE6, 7, and 9 in the region which is equivalent to NHE9 residues p.482-578. Blue highlighting marks conserved amino acids. This area of the proteins is highly conserved, and does not contain sequences that are similar between NHE7 and NHE9 but different in NHE6.

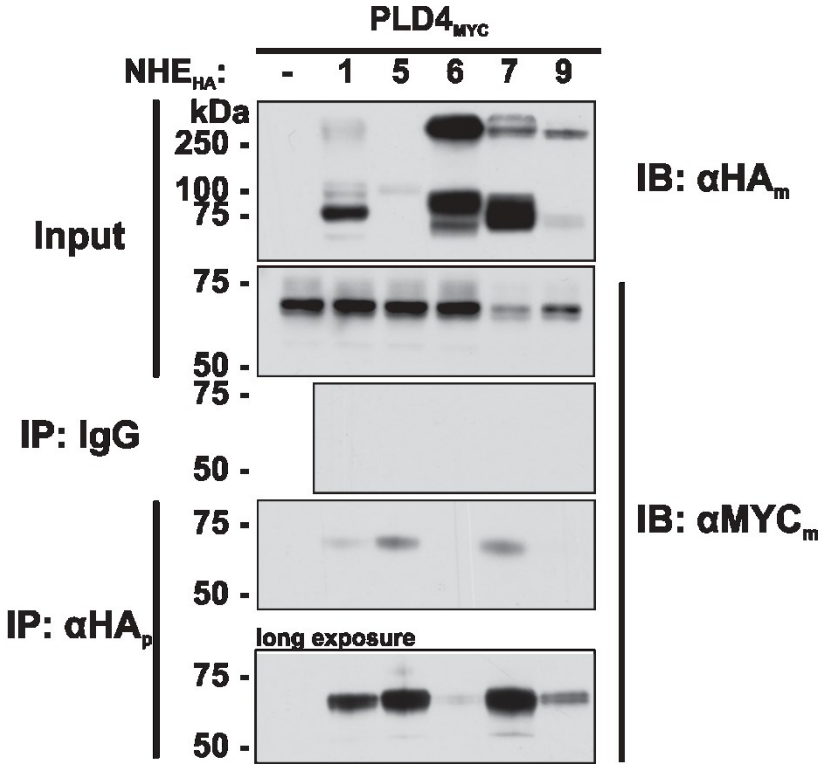

Figure 4: PLD4 also co-immunoprecipitates with some NHE paralogs. PLD4 binds similarly to NHE paralogs as PLD3: NHE5 and NHE7 still indicate strong PLD4 signal. NHE1 appears precipitate PLD4 slightly more strongly, whereas NHE9 appears to precipitate PLD4 slightly more weakly, these conclusions being drawn from four independent experiments with all the isoforms, with three additional independent experiments using NHE6 and NHE9.

results suggest that NHE9 and PLD3 are sequestered during normal cell activity, both in HEK293T cells (**Figure 5A**), and SH-SY5Y neuroblastoma cells (**Figure 5B**), which more faithfully recapitulate neuronal physiology. Moreover, this distribution was not significantly affected by the mutations in PLD3 studied here, the Alzheimer's disease-linked V232M and the putatively catalytically inactive K418R.

Discussion

PLD3 offers an interesting candidate as it has been implicated not only in cell differentiation events but also in trafficking (99, 100, 118) – two themes that are of particular importance in neurodevelopment. The development of the central nervous system encompasses a number of cellular differentiation events, highly coordinated cellular migration, as well as a multitude of particular signaling events which eventually give shape to neuronal structure and function (101, 102, 108). While PLD3 currently has loose implications in neurogenic differentiation, it does play an important role in facilitating myogenic differentiation, potentially by aiding the cell manage stresses of the endoplasmic reticulum which precede and take place during such cellular processes (100). PLD3 shifts localization from the endoplasmic reticulum to other vesicles during stresses and differentiation and its closest viral homologs are involved in membrane fission events (100). The mechanisms underlying these processes, however, are not well understood; by homology PLD3 appears to contain the appropriate catalytic domains for phospholipase D activity but thus far none has been detected (100). Moreover, a putatively catalytically inactive version of PLD3 identified by homology, K418R, diminishes any facilitation that PLD3 provides to myogenic differentiation (100). This suggests that the catalytic domains retain some function, albeit perhaps not in the catalysis of phosphotidylcholine to phosphatidic acid and choline (100). Intriguingly, mutations in PLD3 have also been linked to late onset Alzheimer's disease (125). At first this may seem entirely distinct from neurogenic differentiations, but the two processes involve stress of the endoplasmic reticulum (99, 128). Whether PLD3 actually plays a role in these processes remains to be unearthed.

We sought to investigate the possible interaction between NHE9 and PLD3, two proteins about which not much is known apart from implications in trafficking and neurodevelopment.

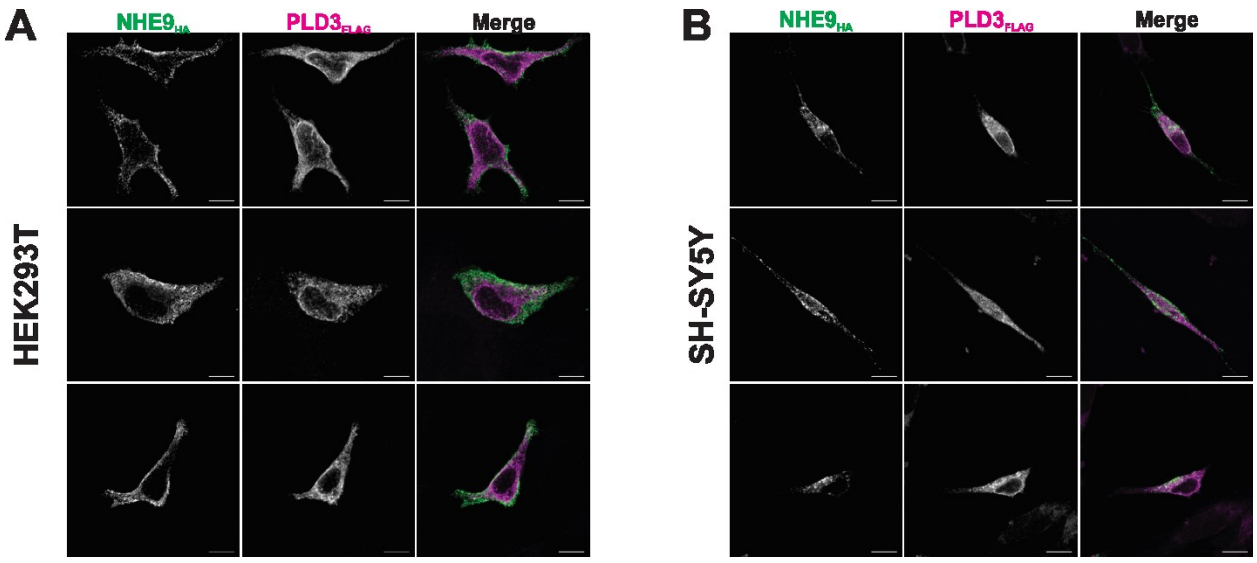

Figure 5: NHE9 does not colocalize with PLD3 in immortalized cell culture. Forty-eight hours post-transfection, neither HEK293T cells (A) nor SH-SY5Y cells (B) indicate a significant amount of co-localization between NHE9 and PLD3. PLD3 retains an endoplasmic reticulum pattern with some punctate pattern, whereas NHE9 has a vesicular localization throughout the cell, particularly peripherally in HEK293T cells. A total of ten cells from three independent experiments were imaged.

Using classical *in vitro* biochemical techniques including immunoprecipitation and GST pull-down, we mapped the interacting domain of NHE9 to PLD3 as the portion of the cytoplasmic carboxy terminal tail closest to the last transmembrane domain. However, in the heterologous systems used here, we did not observe significant colocalization of the two proteins. This suggests that binding occurs during only specific cellular events, such as endoplasmic reticulum stress, or cellular differentiation. Despite the lack of colocalization of NHE9 with the endoplasmic reticulum distribution of PLD3, the interaction appears to be somewhat specific as shown by two of our experiments. First, while PLD3 binds strongly to both NHE7 and NHE9, it does not bind at all to NHE6, which shares very high protein sequence similarity, including at the putative binding site. However, other NHE paralogs, both the plasmalemmal NHE1 and the recycling NHE5 can also precipitate PLD3. Second, these capabilities to precipitate are largely conserved with PLD4, suggesting that the specificity lies in regions shared between PLD3 and PLD4, rather than to regions unique to PLD3.

GENERAL DISCUSSION

NHE9 is a widely-expressed alkali cation/proton exchanger that regulates the trafficking and pH of a subset of early and recycling endosomes. These endosomes make up compartments which serve both as trafficking and as signaling hubs of the cell. Cargo is trafficked from the Golgi apparatus or the plasma membrane through these compartments towards a variety of destinations: to the lysosomes; to be recycled back to the membrane; or even back to the Golgi apparatus. Throughout this process, cargo can continue to partake in biochemical activity which can influence trafficking or signaling, and cell physiology as a whole.

Despite the ubiquitous expression of NHE9 and the great breadth of phenomena that involve the early and recycling endosomes, alterations in NHE9 function have thus far only been linked to a number of neurodevelopmental conditions, including autism and attention deficit/hyperactivity disorder. While the roles of NHE9 as a modulator of trafficking and signaling are beginning to emerge, there has not yet been progress on NHE9's role in neurodevelopment and the function of neurons. My study aimed foremost to characterize how NHE9 may be functioning in trafficking and to use this knowledge to assess the function of six autism-associated mutations. Moreover, I aimed to begin to place NHE9 in the context of neuron physiology and neurodevelopment. To this end, I screened a human brain cDNA library for interacting partners of NHE9, further investigating the putative interaction with PLD3.

In immortalized cell cultures transiently transfected to express NHE9, the six autism-associated variants, a putatively ion exchange deficient D244N, or an unglycosylated N96A (see Appendix A), did not affect the sub-cellular localization, when compared to a number of small RAB GTPases – markers of intracellular compartments. While we did not induce change or conditions of flux in this experiment, we used transferrin uptake as a measure of endocytosis and trafficking in the early and recycling endosomes for subsequent experiments. By our measures, NHE9 greatly enhances transferrin uptake, amounting to 1.5-fold greater after 10 minutes relative to GFP-expressing cells. Importantly, some of the mutations significantly diminished the enhancement that NHE9 confers. In particular, the autism-associated variant S438P and the putatively ion exchange deficient D244N almost completely prevented the enhancement of

transferrin uptake. Similarly, L236S, D495N, and Q609K tended to enhance uptake less than wild-type NHE9, although this was not statistically significant. As trafficking is correlated to pH, and vesicular function requires tight regulation of pH, we sought to determine whether NHE9 contributes to transferrin-containing vesicle pH. Intriguingly, we found that alkalinisation of transferrin-containing vesicle pH did not simply correlate with transferrin uptake. Vesicles with $NHE9_{ChFP}$ were significantly more alkaline than control vesicles (i. e., in ChFP-expressing cells) at 2.5, 10, and at 40 min of endocytosis. For the V176I, L236S, D495N, and Q609K variants, the loss of alkalinisation corresponded well with the effects of those mutations on transferrin uptake. Paradoxically, N96A and P117T exhibited vesicles much more acidic than expected, and D244N, the putative ion-exchange deficient variant, exhibited vesicles which were alkaline, more so than wild-type NHE9 at 2.5 and 10 min.

Superficially, these results may appear to be conflicting. On the contrary, measuring the pH of regions where transferrin and NHE9 are colocalized is a distant proxy to measuring alkali cation/proton exchange. The technique cannot distinguish between alkali cation/proton exchange activity and other processes, such as a diversion of trafficking. For instance, the ion exchange deficient D244N variant may have yielded more alkaline transferrin-containing vesicle pH values than expected not because it exhibits the same alkali cation/proton exchange activity as NHE9, but rather because it precludes transferrin from ever reaching the relatively acidic early endosomes. Hence, to more precisely dissect the cellular and molecular roles that NHE9 plays in the early and recycling endosomes, future experiments should analyze trafficking concomitantly with pH. For instance, our pH measurements were done at room temperature in order minimize trafficking during our imaging. The experiment could be set-up, calibrations included, at 37 °C, at which point one could measure more physiologically-relevant trafficking events in real time. One limitation is that fluorescent probes have to be washed out of the bathing solution prior to imaging, and that transferrin traffics extremely rapidly to the recycling endosomes. Together these facts may largely restrict observations to later points of endocytosis. Alternately, trafficking could be tracked in separate preparations using live-cell colocalization studies with intracellular compartment markers, such as the RAB paralogs used in this study. An additional experiment of interest would target the endogenous endomembrane alkali cation/proton transporters. For

instance, measuring the pH of vesicles in cells with a knockdown of endomembrane NHE expression may reveal whether small amounts of NHE9 expression can indeed impact vesicular pH. Similarly, measuring the trafficking of cargo and pH of vesicles which do not contain NHE9, in NHE9-expressing cells, could reveal whether NHE9 can impact trafficking on a pan-cellular level. In particular, one could measure the trafficking and pH of epidermal growth factor-containing vesicles, which predominantly traffic towards the lysosomes for degradation.

These proposed experiments would broaden our understanding of the relationship between alkali cation/proton exchange and trafficking. Extending these insights into neurodevelopment is a central goal, which we have begun to address by identifying twenty-six putative interacting partners of NHE9 from a human brain cDNA library. We identified proteins involved in adhesion, cytoskeleton regulation, scaffolding, trafficking, and metabolism, among other functions. Presently, the most notable results are: the inhibitory synapse post-synaptic receptor scaffolding protein gephyrin; vacuolar protein sorting homolog 4; axonal contactin 2; Ras suppressor protein 1; the focal adhesion accessory protein zyxin; and phospholipase D 3 (PLD3). For a number of these results, we carried out biochemical experiments to confirm interactions, to then conduct more specialized experiments to shed light on the molecular mechanisms underlying the roles of NHE9.

Co-immunoprecipitation experiments yielded inconsistent results with gephyrin and vacuolar protein sorting homolog 4, but were definitive for PLD3. We found that PLD3 could be co-precipitated by numerous NHE paralogs in addition to NHE9: NHE1, 5, 7, but not NHE6, despite the great similarity that NHE6 shares with NHE7 and NHE9 (58-68% at the polypeptide sequence level). Furthermore, a similar pattern of precipitation was found with PLD4, a paralog of PLD3. By using an *in vitro* affinity chromatography using fragments of the carboxy terminal tail of NHE9, we mapped the binding site of PLD3 to residues p.482-578 of NHE9. Interestingly, no sequences within this region were similar between NHE7 and NHE9 but different from NHE6, as would be expected from the co-immunoprecipitation experiment. Hence, it is possible that the interaction with NHE6 is precluded by protein binding to the same region or by steric hindrance. Despite the binding that occurs between NHE9 and PLD3, we found that NHE9 and PLD3 colocalize minimally in both HEK293T cells and SH-SY5Y neuroblastoma cells. Subsequent experiments should aim to

investigate the interaction in particular cellular events, such as cellular differentiation or endoplasmic reticulum stress – events during which PLD3 has been shown to change localization. For instance, transient treatment with the endoplasmic reticulum stressor tunicamycin may change the co-localization and perhaps the strength of co-immunoprecipitation of PLD3 with NHE9. The necessity of this interaction in cellular homeostasis can then be evaluated in these contexts by attempting to prevent it. Currently, we are constructing GFP-fusions of fragments of the carboxy terminal tail of NHE9 which may be able to out-compete NHE9 in interacting with PLD3 when transfected into cells. Ultimately, investigations should be carried out in neuronal cultures or *in vivo* to elucidate the association of NHE9 with neurodevelopmental conditions.

In summary, NHE9 does regulate the trafficking and pH of vesicles. However, the relationship between these two phenomena is not a simple one; some of the studied NHE9 variants seemingly affect one function but not the other. Hence, it appears as if the structure and ion-exchange function of NHE9 may influence not only the extent of trafficking, but also its direction. These insights along with the molecular tools for investigating NHE9 can be implemented into subsequent efforts to reveal the association between neurodevelopment and the endomembrane alkali cation/proton exchanger NHE9.

REFERENCES

1. Roos A & Boron WF (1981) Intracellular pH pp 296-434.

2. Herriott RM (1962) Pepsinogen and pepsin. J Gen Physiol 45(4)Pt 2:57-76.

3. Dautry-Varsat A, Ciechanover A, & Lodish HF (1983) pH and the recycling of transferrin during receptor-mediated endocytosis. Proceedings of the National Academy of Sciences 80(8):2258-2262.

4. Grinstein S, Rotin D, & Mason MJ (1989) Na+/H+ exchange and growth factor-induced cytosolic pH changes. Role in cellular proliferation. Biochimica et Biophysica Acta (BBA) - Reviews on Biomembranes 988(1):73-97.

5. Cardone RA, Casavola V, & Reshkin SJ (2005) The role of disturbed pH dynamics and the Na+/H+ exchanger in metastasis. Nat Rev Cancer 5(10):786-795.

6. Van Slyke AC, et al. (2012) Proton block of the pore underlies the inhibition of hERG cardiac K+ channels during acidosis pp C1797-C1806.

7. Casey JR, Grinstein S, & Orlowski J (2010) Sensors and regulators of intracellular pH. Nat Rev Mol Cell Biol 11(1):50-61.

8. Becker H, Klier M, & Deitmer J (2014) Carbonic Anhydrases and Their Interplay with Acid/Base-Coupled Membrane Transporters. Carbonic Anhydrase: Mechanism, Regulation, Links to Disease, and Industrial Applications, Subcellular Biochemistry, eds Frost SC & McKenna R (Springer Netherlands), Vol 75, pp 105-134.

9. Marshansky V, Rubinstein JL, & Grüber G (2014) Eukaryotic V-ATPase: Novel structural findings and functional insights. Biochimica et Biophysica Acta (BBA) - Bioenergetics 1837(6):857-879.

10. Shin JM, Munson K, & Sachs G (2011) Gastric H+,K+-ATPase. Comprehensive Physiology, (John Wiley & Sons, Inc.).

11. Morth JP, et al. (2011) A structural overview of the plasma membrane Na+,K+-ATPase and H+-ATPase ion pumps. Nat Rev Mol Cell Biol 12(1):60-70.

12. Cordat E & Reithmeier RAF (2014) Chapter One - Structure, Function, and Trafficking of SLC4 and SLC26 Anion Transporters. Current Topics in Membranes, ed Mark OB (Academic Press), Vol Volume 73, pp 1-67.

13. Merot J, Giebisch G, & Geibel J (1997) Intracellular acidification induces Cl/HCO3 exchange activity in the basolateral membrane of beta-intercalated cells of the rabbit cortical collecting duct. The Journal of membrane biology 159(3):253-262.

14. Parker MD, et al. (2008) Characterization of Human SLC4A10 as an Electroneutral Na/HCO3 Cotransporter (NBCn2) with Cl– Self-exchange Activity. Journal of Biological Chemistry 283(19):12777-12788.

15. Amlal H, Burnham CE, & Soleimani M (1999) Characterization of Na+/ cotransporter isoform NBC-3. American Journal of Physiology 276(6):F903-F913.

16. Grichtchenko II, et al. (2001) Cloning, Characterization, and Chromosomal Mapping of a Human Electroneutral Na+-driven Cl-HCO3Exchanger. Journal of Biological Chemistry 276(11):8358-8363.

17. Pushkin A, et al. (1999) Cloning, Tissue Distribution, Genomic Organization, and Functional Characterization of NBC3, a New Member of the Sodium Bicarbonate Cotransporter Family. Journal of Biological Chemistry 274(23):16569-16575.

18. Virkki LV, Wilson DA, Vaughan-Jones RD, & Boron WF (2002) Functional characterization of human NBC4 as an electrogenic Na+-HCO cotransporter (NBCe2) pp C1278-C1289.

19. Odgaard E, et al. (2004) Basolateral Na+-dependent HCO3− transporter NBCn1-mediated HCO3− influx in rat medullary thick ascending limb. The Journal of Physiology 555(1):205-218.

20. Sinning A, et al. (2011) Synaptic Glutamate Release Is Modulated by the Na+-Driven Cl−/HCO3− Exchanger Slc4a8. The Journal of Neuroscience 31(20):7300-7311.

21. Igarashi T, et al. (1999) Mutations in SLC4A4 cause permanent isolated proximal renal tubular acidosis with ocular abnormalities. Nat Genet 23(3):264-266.

22. Fuster D & Alexander RT (2014) Traditional and emerging roles for the SLC9 Na+/H+ exchangers. Pflugers Arch - Eur J Physiol 466(1):61-76.

23. Orlowski J & Grinstein S (2011) Na+/H+ Exchangers. Comprehensive Physiology, (John Wiley & Sons, Inc.).

24. Noel J, Roux D, & Pouyssegur J (1996) Differential localization of Na+/H+ exchanger isoforms (NHE1 and NHE3) in polarized epithelial cell lines. Journal of Cell Science 109(5):929-939.

25. Lukashova V, et al. (2013) The Na+/H+ Exchanger NHE5 Is Sorted to Discrete Intracellular Vesicles in the Central and Peripheral Nervous Systems. Advances in Experimental Medicine and Biology, ed Annunziato L (Springer US), Vol 961, pp 397-410.

26. Hill JK, et al. (2006) Vestibular Hair Bundles Control pH with (Na+, K+)/H+ Exchangers NHE6 and NHE9. The Journal of Neuroscience 26(39):9944-9955.

27. Numata M & Orlowski J (2001) Molecular Cloning and Characterization of a Novel (Na+,K+)/H+ Exchanger Localized to the trans-Golgi Network. Journal of Biological Chemistry 276(20):17387-17394.

28. Kang'ethe W, Aimanova KG, Pullikuth AK, & Gill SS (2007) NHE8 mediates amiloride-sensitive Na+/H+ exchange across mosquito Malpighian tubules and catalyzes Na+ and K+ transport in reconstituted proteoliposomes pp F1501-F1512.

29. Rotin D & Grinstein S (1989) Impaired cell volume regulation in Na(+)-H+ exchange-deficient mutants pp C1158-C1165.

30. Peti-Peterdi J, et al. (2000) Macula densa Na+/H+ exchange activities mediated by apical NHE2 and basolateral NHE4 isoforms pp F452-F463.

31. Shen M-R, Wilkins RJ, Chou C-Y, & Ellory JC (2002) Anion exchanger isoform 2 operates in parallel with Na+/H+ exchanger isoform 1 during regulatory volume decrease of human cervical cancer cells. FEBS Letters 512(1–3):52-58.

32. Garcia-Romeu F, Borgese F, Guizouarn H, Fievet B, & Motais R (1996) A role for the anion exchanger AE1 (band 3 protein) in cell volume regulation. Cellular and molecular biology 42(7):985-994.

33. Sanchez-Olea R, Fuller C, Benos D, & Pasantes-Morales H (1995) Volume-associated osmolyte fluxes in cell lines with or without the anion exchanger. The American journal of physiology 269(5 Pt 1):C1280-1286.

34. Levine SA, Montrose MH, Tse CM, & Donowitz M (1993) Kinetics and regulation of three cloned mammalian Na+/H+ exchangers stably expressed in a fibroblast cell line. Journal of Biological Chemistry 268(34):25527-25535.

35. Helmle-Kolb C, et al. (1993) Na/H Exchange activities in NHE1-transfected OK-cells: cell polarity and regulation. Pflugers Arch. 425(1-2):34-40.

36. Roussa E, Alper SL, & Thévenod F (2001) Immunolocalization of Anion Exchanger AE2, Na+/H+ Exchangers NHE1 and NHE4, and Vacuolar Type H+-ATPase in Rat Pancreas. Journal of Histochemistry & Cytochemistry 49(4):463-474.

37. Nejsum LN, Praetorius J, & Nielsen S (2005) NKCC1 and NHE1 are abundantly expressed in the basolateral plasma membrane of secretory coil cells in rat, mouse, and human sweat glands pp C333-C340.

38. Garciarena CD, Youm JB, Swietach P, & Vaughan-Jones RD (2013) H+-activated Na+ influx in the ventricular myocyte couples Ca2+-signalling to intracellular pH. Journal of Molecular and Cellular Cardiology 61(0):51-59.

39. Good DW, Watts BA, George T, Meyer JW, & Shull GE (2004) Transepithelial HCO_3^- absorption is defective in renal thick ascending limbs from Na+/H+ exchanger NHE1 null mutant mice pp F1244-F1249.

40. Jinadasa T, Szabó EZ, Numata M, & Orlowski J (2014) Activation of AMP-activated Protein Kinase Regulates Hippocampal Neuronal pH by Recruiting Na+/H+ Exchanger NHE5 to the Cell Surface. Journal of Biological Chemistry 289(30):20879-20897.

41. Diering GH, Numata Y, Fan S, Church J, & Numata M (2013) Endosomal acidification by Na+/H+ exchanger NHE5 regulates TrkA cell-surface targeting and NGF-induced PI3K signaling. Molecular Biology of the Cell 24(21):3435-3448.

42. Schwake M, Schröder B, & Saftig P (2013) Lysosomal Membrane Proteins and Their Central Role in Physiology. Traffic 14(7):739-748.

43. Bhuin T & Roy JK (2014) Rab proteins: The key regulators of intracellular vesicle transport. Experimental Cell Research 328(1):1-19.

44. Lodish H, Berk A, & Kaiser C (2007) Molecular and Cell Biology (WHFreeman) 6 Ed.

45. Marshansky V & Futai M (2008) The V-type H+-ATPase in vesicular trafficking: targeting, regulation and function. Current Opinion in Cell Biology 20(4):415-426.

46. Hoogenraad CC, et al. (2010) Neuron Specific Rab4 Effector GRASP-1 Coordinates Membrane Specialization and Maturation of Recycling Endosomes. PLoS Biol 8(1):e1000283.

47. Solinger JA & Spang A (2013) Tethering complexes in the endocytic pathway: CORVET and HOPS. FEBS Journal 280(12):2743-2757.

48. Rink J, Ghigo E, Kalaidzidis Y, & Zerial M (2005) Rab Conversion as a Mechanism of Progression from Early to Late Endosomes. Cell 122(5):735-749.

49. Posor Y, Eichhorn-Grünig M, & Haucke V (2014) Phosphoinositides in endocytosis. Biochimica et Biophysica Acta (BBA) - Molecular and Cell Biology of Lipids (0).

50. Kim J (2015) Unconventional Mechanics of Lipid Membranes: A Potential Role for Mechanotransduction of Hair Cell Stereocilia. Biophysical Journal 108(3):610-621.

51. Suetsugu S, Kurisu S, & Takenawa T (2014) Dynamic Shaping of Cellular Membranes by Phospholipids and Membrane-Deforming Proteins pp 1219-1248.

52. Anne C & Gasnier B (2014) Chapter Three - Vesicular Neurotransmitter Transporters: Mechanistic Aspects. Current Topics in Membranes, ed Mark OB (Academic Press), Vol Volume 73, pp 149-174.

53. Stauber T & Jentsch TJ (2013) Chloride in Vesicular Trafficking and Function. Annual Review of Physiology 75(1):453-477.

54. Hurtado-Lorenzo A, et al. (2006) V-ATPase interacts with ARNO and Arf6 in early endosomes and regulates the protein degradative pathway. Nat Cell Biol 8(2):124-136.

55. Gidon A, et al. (2014) Endosomal GPCR signaling turned off by negative feedback actions of PKA and v-ATPase. Nat Chem Biol 10(9):707-709.

56. Jean S & Kiger AA (2012) Coordination between RAB GTPase and phosphoinositide regulation and functions. Nat Rev Mol Cell Biol 13(7):463-470.

57. Kandachar V & Roegiers F (2012) Endocytosis and control of Notch signaling. Current Opinion in Cell Biology 24(4):534-540.

58. Zhou P, et al. (2007) Polarized Signaling Endosomes Coordinate BDNF-Induced Chemotaxis of Cerebellar Precursors. Neuron 55(1):53-68.

59. Alzamora R, et al. (2010) PKA Regulates Vacuolar H+-ATPase Localization and Activity via Direct Phosphorylation of the A Subunit in Kidney Cells. Journal of Biological Chemistry 285(32):24676-24685.

60. Hara-Chikuma M, et al. (2005) ClC-3 Chloride Channels Facilitate Endosomal Acidification and Chloride Accumulation. Journal of Biological Chemistry 280(2):1241-1247.

61. Li X, Wang T, Zhao Z, & Weinman SA (2002) The ClC-3 chloride channel promotes acidification of lysosomes in CHO-K1 and Huh-7 cells. American Journal of Physiolog: Cell Physiology 282(6):C1483-C1491.

62. Seksek O, Biwersi J, & Verkman AS (1996) Evidence against Defective trans-Golgi Acidification in Cystic Fibrosis. Journal of Biological Chemistry 271(26):15542-15548.

63. Barasch J, et al. (1991) Defective acidification of intracellular organelles in cystic fibrosis. Nature 352(6330):70-73.

64. Nordeen MH, Jones SM, Howell KE, & Caldwell JH (2000) GOLAC: an endogenous anion channel of the Golgi complex. Biophys J 78(6):2918-2928.

65. Thompson RJ, Nordeen MH, Howell KE, & Caldwell JH (2002) A large-conductance anion channel of the Golgi complex. Biophys J 83(1):278-289.

66. D'Souza S, et al. (1998) The Epithelial Sodium-Hydrogen Antiporter Na+/H+ Exchanger 3 Accumulates and Is Functional in Recycling Endosomes. Journal of Biological Chemistry 273(4):2035-2043.

67. Alexander RT, Furuya W, Szászi K, Orlowski J, & Grinstein S (2005) Rho GTPases dictate the mobility of the Na/H exchanger NHE3 in epithelia: Role in apical retention and targeting. Proceedings of the National Academy of Sciences of the United States of America 102(34):12253-12258.

68. Feldmann T, et al. (2007) Role of endosomal Na+-K+-ATPase and cardiac steroids in the regulation of endocytosis pp C885-C896.

69. Gekle M, et al. (1999) Inhibition of Na+-H+ exchange impairs receptor-mediated albumin endocytosis in renal proximal tubule-derived epithelial cells from opossum. The Journal of Physiology 520(3):709-721.

70. Nakamura N, Tanaka S, Teko Y, Mitsui K, & Kanazawa H (2005) Four Na+/H+ Exchanger Isoforms Are Distributed to Golgi and Post-Golgi Compartments and Are Involved in Organelle pH Regulation. Journal of Biological Chemistry 280(2):1561-1572.

71. Brett CL, Wei Y, Donowitz M, & Rao R (2002) Human Na+/H+ exchanger isoform 6 is found in recycling endosomes of cells, not in mitochondria pp C1031-C1041.

72. Miyazaki E, Sakaguchi M, Wakabayashi S, Shigekawa M, & Mihara K (2001) NHE6 Protein Possesses a Signal Peptide Destined for Endoplasmic Reticulum Membrane and Localizes in Secretory Organelles of the Cell. Journal of Biological Chemistry 276(52):49221-49227.

73. Ohgaki R, Fukura N, Matsushita M, Mitsui K, & Kanazawa H (2008) Cell Surface Levels of Organellar Na+/H+ Exchanger Isoform 6 Are Regulated by Interaction with RACK1. Journal of Biological Chemistry 283(7):4417-4429.

74. Ilie A, Weinstein E, Boucher A, McKinney RA, & Orlowski J (2014) Impaired posttranslational processing and trafficking of an endosomal Na+/H+ exchanger NHE6 mutant (Δ370WST372) associated with X-linked intellectual disability and autism. Neurochemistry International 73(0):192-203.

75. Xinhan L, et al. (2011) Na+/H+ exchanger isoform 6 (NHE6/SLC9A6) is involved in clathrin-dependent endocytosis of transferrin pp C1431-C1444.

76. Prasad H & Rao R (2015) The Na+/H+ Exchanger NHE6 Modulates Endosomal pH to Control Processing of Amyloid Precursor Protein in a Cell Culture Model of Alzheimer Disease. Journal of Biological Chemistry 290(9):5311-5327.

77. Gilfillan GD, et al. (2008) SLC9A6 mutations cause X-linked mental retardation, microcephaly, epilepsy, and ataxia, a phenotype mimicking Angelman syndrome. American journal of human genetics 82(4):1003-1010.

78. Takahashi Y, et al. (2011) A loss-of-function mutation in the SLC9A6 gene causes X-linked mental retardation resembling Angelman syndrome. American Journal of Medical Genetics Part B: Neuropsychiatric Genetics 156(7):799-807.

79. Zanni G, et al. (2014) A novel mutation in the endosomal Na+/H+ exchanger NHE6 (SLC9A6) causes Christianson syndrome with electrical status epilepticus during slow-wave sleep (ESES). Epilepsy Research 108(4):811-815.

80. Schwede M, Garbett K, Mirnics K, Geschwind DH, & Morrow EM (2014) Genes for endosomal NHE6 and NHE9 are misregulated in autism brains. Mol Psychiatry 19(3):277-279.

81. Roxrud I, Raiborg C, Gilfillan GD, Strømme P, & Stenmark H (2009) Dual degradation mechanisms ensure disposal of NHE6 mutant protein associated with neurological disease. Experimental Cell Research 315(17):3014-3027.

82. Ouyang Q, et al. (2013) Christianson Syndrome Protein NHE6 Modulates TrkB Endosomal Signaling Required for Neuronal Circuit Development. Neuron 80(1):97-112.

83. Solecki DJ (2012) Sticky situations: recent advances in control of cell adhesion during neuronal migration. Current Opinion in Neurobiology 22(5):791-798.

84. Baydyuk M & Xu B (2014) BDNF signaling and survival of striatal neurons. Frontiers in Cellular Neuroscience 8.

85. Deane EC, et al. (2013) Enhanced Recruitment of Endosomal Na+/H+ Exchanger NHE6 into Dendritic Spines of Hippocampal Pyramidal Neurons during NMDA Receptor-Dependent Long-Term Potentiation. The Journal of Neuroscience 33(2):595-610.

86. Lin PJC, Williams WP, Kobiljski J, & Numata M (2007) Caveolins bind to (Na+, K+)/H+ exchanger NHE7 by a novel binding module. Cellular Signalling 19(5):978-988.

87. Milosavljevic N, et al. (2014) The Intracellular Na+/H+ Exchanger NHE7 Effects a Na+-Coupled, but Not K+-Coupled Proton-Loading Mechanism in Endocytosis. Cell Reports 7(3):689-696.

88. Lawrence SP, Bright NA, Luzio JP, & Bowers K (2010) The Sodium/Proton Exchanger NHE8 Regulates Late Endosomal Morphology and Function. Molecular Biology of the Cell 21(20):3540-3551.

89. de Silva MG, et al. (2003) Disruption of a novel member of a sodium/hydrogen exchanger family and DOCK3 is associated with an attention deficit hyperactivity disorder-like phenotype. Journal of Medical Genetics 40(10):733-740.

90. Lasky-Su J, et al. (2008) Genome-wide association scan of quantitative traits for attention deficit hyperactivity disorder identifies novel associations and confirms candidate gene associations. American Journal of Medical Genetics Part B: Neuropsychiatric Genetics 147B(8):1345-1354.

91. Zhang-James Y, DasBanerjee T, Sagvolden T, Middleton FA, & Faraone SV (2011) SLC9A9 mutations, gene expression, and protein–protein interactions in rat models of attention-deficit/hyperactivity disorder. American Journal of Medical Genetics Part B: Neuropsychiatric Genetics 156(7):835-843.

92. Morrow EM, et al. (2008) Identifying Autism Loci and Genes by Tracing Recent Shared Ancestry. Science 321(5886):218-223.

93. Kondapalli KC, et al. (2013) Functional evaluation of autism-associated mutations in NHE9. Nat Commun 4.

94. Kondapalli KC, et al. (2015) A leak pathway for luminal protons in endosomes drives oncogenic signalling in glioblastoma. Nat Commun 6.

95. Kondapalli KC, Prasad H, & Rao R (2014) An Inside Job: How Endosomal Na+/H+ Exchangers Link to Autism and Neurological Disease. Frontiers in Cellular Neuroscience 8.

96. Angelidou A, et al. (2011) Brief Report: "Allergic Symptoms" in Children with Autism Spectrum Disorders. More than Meets the Eye? J Autism Dev Disord 41(11):1579-1585.

97. Toh MC & Allen-Vercoe E (2015) The human gut microbiota with reference to autism spectrum disorder: considering the whole as more than a sum of its parts. 2015 26.

98. Theoharides TC, et al. (2012) Mast cell activation and autism. Biochimica et biophysica acta 1822(1):34-41.

99. Satoh J-i, et al. (2014) PLD3 is accumulated on neuritic plaques in Alzheimer's disease brains. Alzheimer's Research & Therapy 6(9):70.

100. Osisami M, Ali W, & Frohman MA (2012) A Role for Phospholipase D3 in Myotube Formation. PLoS ONE 7(3):e33341.

101. Urban N & Guillemot F (2014) Neurogenesis in the embryonic and adult brain: same regulators, different roles. Frontiers in Cellular Neuroscience 8.

102. Barry DS, Pakan JM, & McDermott KW (2014) Radial glial cells: key organisers in CNS development. The international journal of biochemistry & cell biology 46:76-79.

103. Gallo G (2013) Chapter Three - Mechanisms Underlying the Initiation and Dynamics of Neuronal Filopodia: From Neurite Formation to Synaptogenesis. International Review of Cell and Molecular Biology, ed Kwang WJ (Academic Press), Vol Volume 301, pp 95-156.

104. Yin J & Yuan Q (2015) Structural homeostasis in the nervous system: A balancing act for wiring plasticity and stability. Frontiers in Cellular Neuroscience 8.

105. Latapy C & Beaulieu JM (2013) Chapter Eleven - β-Arrestins in the Central Nervous System. Progress in Molecular Biology and Translational Science, ed Louis ML (Academic Press), Vol Volume 118, pp 267-295.

106. Villarroel-Campos D, Gastaldi L, Conde C, Caceres A, & Gonzalez-Billault C (2014) Rab-mediated trafficking role in neurite formation. Journal of Neurochemistry 129(2):240-248.

107. Lazo OM, et al. (2013) BDNF Regulates Rab11-Mediated Recycling Endosome Dynamics to Induce Dendritic Branching. The Journal of Neuroscience 33(14):6112-6122.

108. Cosker KE & Segal RA (2014) Neuronal Signaling through Endocytosis. Cold Spring Harbor Perspectives in Biology 6(2).

109. Mayle KM, Le AM, & Kamei DT (2012) The intracellular trafficking pathway of transferrin. Biochimica et Biophysica Acta (BBA) - General Subjects 1820(3):264-281.

110. Lagache T, Sauvonnet N, Danglot L, & Olivo-Marin J-C (2015) Statistical analysis of molecule colocalization in bioimaging. Cytometry Part A:n/a-n/a.

111. Snedecor GW & Cochran WG (1989) Statistical Methods (Iowa State University Press) 8 Ed.

112. Barriere H & Lukacs GL (2001) Analysis of Endocytic Trafficking by Single-Cell Fluorescence Ratio Imaging. Current Protocols in Cell Biology, (John Wiley & Sons, Inc.).

113. Science AIfB (2014) Allen Developing Mouse Brain Atlas.

114. Wakabayashi S, Pang T, Su X, & Shigekawa M (2000) A Novel Topology Model of the Human Na+/H+ Exchanger Isoform 1. Journal of Biological Chemistry 275(11):7942-7949.

115. Jones S & Rappoport JZ (2014) Interdependent epidermal growth factor receptor signalling and trafficking. The international journal of biochemistry & cell biology 51(0):23-28.

116. Lecoeur H, de Oliveira-Pinto LM, & Gougeon M-L (2002) Multiparametric flow cytometric analysis of biochemical and functional events associated with apoptosis and oncosis using the 7-aminoactinomycin D assay. Journal of Immunological Methods 265(1–2):81-96.

117. Dityatev A & Rusakov DA (2011) Molecular signals of plasticity at the tetrapartite synapse. Current Opinion in Neurobiology 21(2):353-359.

118. Roth MG (2008) Molecular Mechanisms of PLD Function in Membrane Traffic. Traffic 9(8):1233-1239.

119. Gomez-Cambronero J (2014) Phospholipase D in Cell Signaling: From a Myriad of Cell Functions to Cancer Growth and Metastasis. Journal of Biological Chemistry 289(33):22557-22566.

120. Jang J-H, Lee CS, Hwang D, & Ryu SH (2012) Understanding of the roles of phospholipase D and phosphatidic acid through their binding partners. Progress in Lipid Research 51(2):71-81.

121. Husain M & Moss B (2002) Similarities in the Induction of Post-Golgi Vesicles by the Vaccinia Virus F13L Protein and Phospholipase D. Journal of Virology 76(15):7777-7789.

122. Schiestl R & Gietz RD (1989) High efficiency transformation of intact yeast cells using single stranded nucleic acids as a carrier. Curr Genet 16(5-6):339-346.

123. Lane DP & Crawford LV (1979) T antigen is bound to a host protein in SY40-transformed cells. Nature 278(5701):261-263.

124. Goujon M, et al. (2010) A new bioinformatics analysis tools framework at EMBL-EBI. Nucleic acids research 38(Web Server issue):W695-699.

125. Meda SA, et al. (2012) A large scale multivariate parallel ICA method reveals novel imaging–genetic relationships for Alzheimer's disease in the ADNI cohort. NeuroImage 60(3):1608-1621.

126. Yoshikawa F, et al. (2010) Phospholipase D Family Member 4, a Transmembrane Glycoprotein with No Phospholipase D Activity, Expression in Spleen and Early Postnatal Microglia. PLoS ONE 5(11):e13932.

127. Otani Y, et al. (2011) PLD4 Is Involved in Phagocytosis of Microglia: Expression and Localization Changes of PLD4 Are Correlated with Activation State of Microglia. PLoS ONE 6(11):e27544.

128. Hetz C (2012) The unfolded protein response: controlling cell fate decisions under ER stress and beyond. Nat Rev Mol Cell Biol 13(2):89-102.

129. Aebi M (2013) N-linked protein glycosylation in the ER. Biochimica et Biophysica Acta (BBA) - Molecular Cell Research 1833(11):2430-2437.

130. Ohtsubo K & Marth JD (2006) Glycosylation in Cellular Mechanisms of Health and Disease. Cell 126(5):855-867.

131. Xu C & Ng DTW (O-mannosylation: The other glycan player of ER quality control. Seminars in Cell & Developmental Biology (0).

132. Benyair R, Ogen-Shtern N, & Lederkremer GZ (Glycan regulation of ER-associated degradation through compartmentalization. Seminars in Cell & Developmental Biology (0).

133. Srinivasan S, Romagnoli M, Bohm A, & Sonenshein GE (2014) N-Glycosylation Regulates ADAM8 Processing and Activation. Journal of Biological Chemistry 289(48):33676-33688.

134. Takahashi M, et al. (2008) N-glycan of ErbB family plays a crucial role in dimer formation and tumor promotion. Biochimica et Biophysica Acta (BBA) - General Subjects 1780(3):520-524.

135. Counillon L, Pouyssegur J, & Reithmeier RAF (1994) The Na+/H+ Exchanger NHE-1 Possesses N- and O-Linked Glycosylation Restricted to the First N-Terminal Extracellular Domain. Biochemistry 33(34):10463-10469.

136. Tse C-M, Levine SA, Yun CHC, Khurana S, & Donowitz M (1994) The plasma membrane Na+/H+ exchanger 2 is an O-linked but not an N-linked sialoglycoprotein: Use of a polyclonal antibody to identify and characterize glycosylation. Biochemistry 33(44):12954-12961.

137. Bizal GL, et al. (1996) Glycosylation of the Na+/H+ exchanger isoform NHE-3 is species specific. Journal of Laboratory and Clinical Medicine 128(3):304-312.

138. Soleimani M, et al. (1996) Inhibition of glycosylation decreases Na+/H+ exchange activity, blocks NHE-3 transport to the membrane, and increases NHE-3 mRNA expression in LLC-PK1 cells. Journal of Laboratory and Clinical Medicine 127(6):565-573.

139. Liu Y, Zaun HC, Orlowski J, & Ackerman SL (2013) CHP1-Mediated NHE1 Biosynthetic Maturation Is Required for Purkinje Cell Axon Homeostasis. The Journal of Neuroscience 33(31):12656-12669.

140. Maley F, Trimble RB, Tarentino AL, & Plummer Jr TH (1989) Characterization of glycoproteins and their associated oligosaccharides through the use of endoglycosidases. Analytical Biochemistry 180(2):195-204.

141. Vagin O, Kraut JA, & Sachs G (2009) Role of N-glycosylation in trafficking of apical membrane proteins in epithelia pp F459-F469.

142. Kanno T, Yaguchi T, Nagata T, Mukasa T, & Nishizaki T (2010) Regulation of AMPA Receptor Trafficking by O-Glycosylation. Neurochem Res 35(5):782-788.

APPENDIX A

Endomembrane (Na^+, K^+)/H^+ exchanger glycosylation affects the stability and resident vesicle pH

Mark Jacunski, Alina Ilie, Annie Boucher, John Orlowski

The previous chapters explored how NHE9 may fit into the greater context of cellular physiology. In the first chapter, we investigated seven mutations, six of which have been associated with autism and one which is a putatively ion exchange deficient variant, identified by homology. We found that the mutations tended to exhibit some defects, whether it be in pH regulation or trafficking, but that these effects were not directly related with one another. In the second, we sought to confirm a putative interaction with phospholipase D 3, which we believe has potential to be important for neurodevelopment. In this section, we investigate the effects of glycosylation on both NHE6 and NHE9. Some NHE6 mutants – particularly those that are also associated with neurodevelopmental conditions – yield variants which are minimally glycosylated. Given that the biochemical nature of the glycosylation and the properties it may confer onto NHE6 and NHE9 are unknown, we sought to determine how glycosylation affects the maturation, stability, localization, and otherwise the function of these alkali cation/proton exchangers.

Introduction

Glycosylation is among the most prominent of post-translational modifications of a wide variety of proteins (129, 130). Glycosylation largely occurs as a sophisticated sequence of oligosaccharide additions and manipulation as proteins pass through the endoplasmic reticulum and Golgi apparatus (129, 131). Here, glycosylation seems to play roles in protein folding; misfolded and inappropriately glycosylated proteins are selectively eliminated or otherwise trafficked to degrade (129, 131). The endoplasmic reticulum-associated degradation pathways are a prominent example of misfolded protein elimination (132). However, glycosylation can also be permissive or facilitative to other aspects of a protein's lifespan. Even for mature proteins, glycosylation can affect the folding and stability. For instance, A Distintegrin And Metalloproteinase 8 (ADAM8), which plays important roles in the biology of triple-negative breast cancers, requires glycosylation of several key asparagines for both appropriate maturation and trafficking towards the cell surface, rather than towards the lysosomes for degradation (133). Glycosylation can play such roles because it influences how soluble protein domains are and what interactions the proteins can take part in, and it can thereby influence not only the stability but also other aspects of protein function, such as trafficking or enzymatic activity (129). One particularly vivid example lies in the loss of glycosylated residues of the epidermal growth factor receptor, whose ability to dimerize and thus auto-activate becomes greater with less glycosylation (134). Increased epidermal growth factor signaling favours proliferation and migration, among other processes, and a loss of glycosylation has been shown to facilitate tumour malignancy (134).

Many paralogs of the alkali cation proton exchanger (NHE, also known as SLC9A) family are asparagine-linked (nitrogen atom in the amide group) glycosylated and/or O-linked (oxygen atom in serine or threonine) glycosylated (22): NHE1 is both N- and O-glycosylated (135), NHE2 is only O-glycosylated (136), whereas the glycosylation of NHE3 depends on the species (137). In NHE3 in particular, one report suggested that glycosylation facilitated NHE3 trafficking and ion exchange function (138). However, the authors made use of tunicamycin to pharmacologically inhibit all glycosylation, which stresses the cell and confounds the conclusions. Conversely, a recent investigation found that calcineurin homologous protein 1 facilitates the glycosylation and

trafficking of NHE1 in Purkinje neurons and that this process is necessary for the homeostasis of those cells (139). Whether the glycosylation itself mediates these effects remains obscure. Hence, overall the roles of glycosylation on NHE family members are unclear or unknown, and it is possible that in some cases glycosylation is a vestige either for blocking biochemical interactions and/or for stabilization.

Two paralogs of the NHE family recently linked to neurodevelopmental conditions, NHE6 and NHE9 appear to be glycosylated but with unknown consequences. While the glycosylation of NHE6 has been shown to be asparagine-linked (72), not much is known about the oligosaccharide linkages or other post-translational modifications that explain why NHE9 separates into several bands when run by reducing, denaturing polyacrylamide gel electrophoresis. NHE6 and NHE9 share 58% similarity at the level of the polypeptide sequence and indeed one glycosylation site is well-conserved between them. Importantly, some of the mutations in NHE6 that have been linked to intellectual disability do not become fully glycosylated yet are able to persist to some extent, albeit with major defects in both structure and function (74, 77). It is unknown whether some of the defects which the mutated NHE6 exhibits are due to glycosylation directly, or rather through other structural changes incurred as a result of the mutations. Thus far, none of the alterations in NHE9 function that have been associated with neurodevelopmental conditions have been suggested to involve changes in glycosylation. Nonetheless, it is of interest to determine whether glycosylation plays a significant role in the folding of NHE6 and NHE9 or perhaps in other aspects of their function, such as trafficking and ion exchange, and how their glycosylation may play a role in neurodevelopment.

Materials and Methods

Reagents

All chemical compounds were purchased from Bioshop Canada or Thermo Fisher Scientific, unless otherwise indicated. Restriction endonucleases and VENT® polymerase were purchased from New England Biolabs. Small interfering RNA pools were purchased from GE Healthcare: siGENOME SMARTpool of either negative control #2 (UAAGGCUAUGAAGAGAUAC, AUGUAUUGGCCUGUAUUAG, AUGAACGUGAAUUGCUCAA, UGGUUUACAUGUCGACUAA), NHE6

(GUUCAAAUCUAUUGGAAUC, GAAACCGGCCUUGCUAUGA, GAUGAUGUUUGCUGGUCUU, UAUAAGGGUUGGUGUUGAU) or NHE9 (CAACAUCAAUCCUCAUCAA, GAUAGUUGCUGUUCUCUUC, GAUGUGGAAUGCAUUGUAA, CAACUCUGCUGGUUAAUAU). Bafilomycin A1 was purchased from LC Laboratories. Rabbit polyclonal antibody to NHE9 was generated by injecting rabbits with affinity-purified glutathione S-transferase (GST)-tagged NHE9 residues p.581-645, collecting serum, and affinity-purifying as described elsewhere (85). Rabbit polyclonal antibody against NHE6 was generated similarly, as described elsewhere (85).

Cell culture

Cells were grown on polystyrene plates (BD Falcon) in humid air at 37 °C and 5% CO_2. HeLa and AP-1-clone Chinese Hamster Ovary cells lacking plasmalemmal alkali cation/proton exchange activity (29) were maintained in alpha modification of Eagle's minimum essential medium (αMEM) (Invitrogen) at 10% fetal bovine serum (Invitrogen) and 1% penicillin/streptomycin (Invitrogen), 25 mM $NaHCO_3$ (pH 7.4), henceforth referred to as serum-supplemented medium. HeLa were used until passage 19 and AP-1 cells were used to passage 13. For plating onto glass coverslips, glass coverslips were coated with poly-L-lysine (Sigma) (37 °C 2 h to overnight with 1 mg/mL poly-L-lysine in water, followed by four water washes) for HeLa cell culture, and coated with fibronectin (Sigma) for AP-1 cell culture (37 °C for 2 h or overnight at 4 °C with 375 µg/mL fibronectin in phosphate buffered saline [PBS], followed by four PBS washes). For live-cell imaging, cells were transferred to HEPES-buffered (i. e., CO_2 independent) DMEM between 12 and 24 h prior to imaging. For tunicamycin (purchased from Sigma) treatments, AP-1 cells were fed with either 1 µL dimethylsulfoxide (DMSO) per mL media or 1 µL of 1 mg/mL tunicamycin in DMSO per mL media 5 h post-transfection, and once again after incubation in normal growing conditions overnight.

Plasmids and molecular cloning

Human NHE6 was cloned out of a human brain cDNA library and a hemagglutinin tag was added to the carboxy terminal tail using polymerase chain reaction (PCR) methodology, and was inserted it into mammalian expression vector pcDNA3.1 using the restriction endonucleases *HindIII* and *XbaI*. Similarly, NHE6 was also inserted into pAc-GFP-N1 using the restriction

endonucleases *HindIII* and *XhoI*. Human NHE9 was cloned out of a human brain cDNA library and further polymerase chain reaction added a hemagglutinin tag (YPTSCPSYAS) to the carboxy terminal tail of NHE9, and inserting it into pcDNA3.1 (Invitrogen) using the restriction endonucleases *KpnI* and *XbaI*. Alternatively, NHE9 was also inserted into pAc-GFP-N1 (ClonTech) using the restriction endonucleases *KpnI* and *BamHI*, creating a carboxy terminal fusion with green fluorescent protein (GFP). In addition, this vector was further modified by inserting monoclonal Cherry fluorescent protein (ChFP) between the sites for *BamHI* and *NotI*, replacing GFP. Mouse Nhe9 cDNA was obtained from Thermo Fisher Scientific and was cloned into a pcDNA3.1 vector with a carboxy terminal HA fusion between the restriction endonuclease sites *HindIII* and *XbaI*. Mutants were generated by two-step polymerase chain reaction-based mutagenesis and sub-cloned to the same three fusions: HA, GFP, and ChFP.

Plasmid transfection of HeLa cells

Plasmids were transfected into HeLa cells when grown to 10-40% confluence using liposomal-mediated FuGENE6 (Promega) transfection. Transfection mixtures were prepared in approximately one twelfth of the cell media volume of αMEM, according to manufacturer protocols. Four µg of DNA were transfected for 60-mm dishes used in the flow cytometry-based endocytosis assay. In brief, for every microgram of plasmid DNA, 3 µL of FuGENE6 was first mixed into the serum-free media and allowed to stand for 5 min. After, plasmid DNA was added and the tubes were gently mixed. Following an additional 20 min incubation, transfection mixtures were added to cells. Cells were fed after overnight incubation in normal growing conditions.

Plasmid transfection of AP-1 cells

AP-1 cells were transfected when at 20-70% confluence, depending on the experiment. Lipofectamine2000 (Life Technologies) transfection mixtures were prepared in approximately one fifteenth of the cell media volume of serum-free αMEM for AP-1 cells, according to manufacturer protocols. Cells in 35-mm dishes were transfected with 1 µg of DNA. Cells used in imaging were plated on 18-mm coverslips for which 0.5 µg of DNA was used. Briefly, for every µg of plasmid DNA, 2.5 µL of Lipofectamine2000 was first mixed into the serum-free media and allowed to stand for 5 min. Plasmid DNA was subsequently added and the tubes were gently

flicked to mix. After an additional 20 min incubation, transfection mixtures were added to cells bathed in serum-free αMEM. Cells were fed after 5 h of incubation in normal growing conditions.

Lysis of Mammalian Cell Cultures and Protein Detection

Cells were washed twice with ice-cold phosphate buffered saline (PBS) pH 7.4 and scraped into immunoprecipitation buffer (PBS, 0.25% sodium deoxycholate, 0.5% Nonidet-P40, and protease inhibitor cocktail [Roche]). After incubating at 4 °C for 30 min, lysates were clarified by centrifuging at 16,100 x *g* for 20 min at 4 °C. Samples were then taken for protein concentration measurement (Biorad DC™ Protein Assay Kit), and for total lysate samples. Laemmli loading buffer (0.1 M Tris pH 6.8, 25% glycerol, 3.7% SDS, 100 mM dithiothreitol [DTT]) was added to all samples for protein separation (total lysates and beads by 9% acrylamide sodium dodecyl sulfate poly acrylamide gel electrophoresis (SDS-PAGE). Gel contents were transferred onto Immobilon-P (Millipore) membranes, blocked with 5% skim milk PBS, and blotted with the appropriate primary antibodies in 5% skim milk 0.1% Tween-20 PBS (mouse monoclonal anti-HA 1:5000 [Covance] or rabbit polyclonal anti-NHE9 1:1000 [generated in-house]), washed four times with 0.1% Tween-20 PBS, then blotted with either goat anti-mouse IgG constant fragment conjugated to horseradish peroxidase (Jackson ImmunoResearch) at 1:5000 dilution or goat anti-rabbit IgG constant fragment conjugated to horseradish peroxidase (Jackson ImmunoResearch) at 1:10000 dilution. Detection was carried by providing substrate with the ECL™ blotting detection reagents (GE Healthcare), and using traditional film-based exposure and development methods. Developed films were scanned using the “Scan Film” function from HP Solution Center and a HP ScanJet G4050.

Endoglycosidase treatment

AP-1 cells transiently transfected to express either human or mouse NHE9 were washed thrice with ice-cold PBS and collected in a small volume of PBS (i. e., for 35-mm dish, 0.3 mL). Cells were pelleted by centrifuging at 10,000 x *g* for 4 min at 4 °C, the supernatant being discarded. Cells were subsequently resuspended in 200 µL of sucrose dissociation solution (250 mM sucrose, 10 mM HEPES, 1 mM ethylenediaminetetraacedic acid [EDTA], protease inhibitor cocktail, pH 7.5)

and passed fifteen times through at 26.5-gauge needle. Post-nuclear supernatants were obtained by centrifuging samples at 700 x *g* for 15 min at 4 °C.

Post-nuclear supernatants from brain regions (cortex, hippocampus, or cerebellum) from 3 week-old mice were obtained by homogenizing every 10 mg of tissue in 100 µL of sucrose dissociation solution by using a mortar and pestle. Homogenates were rocked overnight at 4 °C then sonicated for 1 min three times with 1 min of cooling in between. Again, solutions were incubated overnight at 4 °C with rocking. Similar to cell culture homogenates, solutions were subsequently passed fifteen times through a 26.5-gauge needle and post-nuclear supernatants were obtained by centrifuging samples at 700 x *g* for 15 min at 4 °C.

From post-nuclear supernatants, a membrane fraction was obtained by centrifuging at 100,000 x *g* for 30 min at 4 °C, discarding the supernatant. Pellets were resuspended in 70 µL sucrose dissociation solution with rocking overnight in addition to micropipetting. Protein concentrations were measured using the BioRad DC Protein Assay Kit and up to 60 µg of protein was diluted into a total 54 µL of sucrose dissociation solution. Six µL of denaturing buffer (0.5% SDS, 1% β-mercaptoethanol) was added to this solution and the mixture was incubated for 20 min at 37 °C. Each 60-µL sample was divided to three reaction tubes, holding 15 µL of the sample in addition to one of: 5 µL water; 1 µL endo-B-N-acetylglucosaminidase H (EndoH), 2 µL G5 buffer (50 mM Na-citrate, pH 5.5), 2 µL water; or 1 µL peptide-N-glucosidase F (PNGase F), 2 µL G7 buffer (50 mM NaH_2PO_4, pH 7.5), 2 µL NP-40. Reactions were incubated at 37 °C for 3 h.

To each 20-µL reaction mixture, 8 µL of 2% Nonidet P-40, 1% Na deoxycholate in PBS was added in order to facilitate the solubilisation of membrane proteins. These mixtures were incubated at 4 °C for 30 min and then clarified by centrifuging at 16,100 x *g* for 20 min at 4 °C, retaining the supernatant. Finally, sample proteins were loaded, separated, and detected as described in the section on mammalin cell culture lysis.

Cell-surface biotinylated protein pull-down

Forty-eight hours after transfection, cells were washed twice with ice-cold PBS 1 mM $MgCl_2$ 0.1 mM $CaCl_2$ pH 8.0 (PBS-CM) then incubated with 0.5 mg/mL sulfo-NHS-SS-biotin (ThermoScientific) for 30 min at 4 °C in the dark. Afterwards, cells were washed once with PBS-CM, twice with PBS-CM 50 mM glycine, and twice with PBS prior to scraping into

immunoprecipitation buffer. Clarified cell lysates and samples were obtained as described in the section on mammalian cell lysis. Equal amounts of protein were diluted to equal volumes and loaded onto 100 µL thrice pre-washed 50% NeutrAvidin bead (ThermoScientific) slurry. Following 2 h of rocking at 4 °C, lysate-bead colloids were washed four times with 650 µL of immunoprecipitation buffer, centrifuging at 1,500 x *g* for 4 min at 4 °C to remove supernatant. To elute proteins from beads, beads were incubated with 50 µL Laemmli protein loading buffer for at least 30 min and then centrifuged at 16,100 x *g* for 5 min to obtain eluent supernatants.

Laser-scanning confocal fluorescence microscopy and analysis

Following two washes with PBS, cells were fixed in 4% formaldehyde in PBS pH 7.4 for 20 min. For immunocytochemistry, cells were washed thrice with PBS and permeabilized for 20 min with 0.1% saponin in PBS pH 7.4. Permeabilized cells were washed then blocked with coverslip staining solution (0.01% saponin, 0.4% glycine, 10% goat serum in PBS) by incubating for 45 min. Primary antibodies were diluted into the same solution and incubated with the cells for 1 h at room temperature or overnight at 4 °C (rabbit polyclonal anti-HA [Abcam] diluted at 1:2000, 3E10 mouse monoclonal anti-MYC tag [Millipore] diluted at 1:200). After four washes with coverslip staining solution, secondary antibodies were diluted into the same solution and left to bathe the cells for 1 h at room temperature protected from light (all AlexaFluor-conjugated secondary antibodies [Molecular Probes] were diluted at 1:2000, in particular, goat anti-rabbit IgG constant fragment conjugated to either AlexaFluor488 or 568). Cells were washed thrice with PBS and once with water prior to mounting onto glass slides in Aqua Poly/Mount mounting medium (Polysciences). Slides were imaged after overnight drying at room temperature protected from light. A Zeiss laser-scanning confocal microscope 710 and ZEN 2011 software were used for image acquisition. Each experiment made us of the same acquisition parameters. Briefly, z-axis images were separated by 0.3 µm, at an x-y sample pixel size of 0.54 µm by 0.54 µm. Images were acquired as an average of two 12-bit images. Only low-to-medium-expressing cells were chosen for acquisition.

For images displayed in figures here, channels were manually thresholded to better display results: digital offsets were removed and channel maxima lowered to scale to the range of signals in the channel, leaving a small population of oversaturated pixels.

Flow cytometry-based transferrin uptake assay

HeLa cells in 60-mm polystyrene dishes (BD Falcon) were serum-starved 48-hour post-transfection by washing with then incubating in 4 mL serum-free αMEM for 2 h in normal growing conditions. Transferrin conjugated to AlexaFluor633 (Tfn-Alexa^{633}) (Molecular Probes) at 10 µg/mL in 2.5 mL was loaded onto cells in serum-free αMEM for 10 min, unless otherwise noted, in normal growing conditions. Immediately following loading, cells were washed with 4 mL αMEM 10% FBS 1% penicillin/streptomycin and then incubated in 4 mL of serum-supplemented αMEM for 1 min in normal growing conditions. Following two 3-mL washes with PBS, cells were incubated with 0.5 mL 10 mg/mL trypsin (Invitrogen) in PBS for 7 minutes at 37 °C. Cells were resuspended by adding 3.5 mL serum-supplemented αMEM and then centrifuged at 200 x *g* for 5 min. The supernatant was aspirated and the cell pellets were resuspended in 0.5 mL PBS, adding 5 µL 7-aminoactinomycin D (7AAD, purchased from Affymetrix eBioscience) to each tube. A BD LSRII flow cytometer and BD FACSDiva software were used for data acquisition and analysis. For each trial, the following compensation controls were used to optimize acquisition and analysis: non-transfected, GFP-transfected, Tfn-Alex^{633}-loaded, and 7AAD-stained cells. The following lasers and filters were used: 488-nm laser (488/10-nm filter for side scatter, 695/40-nm filter for 7AAD, 530/30-nm filter for GFP); 633-nm laser (660/20-nm filter for AlexaFluor633). Finally, total cellular Tfn-Alexa^{633} medians were obtained by excluding intensities in this channel which were exhibited by the compensation controls that were not loaded with Tfn-Alexa^{633}. For four independent trials, the median total cellular Tfn-Alexa^{633} fluorescence for 10^4 live, transfected cells were compared relative to all non-transfected cells from the same trial, i. e. from each plate that was from the same batch of processed plates. The relative values from four independent experiments were statistically analysed. Homogeneity of variances was analysed by a Bartlett test, indicating that variances were homogenous, which validated use of parametric type II one-way ANOVA for statistical analysis.

Fluorescence ratiometric imaging analysis for intracellular pH measurements

HeLa and were grown on poly-L-lysine-coated glass coverslips at normal growing conditions and transfected approximately 24 h after plating as described in the section on plasmid transfection of HeLa cells. Following overnight incubation with the transfection mixture, media was changed

to 10% fetal bovine serum-supplemented HEPES-buffered DMEM and the cells were grown for an additional night in 0% CO_2 37 °C humid air.

To load the cells with transferrin, cells were serum-starved with a with serum-free HEPES-buffered DMEM wash and incubation in serum-free HEPES-buffered DMEM for 40 min in normal growing conditions, changing to fresh medium after 20 min. Next, fluorescein isothiocyanate-conjugated human transferrin (Molecular Probes) at 1 µg/µL in serum-free HEPES-buffered DMEM was placed on the cells for the indicated amount of time in 0% CO_2 humid air at 37 °C. Cells were subsequently washed twice with 10% fetal bovine serum-supplemented HEPES-buffered DMEM, keeping the second wash for a thirty-second chase period, to allow for both internalization and unbinding of remaining plasmalemmal Tfn_{FITC}. Following a wash with a modified Ringer's solution (140 mM NaCl, 5 mM KCl, 10 mM HEPES, 10 mM glucose, 1 mM $CaCl_2$, 1 mM $MgCl_2$, pH 7.3) cells were imaged in the same solution at room temperature within five minutes for time-points, and within thirty minutes for pH calibration. A Carl Zeiss MicroImaging AxioObserver Z1 inverted microscope using a plan-Apochromat 63X/1.4 numerical aperture oil immersion objective and equipped with a X-Cite 120Q fluorescence illumination system (Lumen Dynamics Group Inc.) and a Evolve 512 electron multiplying charged-coupled device camera (Photometrics Technology) with MetaFluor software (Molecular Devices) was used for image acquisition and vesicle region of interest selection. Using 440-, 490-, and 570-nm lasers and acquiring with a long-pass 525 nm filter allowed for optimization of both high signal and low channel cross-talk while imaging FITC and ChFP. For each time point and construct, three images were acquired and 20-275 vesicles selected, depending on the time point and the cell. Distributions of pH values were analysed using Origin 7.5 software (OriginLab).

Standard curves for the experiments were also obtained as described elsewhere (112), with some modifications. In brief, cell culture and imaging was carried out in the same way: cells were imaged in potassium-rich buffer (10 mM NaCl, 10 mM glucose, 135 mM KCl, 1 mM $CaCl_2$, 1 mM $MgCl_2$), buffered with MES for pH's under 6.0 or with HEPES for pH's at 6.0 and above, and pHed using either HCl or KOH. However, proton concentration was equilibrated by adding a number of proton ionophores in addition to 10 µM nigericin immediately prior to imaging: 10 µM monensin, 25 µM carbonyl cyanide m-chlorophenyl hydrazine (CCCP). Furthermore, the V-

ATPase was inhibited through the addition of 0.4 μM bafilomycin. Cells were imaged at pH 4.5, 5.5, 6.0, 6.3, 6.6, 7.2, and 8.3, thrice independently for untransfected HeLa cells, and twice each for ChFP-transfected and NHE9-ChFP-transfected cells.

Results

NHE6 and NHE9 share 59% protein sequence similarity and separate into multiple bands when immunoblotting after sodium dodecyl sulfate polyacrylamide gel electrophoresis (SDS-PAGE) after reductive conditions (dithiothreitol being in the loading buffer). NHE6 was previously shown to be N-glycosylated (72) but the source of multiple bands for NHE9 has not been determined. To this end, AP-1 cells – a cell line derived from Chinese hamster ovary cells which lacks plasma membrane alkali cation/proton exchange activity – transiently expressing human or mouse NHE9 were put through multiple fractionation steps (see methods and materials section) and treated with endoglycosidase H (EndoH) or peptide-N-glycosidase F (PNGase F) following denaturation. Endoglycosidase H cleaves within the core of asparagine-linked oligosaccharides, leaving fully glycosylated protein intact, whereas peptide-N-glycosidase F removes complex asparagine-linked oligosaccharides by breaking the bond to the protein's asparagine (140). As expected, both human (**Figure 1A**) and mouse NHE9 (**Figure 1B**) are core glycosylated and further matured: the core-glycosylated band shifts downwards with endoglycosidase H treatment, but the fully-glycosylated band does not; both bands shift downwards to an unglycosylated form with peptide-N-glycosidase F treatment. However, there are more bands than expected than for a simple distribution of unglycosylated, core glycosylated, and fully-glycosylated forms, indicating that NHE9 may have other post-translational modifications (**Figure 1A, B**). Corroborating these data from heterologous expression in AP-1 cells are endoglycosidase treatments from mouse brain lysates of the hippocampus, cerebellum, and cortex (**Figure 1C**). As in transiently-transfected immortalized cells, the slowest-running band of NHE9 can be quickened by treatment with PNGase F, but not EndoH. In these tissues there appear to be undetectable amounts of core-glycosylated NHE9, as even in the over-exposed immunoblots shown here there is no signal whose migration is affected by EndoH treatment. Again, it is possible that the remaining bands here are made up of NHE9 with alternate post-translational modifications or are otherwise non-specific (**Figure 1C**).

Glycosylation is used as a marker for trafficking for certain proteins (141, 142). NHE6 and NHE9 are trafficked towards distinct and overlapping pools of early and recycling endosomes (70), but seem to have a small plasmalemmal pool when overexpressed in AP-1 cells, as measured by pull-down of cell-surface biotinylated protein (**Figure 1B**). Interestingly, precluding glycosylation by using an inhibitor of asparagine glycosylation – tunicamycin – does not greatly affect this plasmalemmal pool (**Figure 1B**). In order to investigate the effects of a loss of glycosylation on the function of NHE6 and NHE9 without pharmacologically stressing the endoplasmic reticulum, we searched for putative glycosylation sites using PROSITE and investigated two residues of interest for NHE6 – N128 and N145. By homology, the N128 residue in NHE6 corresponds to the N96 residue in NHE9, which we likewise chose for further investigation. Moreover, we chose to investigate a splice variant of NHE6 which, similarly to NHE9, lacks a short amino acid sequence which contains the second, N145, glycosylation site (**Figure 2A**). Thus far, no known functional difference exists between the longer variant, NHE6v1, and the shorter, singly-glycosylated variant, NHE6v2. Other splice variants exist but these will not be discussed further in this report. For this report, we generated mutant constructs with the glycosylated residues substituted for alanine. In NHE6v1, mutations of only one residue reduced but did not eliminate glycosylation, and accordingly mutating both residues entirely eliminated glycosylation (**Figure 2B**). Similarly, by mutating the only asparagine of interest in NHE6v2 and NHE9 to alanine, we were able to prevent glycosylation of the proteins (**Figure 2B**).

We had observed that NHE6v2 is expressed in much greater amounts than NHE6v1, by immunoblot analysis. However, it tends to retain a core glycosylated form for longer than NHE6v1 (**Figure 3**). We chose to measure the relative maturation – the ratio between the fully glycosylated signal and the total signal – in AP-1 cells to quantify this phenomenon, and to determine whether this is related either to the rate of maturation or perhaps to the larger amount of protein present. Additionally, we investigated the maturation of the single mutations of NHE6v1 to determine whether this curtailed relative maturation was due to the higher expression of NHE6v2 and limited glycosylation capacity or perhaps to facilitated protein folding due to the presence of a second glycosylated residue. We confirmed that NHE6v1 had a marginally faster relative maturation rate than NHE6v2 and we found that the N128A mutation

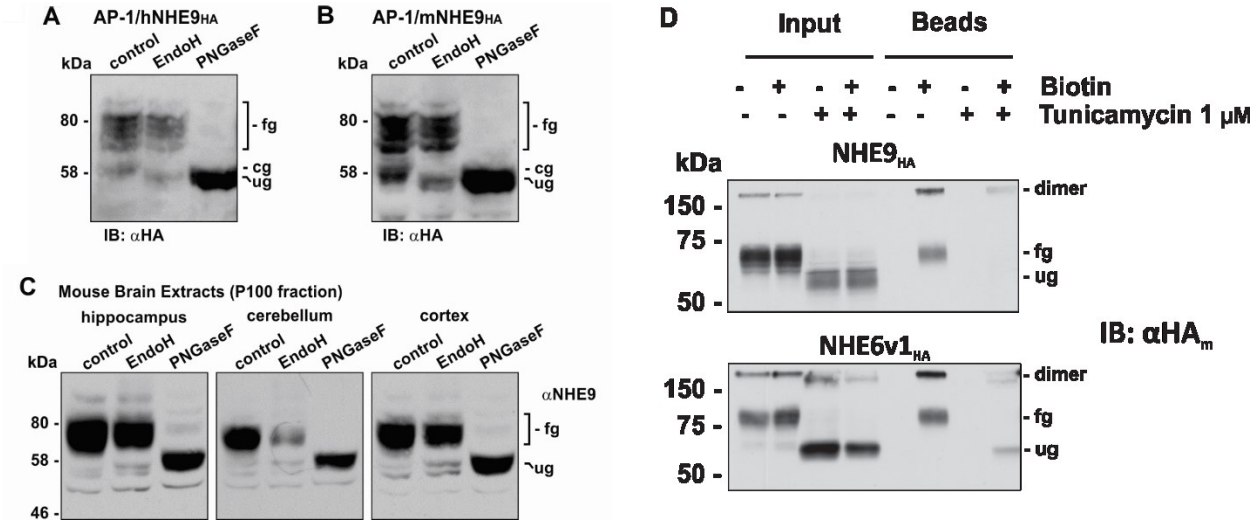

Figure 1: NHE9 is N-glycosylated, and N-glycosylation does not affect NHE6 or 9 plasmalemmal localization. By reducing, denaturing gel electrophoreses NHE9 separates into multiple bands, a fully glycosylated (fg), and a core glycosylated (cg) form, among others. Removal of all oligosaccharides results in an unglycosylated (ug) band. Endoglycosidase treatments of human NHE9 (A) and mouse NHE9 (B) transfected into AP-1 cells indicates that NHE9 is asparagine glycosylated as the asparagine-linked oligosaccharide cleavage enzymes endoglycosidase H, which shifts removes core glycosylations but not full glycosylations, and peptide-n-glycosidase, which removes all such glycosylations, yield the expected shifts in bands. These effects are largely the same in mouse brain extracts (C), although in these tissues there is an undetectable amount of core glycosylated NHE9. The other bands are either due to other post-translational modifications or are otherwise non-specific. (D) Preventing glycosylation by treatment with tunicamycin did not preclude trafficking of NHE9 or NHE6v1 to the plasma membrane in AP-1 cells, suggesting that glycosylation does not significantly affect the structure or function of NHE6 and NHE9.

curtailed this process in NHE6v1. However, the N145A mutation in NHE6v1, which recapitulates the glycosylation pattern of NHE6v2, actually modestly increased the rate of relative maturation. Moreover, NHE9, which shares the single glycosylation site with NHE6v2, was the quickest to achieve full relative maturation (**Figure 3**). While the molecular mechanisms underlying these processes are unclear, our results suggest that increased glycosylation does not necessarily favour quicker maturation. Instead, the singly-glycosylated NHE6v2 may have a slower relative maturation rate due to its strong expression or through other mechanisms.

Many proteins are thought to be stabilized by glycosylation through numerous mechanisms (132): by favouring protein folding; by allowing for higher-order protein structures to be solubilized in water; by permitting biochemical interactions which affect protein function. To determine whether NHE6 and NHE9 were stabilized by glycosylation, we performed a cycloheximide chase assay. Cultures were switched to 150 µg/mL cycloheximide-containing medium forty-eight hours after transient transfection with NHE6 or NHE9, or their mutant forms. This concentration of cycloheximide significantly inhibits protein synthesis at the level of the ribosome. Both NHE6 and NHE9 levels steadily decreased over twenty-four hours whether glycosylated or not (**Figure 4**). Exponential curve fitting (**Figure 4B, D, F**) to densitometrically-quantified immunoblot signal (**Figure 4A, C, E**) indicated that a lack of glycosylation modestly increased the degradation of NHE6 and NHE9.

To determine whether glycosylation was affecting trafficking of NHE9 within the cell, we used laser-scanning confocal microscopy to localize the protein and its mutant form in relation to transferrin, a cargo which traffics through early endosomes to the recycling endosomes (109), and RAB11, a small RAB GTPase which serves as a marker of slow recycling endosomes. The mutant form of NHE9 did not yield a striking difference in co-localization when overexpressed in AP-1 cells, neither with transferrin (**Figure 5A**), nor with RAB11 (**Figure 5B**). Additionally, the colocalization with RAB11 was also not affected by the mutation in HeLa cells (**Supplementary Figure 1**) Therefore, corroborating our cell-surface biotinylation experiment, we conclude that a lack of glycosylation does not impair the intracellular distribution of either NHE9. A limitation of using populations of cells forty-eight hours of transfection is that it is difficult to determine whether one is imaging conditions of net flux or of steady-state.

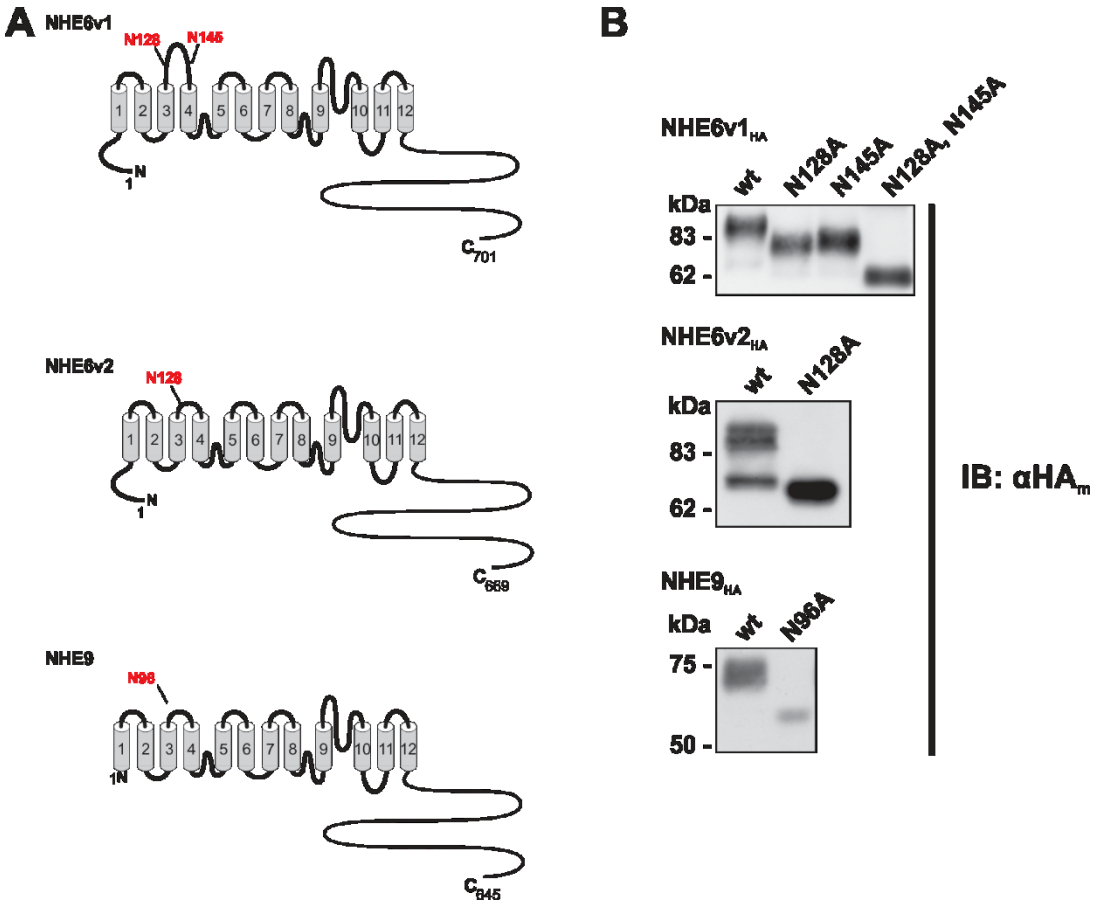

Figure 2: Identification of glycosylated residues. Using a PROSITE scan and homology studies, we identified the putative glycosylation sites as indicated in panel A. Panel B shows the expression of these variant in carboxy terminal hemagglutinin-tagged form in AP-1 cells. Bands migrate quicker, indicating a loss of glycosylation.

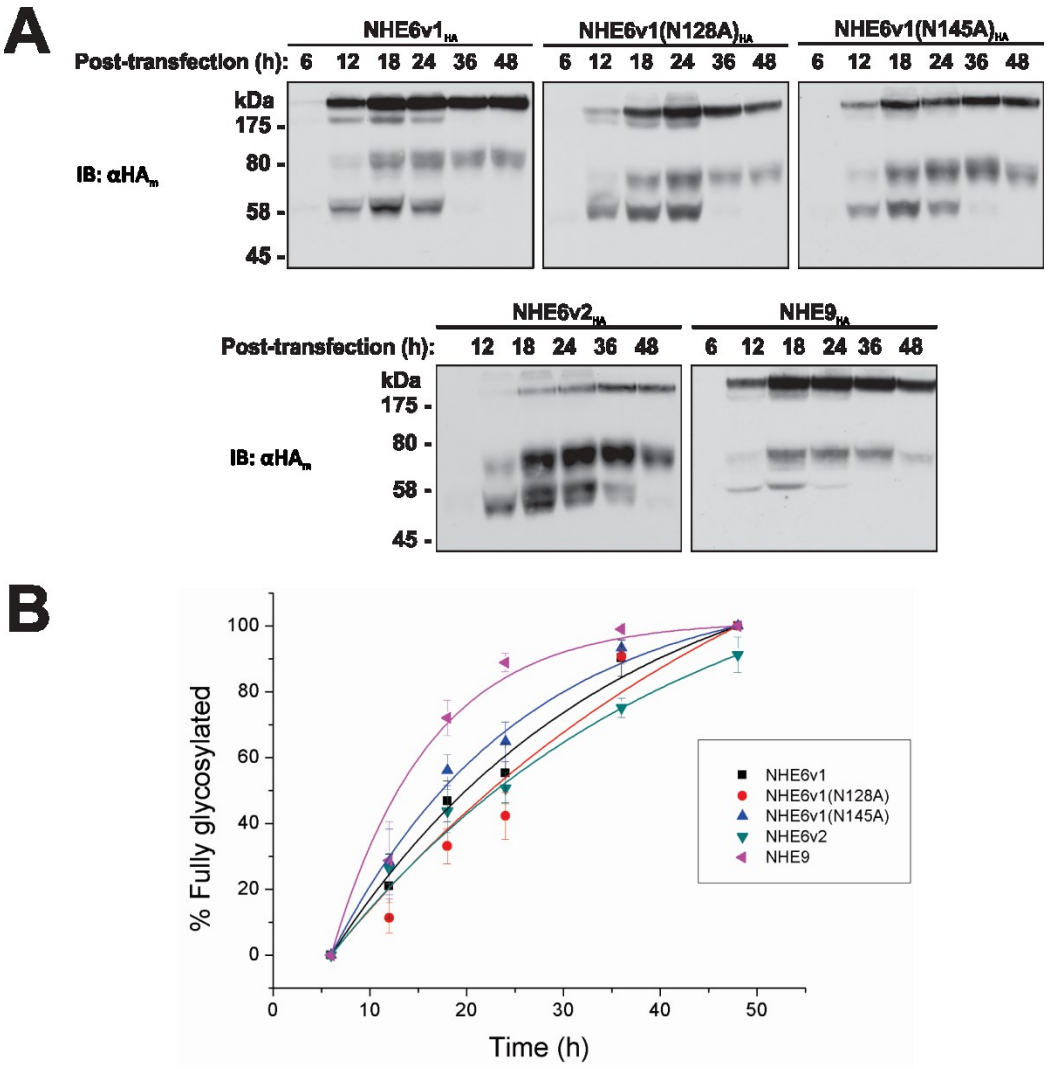

Figure 3: Maturation of glycosylation in NHE6 and NHE9. We tracked the progress of NHE6 and NHE9 synthesis and maturation by lysing cells are intervals after transfection (A). Immunoblot quantification indicates that NHE6v2 retains core and unglycosylated forms minutely longer than the other test proteins (B). While we expected this effect to be recapitulated by the N145A mutation of NHE6v1, we found that it actually increased the relative maturation. Moreover, NHE9 was expected to be more similar to NHE6v2 than to NHE6v1, as it also only contains one glycosylated residue. In contrast, NHE9 appeared to mature significantly faster than all NHE6 variants tested.

While a lack of glycosylation does not affect the intracellular distribution of NHE9, it may still exhibit defects in ion exchange function or scaffolding, particularly in conditions of flux. Since both NHE6 and NHE9 enhance transferrin endocytosis, a function which is thought to be diminished by losing ion exchange function (75, 93), we undertook a flow cytometry-based transferrin endocytosis assay to determine whether the mutations in question affected this aspect of NHE6 or NHE9 function. In this assay, serum-starved HeLa cells transiently transfected with carboxy terminal GFP fusions of NHE6 or NHE9 are loaded with fluorescently-conjugated Tfn-Alexa^{633} for 10 min and stained with 7-actinomycin D (7AAD), selecting for live (7AAD-negative) and GFP-expressing cells from which to record total cellular transferrin fluorescence. We chose HeLa cells because AP-1 cells uptake much less transferrin, reducing the signal-to-noise ratio and the resolution of any changes due to different experimental conditions. Twenty-four hours after transfection, transferrin uptake is enhanced by NHE6v1 and NHE6v2, but this enhancement is not significantly affected by the glycosylated variants (**Figure 6G, H**). For further study, we chose a 10-minute time point because we found that HeLa cells uptake transferrin linearly with time for at least the first 20 min of uptake when measured twenty-four hours after transfection, and this time point yielded more consistent results than the 5 min time point used in previous experiments (74). Forty-eight hours after transfection, both the expression of NHE6$_{GFP}$ (**Figure 6A, C**) and the expression of NHE9$_{GFP}$ (**Figure 6E**) enhanced transferrin uptake, though for the v2 splice variant of NHE6, this effect was not statistically significant (**Figure 6B, D, F**). While for NHE6v1, all the mutants tested yielded slightly lesser enhancements of transferrin uptake, these differences were not statistically significant (**Figure 6B**). Similarly, the unglycosylated variant of NHE9 did not differ in its enhancement of transferrin endocytosis from wild-type NHE9 (**Figure 6F**).

Though measuring intracellular trafficking in populations of cells is enabled by flow cytometry, direct measures of ion exchange across endomembranes remains experimentally limited. Transferrin endocytosis serves as a loose proxy for ion exchange function of both NHE6 and NHE9. However, more direct methods for measuring intracellular compartment pH have been developed using ratiometric imaging analysis (112). Thus, we calibrated our ratiometric imaging analysis in untransfected cells (**Figure 7A**), cells expressing monomeric Cherry

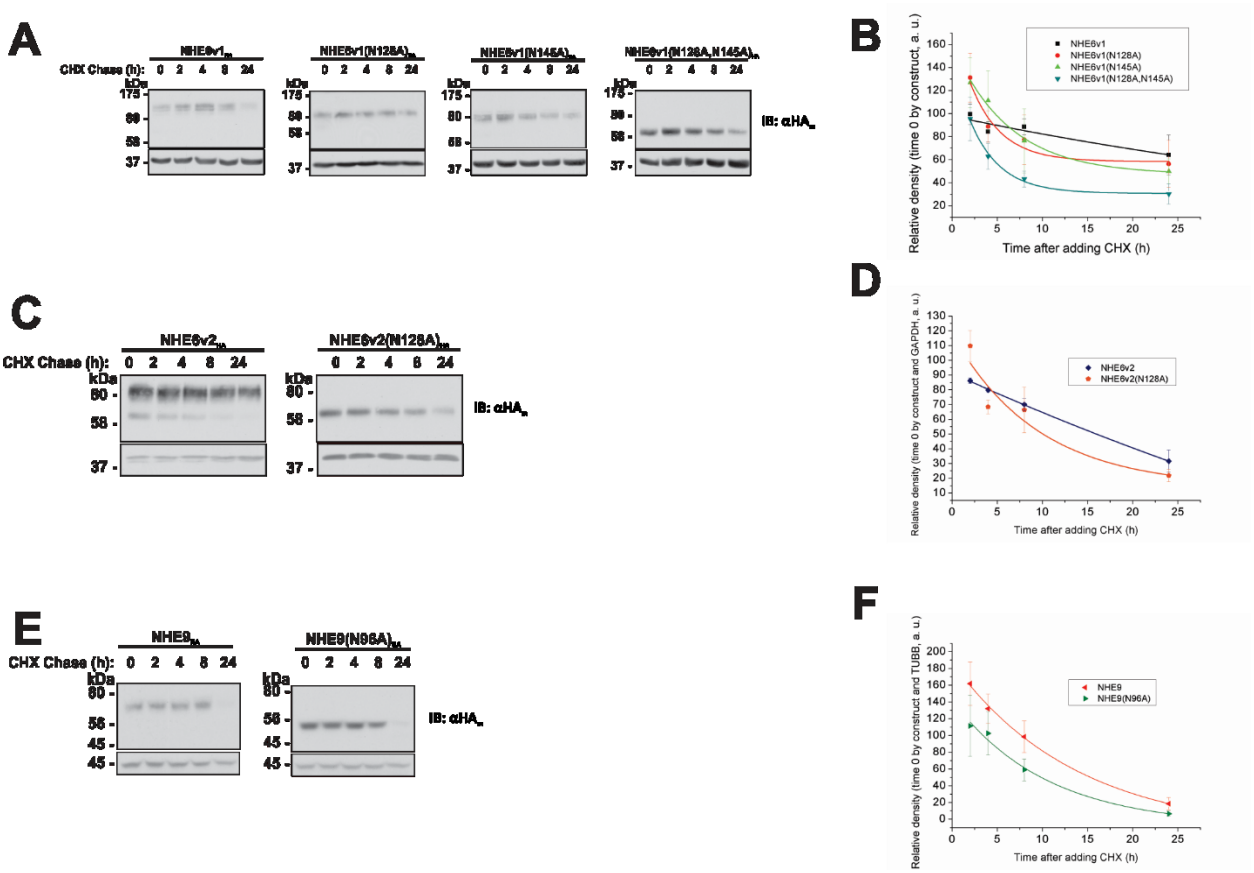

Figure 4: A lack of glycosylation modestly compromises the stability of NHE6 and NHE9. A cycloheximide chase assay inhibits protein synthesis, allowing to track the rate of protein loss while minimizing new protein production. Quantifying immunoblots (A, C, E) and fitting exponential curves using Origin 8.0 (B, D, F) indicated that unglycosylated variants degraded with shorter time constants, i. e. quicker. This is particularly pronounced with NHE6v1 and less so for NHE6v2 and NHE9.

fluorescent protein (ChFP) (**Figure 7B**), and cells expressing NHE9 fused at the carboxy terminus with ChFP (**Figure 7C**) after loading with transferrin conjugated to fluorescein isothiocyanate for 40 min. We then measured the pH of transferrin containing endosomes (colocalized with $NHE9_{ChFP}$, if applicable) in these cells at 2.5, 10 and 40 min (**Figure 7D**). Transferrin is distributed in a relatively acidic, early endosomal lumen at 2.5 min and transitions to a more alkaline lumen as trafficking continues. Just the expression of ChFP led to an apparent acidification of this compartment. Relative to these cells, transferrin vesicle luminal pH was alkalinized when NHE9 was present, and this effect was entirely abrogated by the N96A mutation. However, the molecular mechanisms of this phenomenon are not necessarily due to any change in ion exchange function of the N96A variant of NHE9. Many possible relationships between transferrin uptake and an acidic lumen can be proposed, including altered trafficking patterns.

Discussion

Many proteins which pass through the endoplasmic reticulum and the Golgi apparatus are glycosylated as a part of a protein folding and maturation process (129). Improper glycosylation during these steps can lead to degradation of the proteins through endoplasmic reticulum-associated degradation pathways; glycosylation can serve as a marker of protein folding (132). However, even if or while the improperly glycosylated proteins are able to persist, their structure can be perturbed such that their stability or function are deficient. Numerous members of the mammalian alkali cation/proton exchanger family are glycosylated (23), but the functional consequences of this glycosylation have by and large remained unknown. Hence, we investigated the role of glycosylation in both NHE6 and NHE9, which we found tended to modestly stabilise the proteins.

Both NHE6 and NHE9 have been linked to neurodevelopmental conditions: NHE6 with Christianson syndrome (77); NHE9 with autism (92) and attention deficit/hyperactivity disorder (89). Certain disease-associated mutations in NHE6 such as the deletions 287ES288 and 370WST372 exhibit profound deficiencies in stability and function, concomitant with greatly decreased glycosylation. Our experiments sought to determine the extent to which these

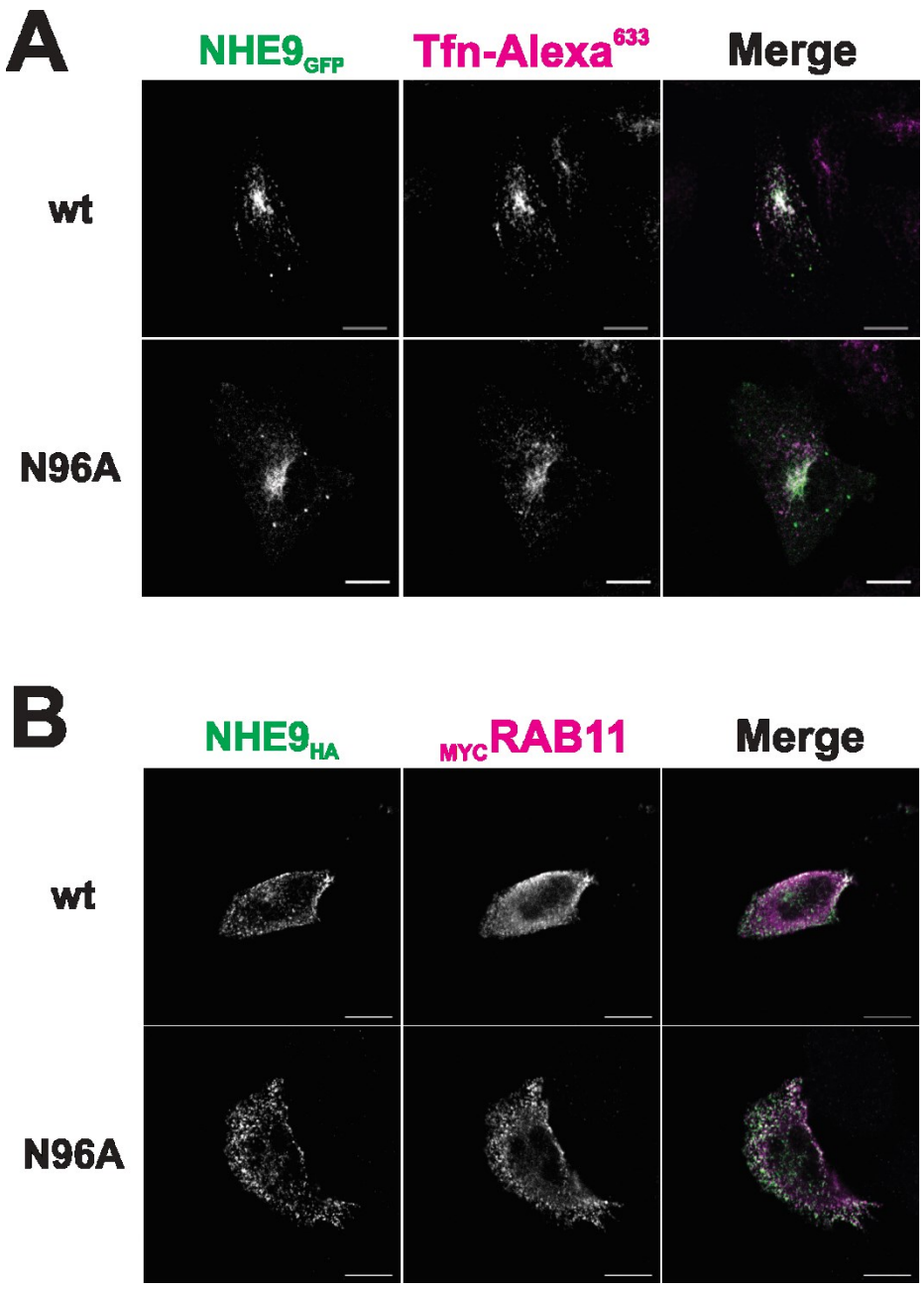

Figure 5: Sub-cellular localization of unglycosylated mutants remains unperturbed in AP-1 cells. Colocalizing transiently-transfected $NHE9_{GFP}$ with either transferrin (A) or RAB11 (B) did not indicate a shift away from the recycling endosomal compartment when the glycosylation site was mutated.

functional consequences could be explained by the diminished glycosylation, rather than to other alterations in protein structure more directly related to the aforementioned mutations.

The highly-similar paralogs NHE6 and NHE9 present an additional interesting point to investigate the functional consequences of glycosylation on endomembrane alkali cation/proton exchangers. These paralogs share 58% similarity at the level of the polypeptide sequence, differing modestly throughout the proteins. One notable difference between the two proteins occurs with glycosylation sites. Compared to NHE9, the primary splice variant of NHE6, NHE6v1, contains a 20-amino acid insertion which grants it an additional glycosylation site (NHE6v1p.N145). Interestingly, the splice variant of NHE6 investigated here, NHE6v2, is similar to NHE9 in missing this glycosylation site, and yet thus far no functional difference has been noted for these two splice variants of NHE6.

NHE6 and NHE9 are emerging as proteins with similar cellular functions: they are present in a subset of early and recycling vesicles, they tend to alkalinize the compartments which they decorate, and they enhance transferrin endocytosis. Conversely, a recent study found that the severity of autism was correlated with both a down-regulation of NHE6 and an up-regulation of NHE9 expression. Our study aimed to investigate whether these paradoxical findings could be explained by the differences in glycosylation of NHE6 and NHE9. We found that while glycosylation does not significantly affect transferrin endocytosis, it does modestly improve protein stability and possibly ion exchange function. Stability was assessed by a cycloheximide chase assay, wherein unglycosylated variants of both NHE6 and NHE9 degraded modestly but significantly quicker than wild-type or partially glycosylated forms. Our measures of function relevant to cellular physiology, however, are somewhat limited. We used transferrin as an archetypal recycling vesicle cargo with many commercially available forms allowing for a wide breadth of experimentations. However, thus far physiologically relevant roles of either NHE6 or NHE9 in transferrin internalization have not been studied, and particularly not in neurodevelopment. Another limitation lies in the measurement of ion exchange function on endomembrane proteins, as we rely on ratiometric wide-field micrograph analysis to measure the pH of vesicles which contain NHE9. It is difficult to dissect the causality of pH changes as it may either be that impairing glycosylation increases the fraction of these proteins that lie in acidic

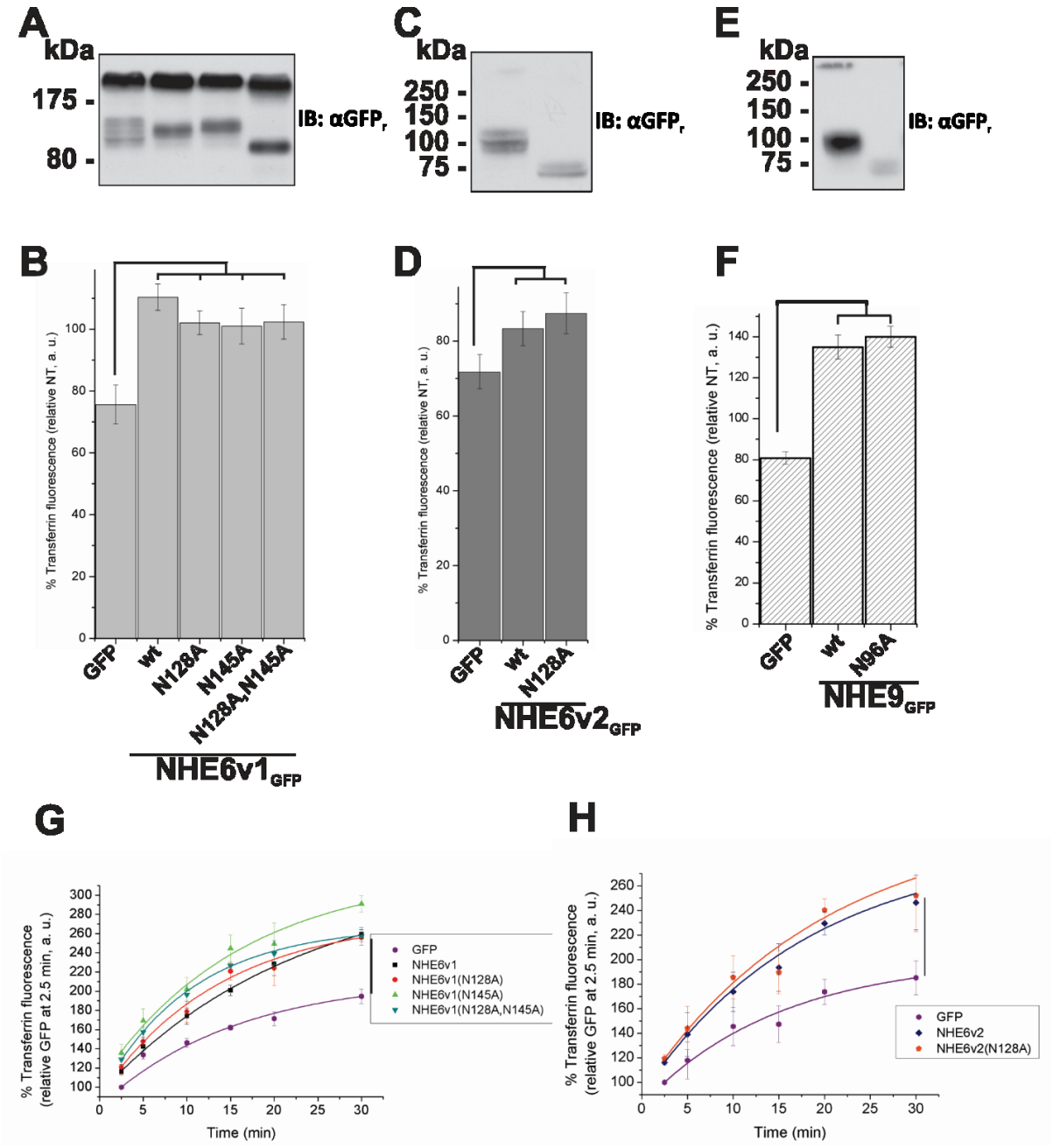

Figure 6: Enhancement of transferrin endocytosis is not affected by glycosylation of NHE6 and NHE9 in HeLa cells. Forty-eight hours after transfection, all of NHE6v1 (A, B), NHE6v2 (C, D), and NHE9 (E, F) enhance transferrin uptake at 10 min, lanes contents correspond to the bar graphs underneath them. This enhancement was not affected by the loss of glycosylation significantly, although NHE6v1 mutants tended to have a lower enhancement than wild-type NHE6v1. We chose a 10-min time point after having measured the time course of transferrin uptake, 24 hours after transfection for both NHE6v1 (G) and NHE6v2 (H). The increase in transferrin is enhanced up at all the studied time points by the expression of NHE6, and this was not significantly affected by the mutations. Here we display exponential curve fittings to reflect a hypothetical steady state that would occur beyond our time course. However, linear curve fittings had similar R-squared values. Data from three independent experiments, error bars represent standard error of the mean, we used one-factor type II ANOVA for panels B, D, and F, and two-factor ANOVA for panels G and H, significance is taken as $p > 0.05$.

vesicles in the degradative pathway, such as late vesicles and lysosomes, or that decreased ion exchange function is responsible for the acidification, or a combination of the two. However, since the sub-cellular localization of NHE9 relative to markers such as transferrin and RAB11 was not greatly affected, we suggest that indeed ion exchange function was affected.

However, we believe a more complicated molecular mechanism underlies our observations. Perhaps there are compartment-specific effects of glycosylation on ion exchange function, but this remains speculative. We can confidently conclude that the glycosylation of NHE6 and NHE9 stabilizes the proteins but does not greatly change how they function in transferrin endocytosis. Whether glycosylation is important for ion exchange in these proteins remains uncertain. The unglycosylated variant of NHE9 is found in more acidic compartments, suggesting a decrease in ion exchange function, or alternatively NHE9(N96A) and transferrin only co-localize in acidic compartments while still permitting for an enhancement in uptake. Importantly, we believe that the lack of glycosylation is contributing to some of the defects observed in neurodevelopmental disease-linked variants of NHE6, but that the mutations themselves are most responsible for the defects in protein function.

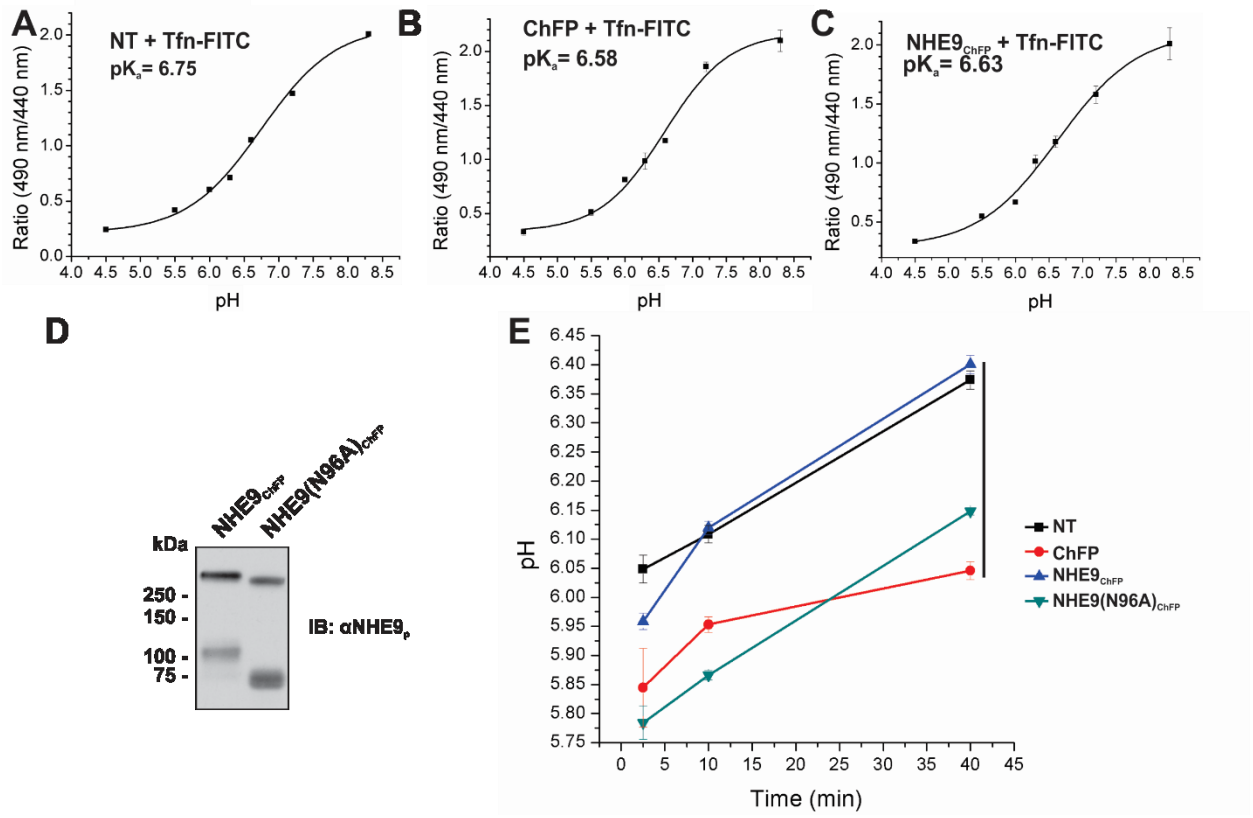

Figure 7: NHE9 alkalanizes transferrin vesicles but unglycosylated NHE9 does not in HeLa cells. Calibrations for ratiometric imaging analysis of transferrin$_{FITC}$ in non-transfected cells (A), ChFP-transfected cells (B), and NHE9$_{ChFP}$-transfected cells (C) are shown. The pH was obtained from regions that contained Tfn-FITC signal, colocalizing with NHE9$_{ChFP}$ signal, if appropriate, at 2.5 min, 10 min, and 40 min (D). We find that as trafficking progresses, the pH alkalinizes. While NHE9 alkalinized vesicles relative to ChFP, the unglycosylated mutant precluded this function. Alkalinization occurred at similar rates in all four cases but remained more acidic for both ChFP and NHE9(N96A)$_{ChFP}$.

Supplemental Data

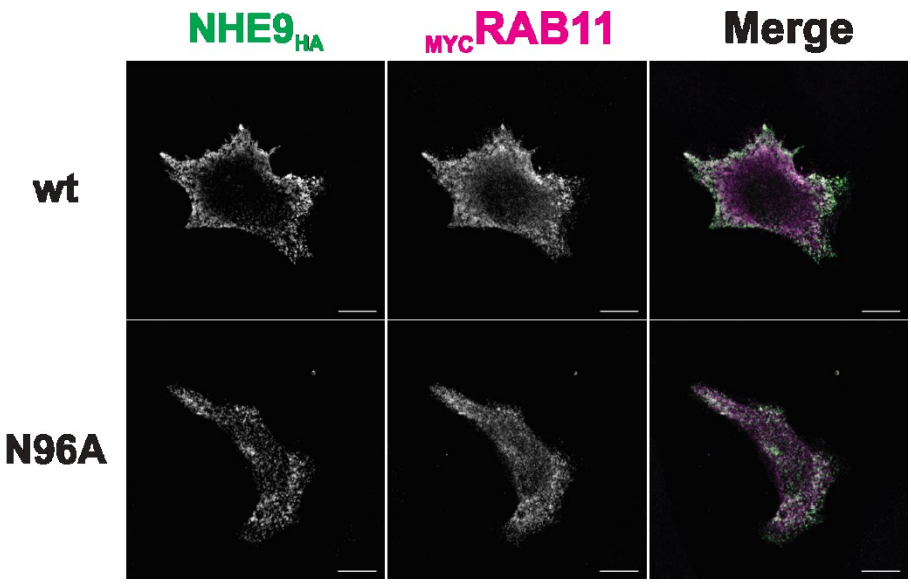

Supplementary Figure 1: Glycosylation does not affect the sub-cellular localization of NHE9 in HeLa cells. Forty-eight hours after transfecting HeLa cells with $NHE9_{HA}$ and $_{MYC}$RAB11, cells were fixed and stained as described in the Materials and Methods section. The unglycosylated variant retained significant colocalization with RAB11, indicating that the sub-cellular localization was not greatly affected.

Supplemental Methods

Plasmid transfection of HeLa cells

Plasmids were transfected into HeLa cells when grown to 10-40% confluence using liposomal-mediated FuGENE6 (Promega) transfection. Transfection mixtures were prepared in approximately one twelfth of the cell media volume of αMEM, according to manufacturer protocols. One µg of DNA was used per 35-mm plate. For 20-mm wells, as was used in for imaging experiments, 0.5 µg of DNA was transfected. For 60-mm plates used in flow cytometry-based endocytosis assays, 4 µg of DNA was transfected. In brief, for every µg of plasmid DNA, 3 µL of FuGENE6 was first mixed into the serum-free media and allowed to stand for 5 min. After, plasmid DNA was added and the tubes were gently mixed. Following an additional 20 min incubation, transfection mixtures were added to cells. Cells were fed after overnight incubation in normal growth conditions.

N. B. References for this appendix are in the preceding section.

APPENDIX B

Supplemental data – figures and protocols

Supplemental Figures

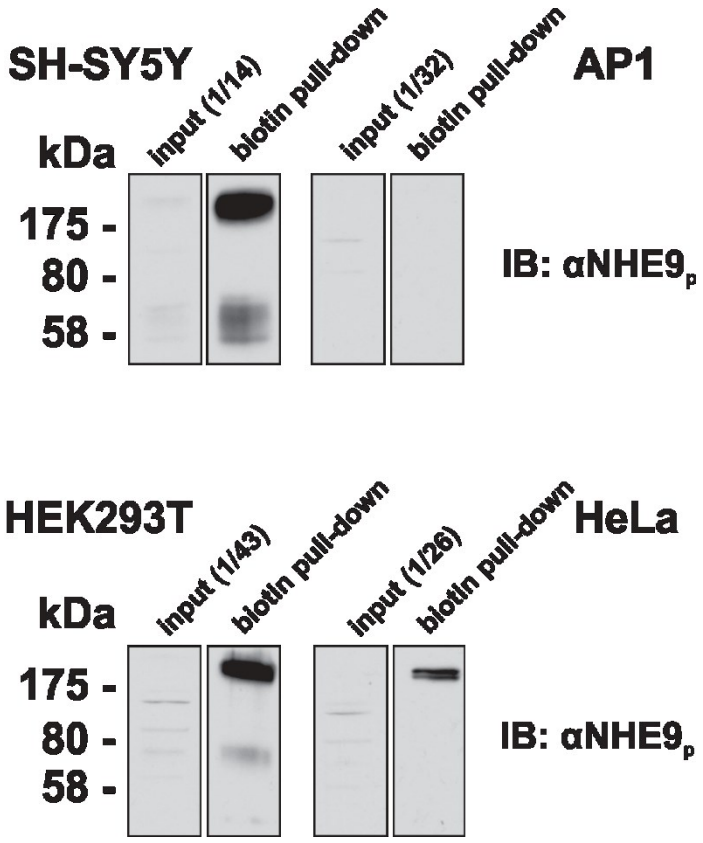

Supplementary Figure 1: Endogenous NHE9 expression and surface presence in common cell lines. All studied cell-lines contain a minute amount of NHE9, though AP-1 cells are Chinese hamster cells, and not human cells and our confidence in our antibody in this species is lesser. SH-SY5Y human neuroblastoma cells (cultured in DMEM/F12 1:1 mixture and 10% fetal bovine serum) and HEK293T cells do exhibit NHE9 immunoblot signal in total lysates while HeLa and AP-1 cells contain miniscule amounts, if any. This pattern is recapitulated at the membrane, in which NHE9 is enriched, wherein SH-SY5Y and HEK293T contain considerably more NHE9 than HeLa or AP-1 cells.

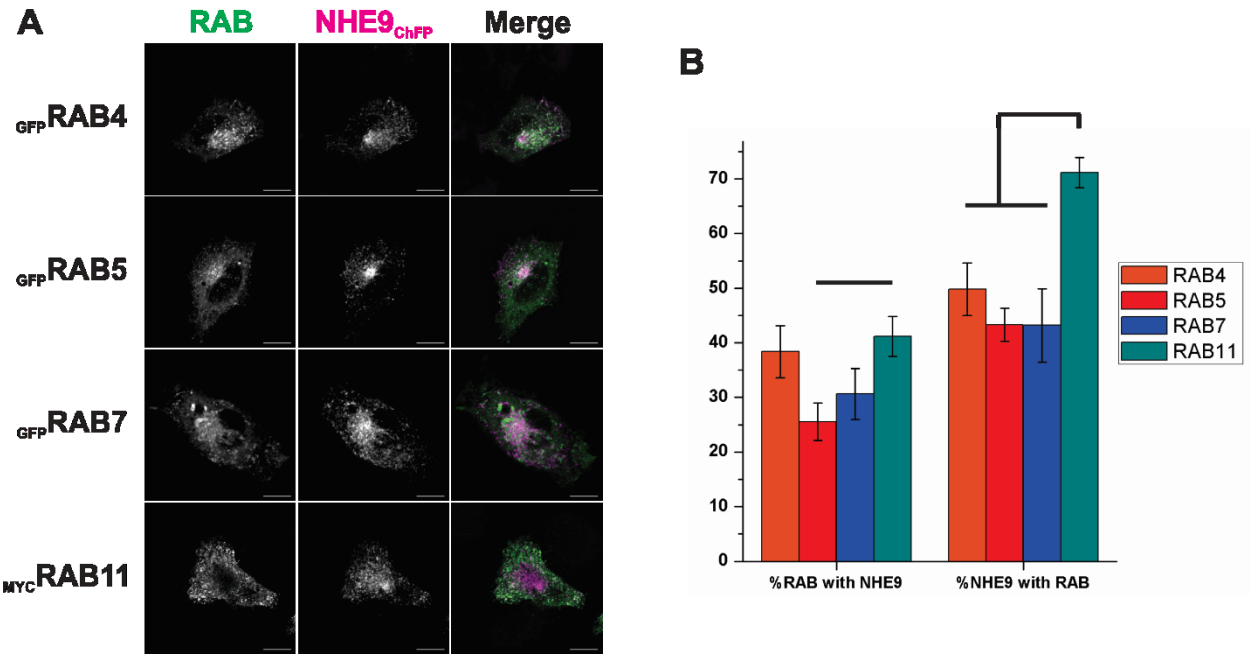

Supplementary Figure 2: NHE9 is present in early and recycling endosomes in AP-1 cells. At least ten micrographs from a total of three independent experiments acquired with identical imaging parameters were used for colocalization analysis. Imaging the green channel was adjusted identically for all RAB11 immunostainings, as the signal was considerably weaker. A representative sample of micrographs is shown in panel A. MYC tag secondary immunostaining was done with goat anti-mouse IgG conjugated to AlexaFluor488. After deconvolution and manual thresholding, Mander's coefficients of coincidence were obtained using Imaris 7.0 software, which recapitulates our qualitative findings (B). NHE9 signal coincides most with RAB11, a slow recycling endosomal marker. Scale bar represents 10 µm. Significant differences indicate $p < 0.05$ by type II one-factor ANOVA.

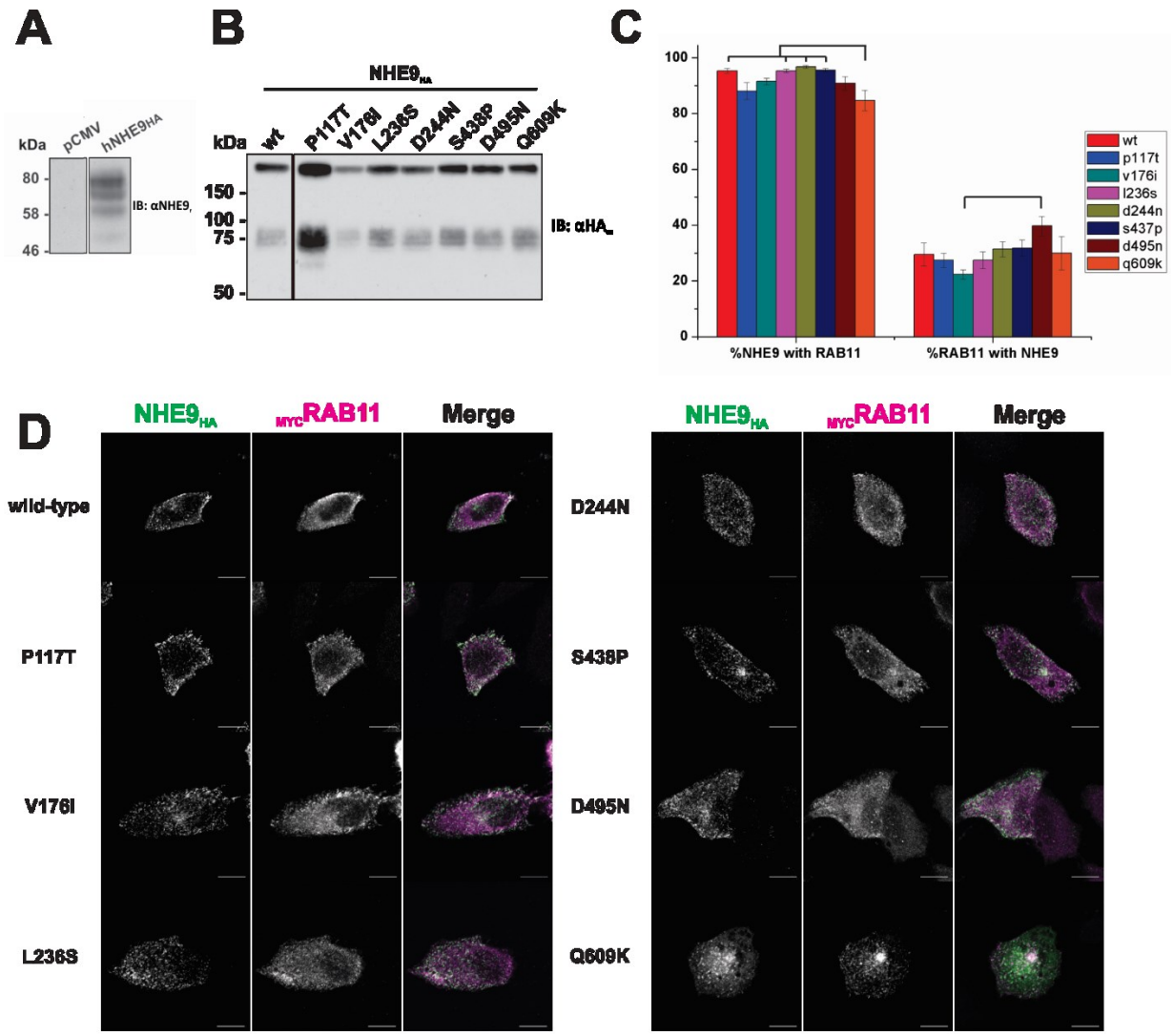

Supplementary Figure 3: Autism-associated variants do not affect the sub-cellular localization of NHE9 in AP-1 cells. AP1 cells do not contain detectable traces of NHE9 by immunoblotting (A). Autism-associated variants and the putatively ion exchange variant D244N in carboxy terminal HA-tagged forms were expressed in AP-1 cells and lysed to assess expression (B). Any variation in signal strength was not found consistently and thus did not warrant further investigation. None of the variants' sub-cellular localization relative to RAB11 differed significantly (C), as indicated by Mander's coefficients of coincidence. This quantification recapitulates our qualitative assessment of the micrographs, at least ten of which were used for analysis from three separate experiments (D). Scale bar represents 10 µm. Significant differences indicate $p < 0.05$ by type II one-factor ANOVA. Panel A is modified from Das Gupta, et al, manuscript in preparation.

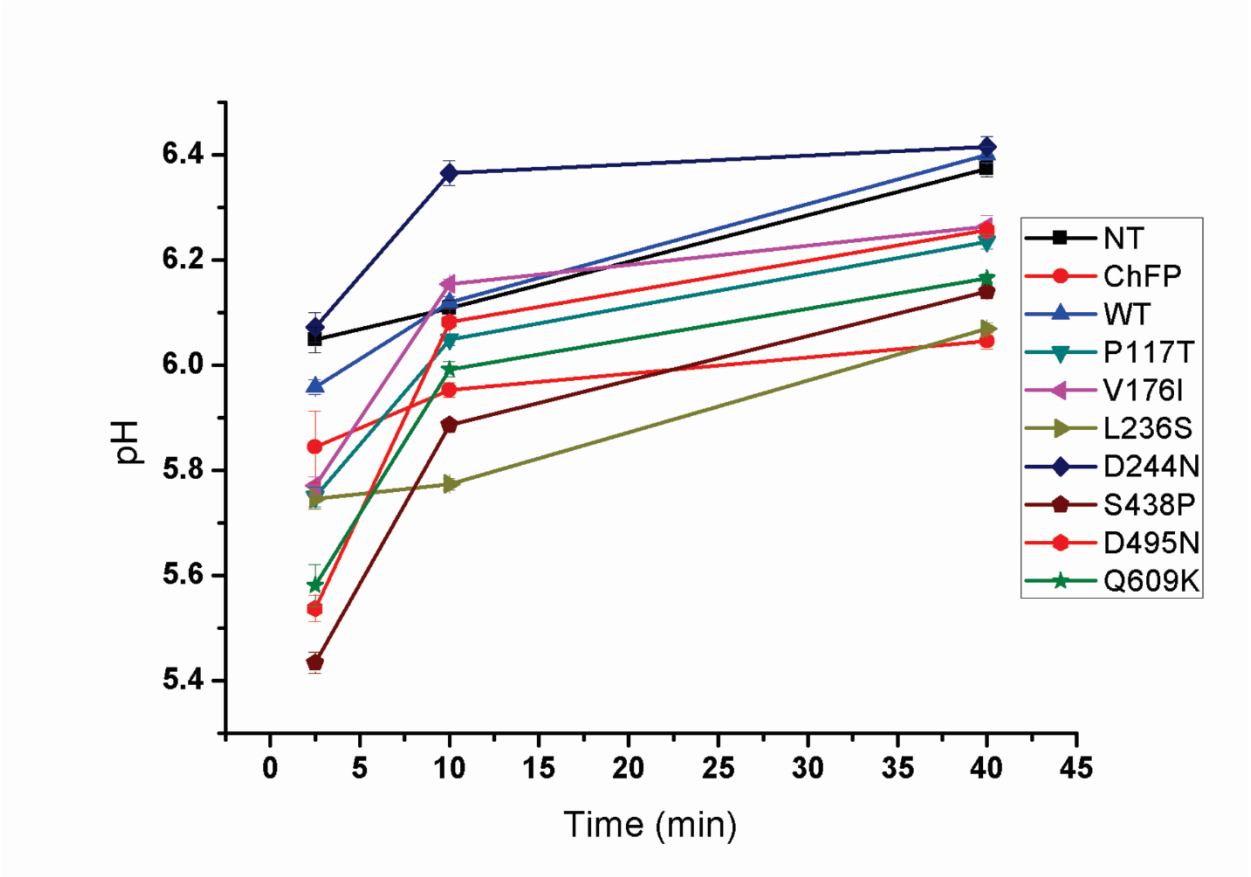

Supplementary Figure 4: NHE9 contributes to transferrin vesicle pH during endocytosis. Transferrin vesicles are distributed among relatively acidic compartments at 2.5 min and progress to vesicles with more alkaline pH at 10 and 40 min. Expressing ChFP decreased the pH of transferrin vesicles throughout this trafficking. When colocalized with transferrin, NHE9 alkalinizes transferrin vesicles. The effects of the mutations on transferrin vesicle pH were largely preserved throughout the timeframe. Error bars represent standard error of the mean. Statistically analysis was only done on the 40 min time point, as shown in Figure 6.

Supplemental Protocols

Cell Culture

HEK293T cells were cultured as HeLa and AP1 cells were. SH-SY5Y cells were similarly cultured except a 50-50 mixture of Dulbecco's Modified Eagle's Medium and nutrient mixture F-12 mixed (DMEM/F12) (Gibco) with an additional 10% fetal bovine serum.

Cell-surface biotinylated protein pull-down

Forty-eight hours after transfection, cells were washed twice with ice-cold PBS 1 mM $MgCl_2$ 0.1 mM $CaCl_2$ pH 8.0 (PBS-CM) then incubated with 0.5 mg/mL sulfo-NHS-SS-biotin (ThermoScientific) for 30 min at 4 °C in the dark. Afterwards, cells were washed once with PBS-CM, twice with PBS-CM 50 mM glycine, and twice with PBS prior to scraping into immunoprecipitation buffer. Clarified cell lysates and samples were obtained as described in the section on mammalian cell lysis. Equal amounts of protein were diluted to equal volumes and loaded onto 100 µL thrice pre-washed 50% NeutrAvidin bead (ThermoScientific) slurry. Following 2h of rocking at 4 °C, lysate-bead colloids were washed four times with 650 µL of immunoprecipitation buffer, centrifuging at 1,500 x *g* for 4 min at 4 °C to remove supernatant. To elute proteins from beads, beads were incubated with 50 µL Laemmli protein loading buffer for at least 30 min and then centrifuged at 16,100 x *g* for 5 min to obtain eluent supernatants.